Quantifying vein patterns in growing leaves

Thesis submitted
To the Faculty of Graduate and Postdoctoral Studies
As partial fulfillment of the requirements for the
Degree of Master of Science

by Rebecca Assaf

Faculty of Science
Department of Biology
University of Ottawa

Acknowledgements:

I would like to thank my supervisor, Dr. A-G. Rolland-Lagan for her valuable guidance and assistance during the course of this study.

I would like to thank Megan Tu for helping out with the digitization and the analysis of the data, and Lauren Remmler for letting me use some of her data and a program for the analysis she wrote for me.

I would like to thank Dr. E. Scarpella (University of Alberta, Canada) and Dr. R. Stadler and N. Sauer (University of Erlangen, Germany) for providing seeds of transgenic plants.

I would like to thank my parents for all the unconditional love and support they gave me over my whole life.

I would like to thank all the Rolland-Lagan lab members present and past for all the good times we had working together.

Abstract:

How patterns arise from an apparently uniform group of cells is one of the classical problems in developmental biology. The mechanism is complicated by the fact that patterning occurs on a growing medium. Therefore, changes in an organism's size and shape affect the patterning processes. In turn, patterning itself may affect growth. This interaction between growth and patterning leads to the generation of complex shapes and structures from simpler ones. Studying such interactions requires the possibility to monitor both processes *in vivo*. To this end, we developed a new technique to monitor and quantify vein patterning in a growing leaf over time using the leaves of *Arabidopsis thaliana* as a model system. We used a transgenic line with fluorescent markers associated with the venation. Individual leaves are followed in many samples *in vivo* through time-lapse imaging. Custom-made software allowed us to extract the leaf surface and vein pattern from images of each leaf at each time point. Then average spatial maps from multiple samples that were generated revealed spatio-temporal gradients. Our quantitative description of wild type vein patterns during leaf development revealed that there is no constant size at which a part of tissue enclosed by vasculature will become irrigated by a new vein. Instead, it seemed that vein formation depends on the growth rate of the tissue. This is the first time that vein patterning in growing leaves was quantified. The techniques developed will later be used to explore the interaction between growth and patterning through a variety of approaches, including mutant analysis, pharmacological treatments and variation of environmental conditions.

Résumé

Savoir comment un groupe de cellules initialement identiques devient hétérogène, formant des motifs spatiaux, est une question fondamentale en biologie du développement. Le mécanisme est compliqué par le fait que la formation de motifs a lieu dans un système en croissance. Ainsi, tout changement dans la taille et la forme d'un organisme peut affecter la formation de motifs. De même, les motifs peuvent affecter la croissance, et dons la forme et la taille de l'organisme. Cette interaction entre croissance et formation de motifs engendre des formes de plus en plus complexes au cours du développement. Étudier ce genre d'interactions requiert la possibilité de suivre croissance et formation de motifs *in vivo*. A cette fin, nous avons développé une nouvelle technique pour suivre et quantifier la formation des motifs de nervures foliaires dans les feuilles en croissance. Nous avons utilisé comme système d'étude une lignée transgénique d'*Arabidopsis thaliana* aux nervures fluorescentes. La formation des nervures peut ainsi être suivie au cours du temps, pour de nombreux échantillons. Des programmes informatiques créés spécialement pour notre étude nous permettent de quantifier la surface de chaque feuille et ses nervures, pour chaque stade de développement analysé. Les données de multiples échantillons sont combinées pour générer des cartes spatio-temporelles des valeurs de différentes variables liées à la formation des nervures. Ces cartes révèlent des gradients spatiaux qui varient au cours du temps. Notre description quantitative des motifs de nervures foliaires au cours du développement de la feuille indique que la formation de nouvelles nervures à l'intérieur d'une aréole ne dépend pas de la taille de l'aréole mais du taux de croissance du tissu. Ceci est la première fois que la formation des nervures foliaires a été quantifiée *in vivo*.

Les techniques développées pourront être utilisées pour explorer l'interaction entre la croissance et la formation de motifs chez différents mutants ou dans différentes conditions environnementales.

Table of Contents

Figure List

Tables list:

Abbreviations

- DAS= Days After Sowing
- DAG= Days After Germination
- FL= Fluorescent Light
- BF= Bright Field
- destructive method = recent method that quantifies vein patterning in cleared leaves (Rolland-Lagan *et al.*, 2009)
- live imaging method= new method for quantifying vein patterning and growth
- 2D = two dimension
- 3D= three dimension
- Col0 = Columbia
- pEPS1= AtSuc2prom:GFP

Chapter 1:

1. Introduction:

1.1. Leaf vein patterning as a model system to study the interaction between growth and pattern formation

Trying to understand how patterns arise from apparently uniform groups of cells is one of the classical problems in developmental biology.

As a multicellular organism develops, different sets of genes are expressed in different tissues at different times. The mechanisms controlling the spatio-temporal patterns of gene expression are affected by growth, and gene expression itself may affect growth. There is therefore a feedback loop between patterning processes and growth (Figure 1). Interactions between patterning and growth during development have been little studied. Studying such interactions requires an experimental system where both growth and patterning can be monitored, ideally independently and *in vivo*.

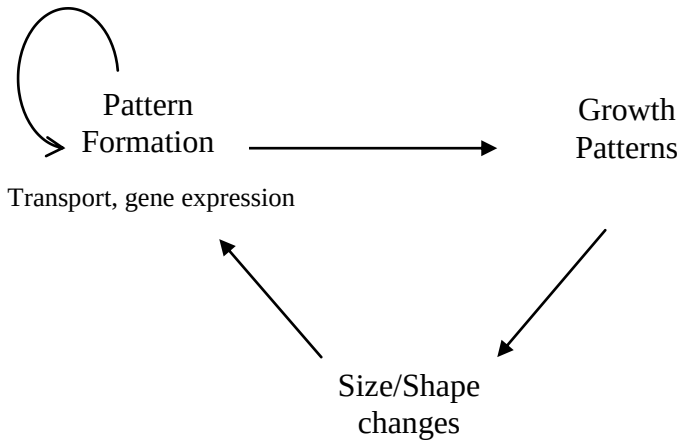

Figure 1: Interaction between growth, gene expression and patterning. (Redrawn from http://mysite.science.uottawa.ca/arolland//Research.html)

In order to monitor growth and patterning, we used an organ that is easily accessible, where growth processes are simple enough and with some pattern features that we can track. The plant leaf and its vasculature fit these requirements well; a leaf is easily accessible to track growth and changes in shape during growth are only due to cells expanding and dividing. Moreover a leaf is relatively thin and can be approximated as a three dimensional surface. It should therefore be possible to track its development and growth through *in vivo* imaging. In order to monitor vein patterning, we can make use of transgenic lines with fluorescently labelled gene expression that is visible on the plant surface (e.g. trichomes, genes expressed in the epidermis, or in the vasculature). In addition, vascular patterns arise progressively as the leaf grows and there is evidence that both processes are coupled (Dengler & Kang, 2001). Extensive work has been done on leaf vascular patterning, from both experimental and theoretical perspectives (Berleth & Sachs, 2001; Dengler & Kang, 2001; Mattsson *et al.*, 1999; Rolland-Lagan & Prusinkiewicz, 2005; Rolland-Lagan *et al.*, 2009; Sachs, 1981; Scarpella *et al.*, 2004; Scarpella *et al.*, 2006). It should therefore be possible to monitor leaf growth and leaf vein patterning *in vivo*, and test the interaction between both processes based on our current knowledge of vein patterning mechanisms.

1.2. Background on leaf vascular tissues

A leaf is an important organ of plants. Through photosynthesis, it is responsible for the production of carbohydrates, which are then transported, to other parts of the plant. Leaves play a major role in evapotranspiration and the upwards movement of water from the roots to the air. Transport throughout the leaves occurs through the

vascular tissue, which is organized in a network. The vascular tissue is mainly composed of xylem and phloem. The xylem conducts water and minerals from the root to upper parts of the plant, and is involved in evapotranspiration; whereas the phloem is responsible for the circulation of nutrients from photosynthesis. In leaves, phloem and xylem tissues are juxtaposed, with the xylem located on the adaxial (upper side) of leaves whereas the phloem is located on the abaxial side of leaves (lower side, Figure 2, Bowman *et al.*, 2002). The phloem and xylem are formed by specialized vascular cells; tracheary in xylem and sieve elements in phloem. Those specialized cells originate from the same provascular cells, which can be labelled by genetic markers at early stages of vein formation (Scarpella & Meijer, 2004). The spatial organization of provascular cells prefigures the venation pattern of the leaf (Scarpella *et al.*, 2004). Therefore, when we talk about venation patterns, we refer to the network pattern that can be seen from the stage when provascular cells appear and onwards. In this thesis, we are more particularly concerned with the spatial organization of the vasculature in the main plane of the leaf (as viewed from above the leaf surface), rather than the spatial organization of xylem and phloem along the adaxial/abaxial axis. Formation of xylem and phloem tissues along the adaxial-abaxial axis has been discussed in several reviews and we refer the reader to those

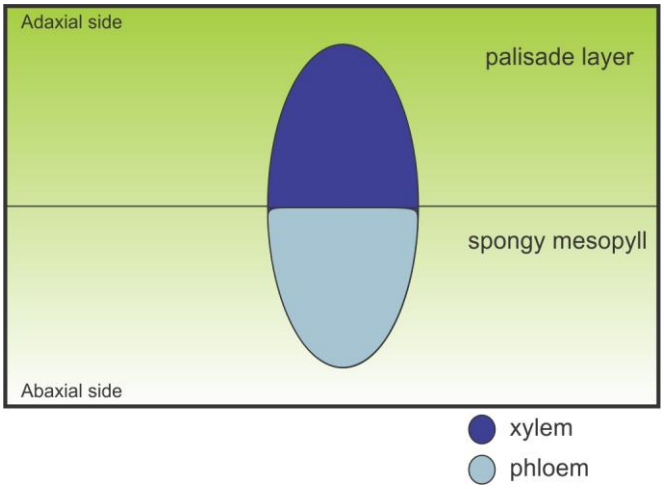

Figure 2: A cross section of a leaf showing the adaxial (upper) and abaxial (lower) sides of the leaf tissue.

reviews for more details (Jung & Park, 2007; Lehesranta *et al.*, 2010; Sieburth & Deyholos, 2006).

At maturity, the venation pattern of whole leaves can be visualized by clearing leaves (Mattsson *et al.*, 1999; Rolland-Lagan *et al.*, 2009), which reveals the xylem, or by imaging transgenic plants with phloem-specific fluorescent markers under an epifluorescence microscope (Donner *et al.*, 2009; Sawchuk *et al.*, 2007; Scarpella *et al.*, 2004; Scarpella *et al.*, 2006; Wenzel *et al.*, 2007, see Chapter 2).

1.2.1. Vein pattern formation: qualitative description

In each primordium, the vascular system is setup *de novo* (Scarpella *et al.*, 2006). Veins are formed as the leaf grows, in spatial arrangements that vary between species, and in some cases between leaves of the same plant. Monocots generally have a striate vein pattern with veins that diverge at the base and converge at the top of the leaf (Figure 3a), while dicots have a reticulate vein pattern with a mid-vein and many higher order veins that connect to each other and form areoles also called loops; a loop is a growing area

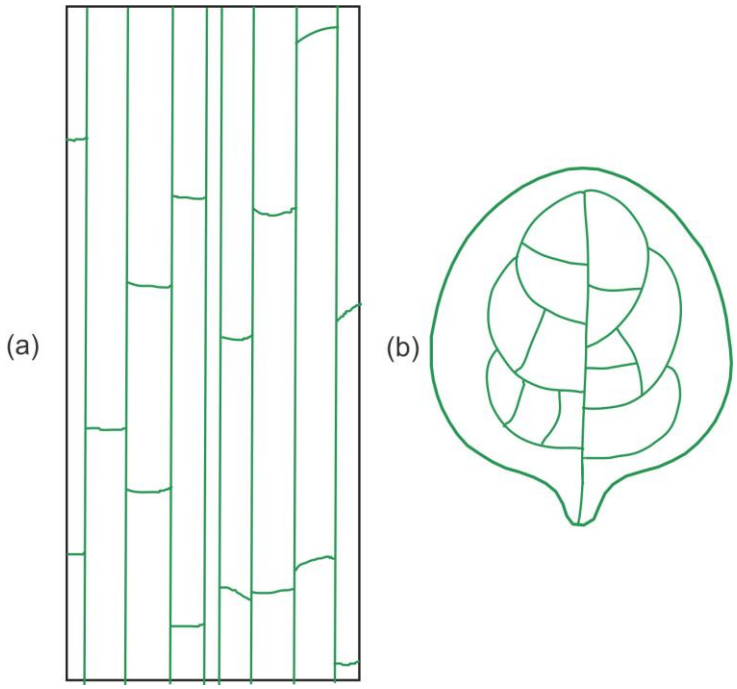

Figure 3: Vascular patterns in dicots vs. monocots. (a)Monocot rice leaf showing striates vascular pattern. (b) Dicot Arabidopsis leaf showing reticulate vein pattern that connect to each other and form loops. Redrawn from Scarpella & Meijer, 2004.

of tissue that is enclosed by veins (Figure 3b, Fujita & Mochizuki, 2006b; Nelson & Dengler, 1997; Runions *et al.*, 2005). Modeling studies suggest that differences in venation patterns between species and between monocots and dicots are likely due to differences in growth patterns (Fujita & Mochizuki, 2006b; Runions *et al.*, 2005).

The sequence of early vascular development events in the first rosette leaf of the dicot species *Arabidopsis thaliana* has recently been characterized qualitatively (Scarpella *et al.*, 2004), and is summarized in Figure 4. At 2 days after germination (DAG), the leaf primordium can be recognized. At 2.5 DAG, the leaf starts growing along the proximodistal axis. Some vascular tissues become visible as the primordium is growing. All vascular cells arise from the vascular meristematic tissue or the procambium (procambium cells are the anatomically identifiable precursor cells of vascular cells, Scarpella *et al.*, 2004). The earliest available markers for vascular pattern formation show a network expression pattern even before cells that will later differentiate into vasculature can be distinguished from the cells around it. The cells that express those early markers have been termed preprocambial cells (Kang Scarpella *et al.*, 2004). The preprocambial cells are originally isodiametric, but later become narrower and cytoplasmic dense compared to surrounding cells. At this stage, the future vascular cells are called procambial cells. The division of procambial cells and preprocambial cells is parallel to the growth direction of the cells (Scarpella & Meijer, 2004; Scarpella *et al.*, 2004). At 3 DAG, the blade is well defined and the first order procambial strands, which will form the mid vein, start showing up. At 5 DAG, the second order procambial cells and two areoles are seen. After 5.5 DAG, the third and higher order procambial strands start appearing. The differentiation of procambial cells

into xylem is completed by DAG 6.5 for first order veins and by DAG 10 for the second order veins. The phytohormone auxin seems to be involved in the differentiation of procambial cells into xylem (Mattsson *et al.*, 1999; Scarpella *et al.*, 2004). At 14 DAG, all veins have already differentiated. The differentiation of veins occurs in a wave starting at the tip of the leaf and then ends at the base (Scarpella & Meijer, 2004; Scarpella *et al.*, 2004).

The molecular mechanism behind the formation of veins in leaves is still unknown. Different models have been suggested to try to explain how veins arise from an initially uniform group of cells.

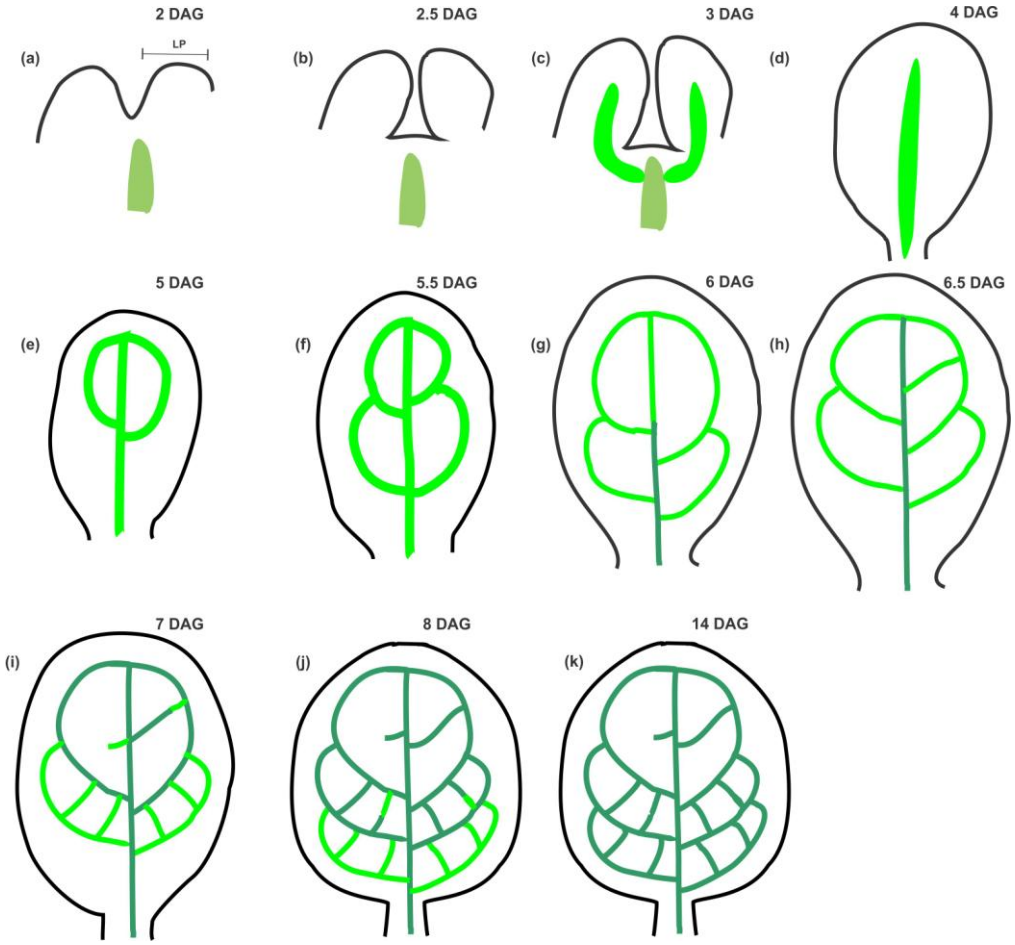

Figure 4: Vein formation in leaf 1 of Arabidopsis. (A-C) Lateral view. (D-K) Abaxial view. Colors in A-K: procambium, bright green, xylem, light green, for more details refer to text. Redrawn from Scarpella *et al.* (2004).

1.2.2. Proposed mechanisms controlling vein pattern formation:

Three types of mechanisms have been proposed to explain vein patterning, and are based either on the transport of some chemicals driving patterning, or on physical constraints.

1.2.2.1. Reaction-diffusion

The reaction- diffusion model postulates the presence of two or more substances that interact to give rise to different patterns. Reaction-diffusion equations were originally proposed by Turing (1952) to show how spatial patterns may arise. More precisely from an initially homogeneous state, spatial heterogeneities can appear due to the interaction of two chemicals A and B where A is an activator and B is an inhibitor. A local maxima of A can be generated, A triggers its own production and the production of B, the two chemicals diffuse and degrade at different rates causing the production of different patterns depending on how the parameters are altered (Figure 5a, Berleth, 2000). Gierer & Meinhard (1972) used this model to predict how patterns form in biological systems; using different parameters, spots, stripes or network patterns can be seen (Figure 5a).

1.2.2.2. Signal canalization

Sachs (1981) proposed the presence of a signal that passes through cells and causes the differentiation of cells into procambial cells. More precisely, Sachs proposed a positive feedback mechanism where a signal goes through cells; some cells will start transporting it more than others will, which will then increase the ability of these cells to transport the signal more efficiently. This signal is responsible for the differentiation of veins. Hence, this signal is transported in the leaf causing the

differentiation of cells into veins (Figure 5b, Sachs, 1981). At least part of the proposed signal involves auxin (Mattsson *et al.*, 1999; Scarpella *et al.*, 2006; Wenzel *et al.*, 2007).

1.2.2.3. Physical forces

Couder *et al.* (2002) demonstrated that the formation of veins occurs in a pattern similar to the pattern of cracks in drying gels and point to the role of forces during growth to explain vascular formation. As pointed out by the authors, veins are not tree-like branching structures; instead, veins reconnect to form reticula (loops). Such patterns also arise when a gel cracks as it dries. To explore the similarities between the two processes, the authors performed different experiments using a concentrated suspension of latex particles and water poured onto a glass plate or silicon wafer. The suspension first became a gel that shrank while drying. The first crack to happen is the longest (analogous to the formation of a mid vein in leaves) and as new cracks form they are limited in their progression by pre-existing cracks (second and higher order veins in leaves). At the end of the experiment, little elastic energy is left and then the last cracks cannot cross to reach the older neighbour cracks and stay open, which explains the free-ending veins in leaves. Different boundaries and conditions were used to be able to explain different leaf vein patterns present in nature (Figure 5c-d). The authors' hypothesis states that the procambium differentiates because of compressive stress that the cell is put through, which exceeds a stress threshold. A difference between a leaf and a drying gel is that the gel is shrinking, not growing (Couder *et al.*, 2002).

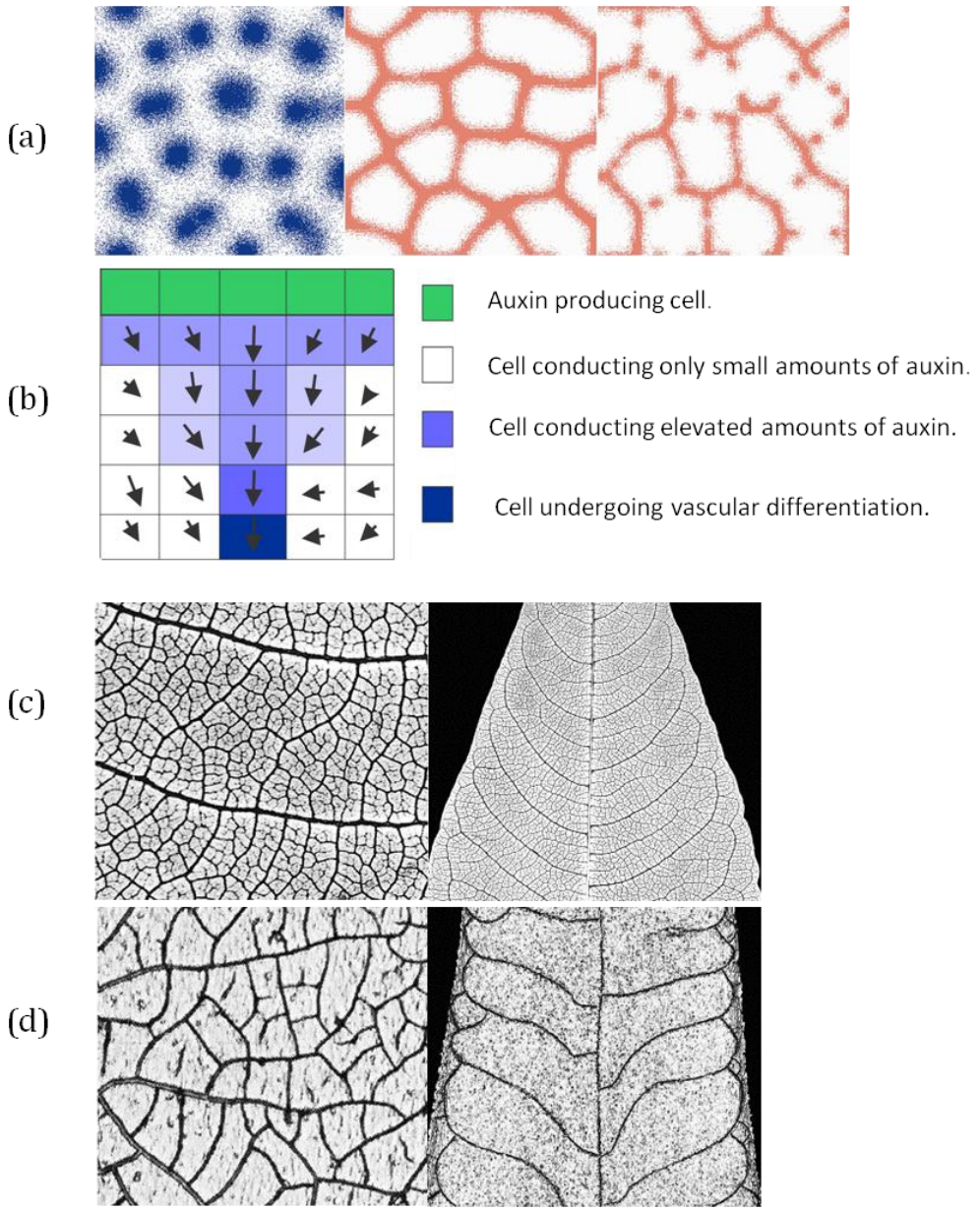

Figure 5: Different hypotheses have been proposed to explain vein patterning. (a) Different patterns generated by the Reaction-Diffusion model. Reproduced from Berleth (2000) with permission from The Copyright Clearance Center. (b) Vein formation according to the canalization hypothesis, efficient auxin transport drains away enough auxin to keep overall auxin below the threshold for vascular differentiation. Redrawn from Mattsson *et al.(*1999). (c) Vein patterns formed in nature (left) veins in a Polygonum Polystachium, (right) the brochidodromous organization of where loops forming the margin. Reproduced from Couder *et al.*, (2002) with permission from The Copyright Clearance Center. (d) Patterns formed in a gel; (left) matching the picture in 5b left. (Right) Matching the leaf in 5c right. Reproduced from Couder *et al.*,(2002) with permission from The Copyright Clearance Center.

1.2.3. Evaluation of existing hypotheses

A hypothesis for the formation of vasculature needs to account for many characteristics in leaves such as the vein formation in monocots and dicots, the formation of loops or reticulations, formation of a mid vein, first order vein, and higher order veins, the formation of discontinuous vasculature in some mutants, the role of growth in vein formation, and the formation of altered patterns in altered environmental conditions, specifically when auxin transport is inhibited (Nelson & Dengler, 1997; Rolland-Lagan & Prusinkiewicz, 2005).

While all proposed vein patterning mechanisms can account for the formation of networks in tissues, the reaction-diffusion model needs at least two substances that interact to give rise to the veins. The existence of such substances in leaves is still not experimentally proven. The current experimental evidence is consistent with the canalization hypothesis. It is proven that auxin is an important signal involved in the formation of vasculature (Mattsson *et al.*, 1999), but the molecular mechanism by which canalization would occur is unknown. Forces during growth may influence vein patterning, but currently such forces have not been measured. The mechanisms at play during vascular pattern formation in leaves are a combination of physical and molecular mechanisms, and a unifying model still remains to be proposed. Creating and testing such a model will require the possibility to monitor, and possibly experimentally alter, growth and vein patterning in space and time as a leaf develops.

1.2.4. From theoretical models to molecular mechanisms

1.2.4.1. Mechanisms for the formation of loops - Further considerations

As previously stated the leaves of dicots are characterized by a mid vein with extended veins forming a closed reticulum or loops (Nelson & Dengler, 1997). Several recent studies qualitatively followed loop formation using different stage-specific fluorescent markers (Donner *et al.*, 2009; Scarpella *et al.*, 2004; Scarpella *et al.*, 2006). However, the underlying mechanism for loop formation is still unknown.

As mentioned previously, a loop is an area of tissue that is enclosed by veins, and as the leaf grows loops will enlarge. To maintain proper irrigation of the tissue, we expect that once a loop reaches a certain size new veins will need to form within it. Those veins may in some cases completely split the loop, leading to the formation of new loops. This phenomenon is called loop subdivision. In terms of patterning mechanism, we postulate that there may be an optimal size that the loop will reach before it subdivides (Figure 6). This optimal size could possibly be directly dependent on the number of cells in the tissue area or the tissue area itself, or depend on the level of given patterning substances necessary for vascular formation. A potential candidate for such a substance is auxin.

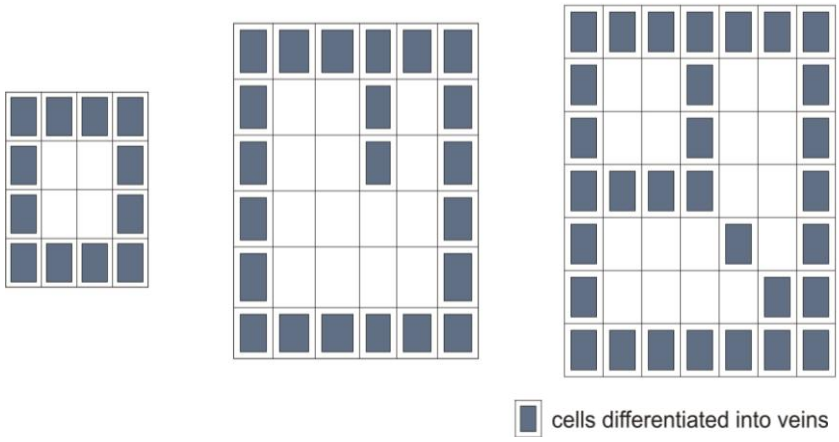

Figure 6: Loop subdivision or splitting. We postulate that if an area of tissue is enclosed by veins, there is an optimal size at which the tissue will get to before new segments arise to maintain proper irrigation.

1.2.5. Auxin

Auxin is a plant hormone involved in many growth and physiological processes in the plant, including vein patterning. The most naturally abundant form of auxin is indole-3-acetic acid (IAA). Auxin is transported between cells via specialized efflux carrier proteins, such as the P-glycoproteins of the ABCB transporter family (ABCB/PGP) and PIN proteins (Wisniewska *et al.*, 2006). PIN proteins localize polarly at the plasma membrane and are in effect guiding auxin movement out of the cells. The pattern of polar localization of efflux carriers across a tissue gives a polarity to auxin transport (Paciorek *et al.*, 2005; Sauer *et al.*, 2006). Until this day, auxin is the main plant hormone for which a role in the vascular differentiation process has been shown. Sachs (1981) proposed that vasculature formation and differentiation is restricted to areas with high auxin fluxes. He performed applications of artificial auxin to stems, causing the formation of new strands that channel auxin into pre-existing vasculature (Sachs, 1981). Sachs proposed the canalization hypothesis based on his work on stems, and the hypothesis was later extended to leaves (Sachs, 1981).

Figure 7a shows how auxin is transported inside the cell according to the chemiosmotic hypothesis. This hypothesis was formulated in 1970 to explain the polar auxin transport (Goldsmith, 1977). Recent findings on auxin influx (AUX1) and efflux carriers (PIN proteins and ABCB/PGP) are now incorporated in the hypothesis (Vanneste & Friml, 2009; Vieten *et al.*, 2007). Auxin is a weak acid (pKa=4.75), it is present in the cell wall (pH=5.5) in two forms ionized IAA^- and protonated IAAH. IAA^- needs AUX1 carriers to be transported inside the cells while IAAH can diffuse passively through the cell plasma membrane into the cytoplasm where the

environment is more neutral (pH=7). Once inside the cells, the proton dissociates and auxin becomes trapped inside the cell. To exit the cell, specific auxin efflux carriers (PIN proteins and ABCB/PGP) are needed to take auxin (IAA^-) outside the cell (Vanneste & Friml, 2009; Vieten *et al.*, 2007).

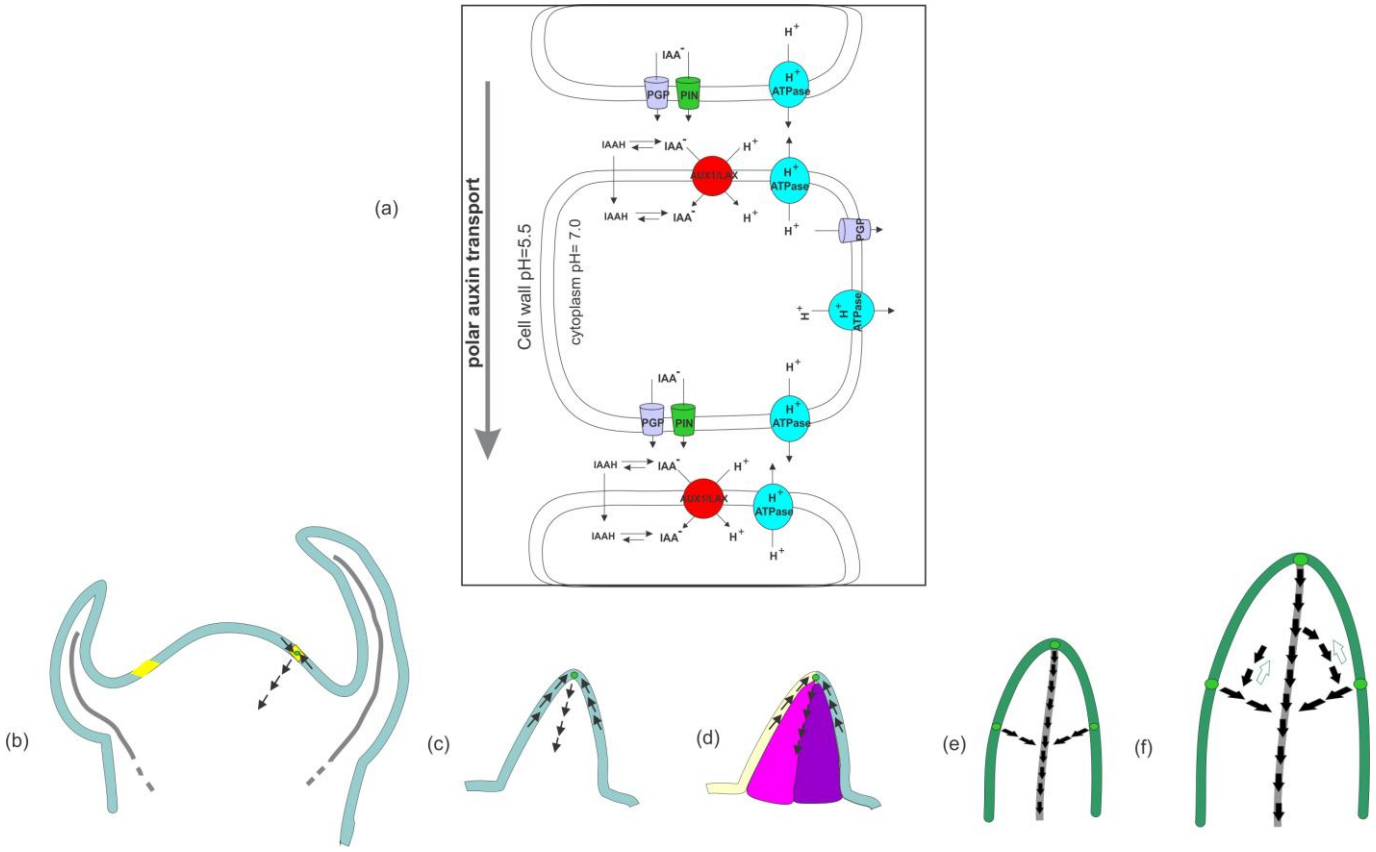

Figure 7: Auxin transport and patterning. (a) Cellular model for polar auxin transport. Redrawn from Vanneste & Friml (2009). For more details, refer to text. (b) Longitudinal section of the shoot apical meristem showing site of leaf initiation (Rolland-Lagan, 2008). (c) Leaf outgrowth corresponding to the boxed area in (b). (d) Adaxial (pink) and abaxial (purple) domains. The epidermis is shown in lighter color (white and light blue). (e) Median section (plane perpendicular to the adaxial–abaxial axis) through the growing primordium (Rolland-Lagan, 2008). (f) Later PIN expression domains extend from existing strands of PIN expression, in a direction opposite to PIN polarity (black arrows). Blue arrows show the direction of PIN expression progression. (b-f) redrawn from Rolland-Lagan (2008).

1.2.5.1. Auxin and patterning

In vivo imaging of transgenic Arabidopsis showed that patterns of PIN: GFP localization in leaves prefigure vein localization (Scarpella *et al.*, 2006) . These patterns must also reflect routes of auxin transport. Figure 7b shows the routes of auxin transport as directed by PIN1 (black arrows) during leaf formation; auxin is transported through the epidermis and towards a convergence point (blue dot) which is the point of leaf primordium outgrowth. As the adaxial (in pink) and abaxial (in purple) regions of the leaf are specified, auxin is transported within the leaf at the junction between adaxial and abaxial domains. As the leaf grows further, new convergence points appear and further auxin paths within the blade appear. The first veins formed progress from the auxin convergence points towards existing veins, but later veins proceed from existing veins (blue arrows, Rolland-Lagan, 2008). This is consistent with canalization models that indicate that veins can proceed from auxin source to auxin sink if localized sources are present, or from sink to source in absence of localized maxima (Rolland-Lagan & Prusinkiewicz, 2005).

However, no model so far is consistent with all experimental data available on vein formation, and it is still unclear where auxin is produced in the leaf. Experimental work on the effect of auxin on vein formation showed that inhibited auxin transport altered vein pattern formation. More particularly, plants treated with auxin transport inhibitors displayed smaller leaves than wild type, and veins were increasingly restricted to the leaf margin with higher concentrations of inhibitors (Mattsson *et al.*, 2003; Sieburth, 1999). However, even though many studies have looked at the auxin involvement in vein initiation (Aloni, 2001; Aloni *et al.*, 2003; Mattsson *et al.*, 1999;

Nelson & Dengler, 1997; Sachs, 1981; Scarpella *et al.*, 2006; Scarpella *et al.*, 2010), until this day, the location of auxin production in the leaf is still unknown, and it is unclear whether vein formation is triggered by high auxin fluxes, high auxin concentrations, or both (Rolland-Lagan *et al.*, 2005). Nevertheless, small pieces of the puzzle are starting to be uncovered in how and where auxin is produced. Recent studies have shown the involvement of YUC gene family (YUC1, YUC2, YUC4 and YUP6) in auxin biosynthesis and plant development. These genes manipulate auxin production spatially and temporally (Cheng *et al.*, 2006; Cheng *et al.*, 2008).

1.3. Vascular formation in a growing leaf: Monitoring growth of tissue surfaces

As vasculature forms in growing tissues, understanding how vascular patterns arise and change throughout development requires studying this pattern formation in the context of a growing leaf. Therefore growth patterns across the surface of the leaf have to be monitored in space and time as the leaf develops.

Monitoring growth generally requires the possibility to track the position of visible landmarks on the tissue across time (Avery, 1933; Dumais & Kwiatkowska, 2002; Reddy *et al.*, 2004; Richards, 1943; Rolland-Lagan *et al.*, 2003; Rolland-Lagan *et al.*, 2005). To study growth of an area or tissue, we need to divide this area into smaller surfaces (Coen *et al.*, 2004).

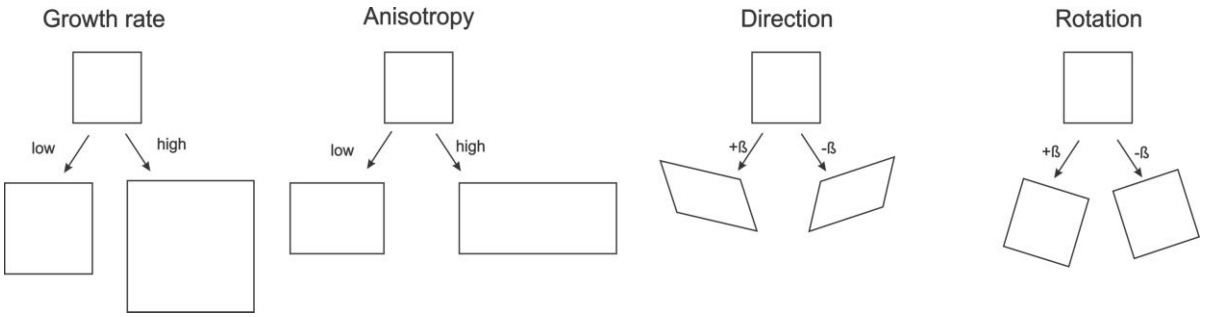

Figure 8: Growth parameters. Redrawn from Coen *et al.* (2004).

Growth in two dimensions (2D) can be characterized by four types of parameters (Coen *et al.*, 2004; Rolland-Lagan *et al.*, 2003; Rolland-Lagan *et al.*, 2005); growth rate, anisotropy, direction of growth and rotation (Figure 8). The growth rate is how much the tissue is growing, and that rate becomes zero at maturity. The anisotropy is the amount of growth along the main direction of growth compared to its growth in the perpendicular direction. If growth is equal in all directions, the area grows from a sphere to a sphere. This is called isotropic growth. If there is a preferred orientation of growth, a sphere grows to an ellipse. This type of growth is called anisotropic (the more anisotropy, the more elongated in shape the ellipse will be). The direction of growth is the angle or orientation of the main direction of growth. Different parts of an organ may grow at different rates along different main directions of growth and with different levels of anisotropy, which may lead to shape changes as the organ increases in size. If in a tissue growth occurs at the same rate everywhere in an isotropic fashion, growth is said to be isogonic. In this case, as the tissue grows it does not change shape (Coen *et al.*, 2004; Richards, 1943). As neighbouring regions grow at different rates and possibly in different orientations, the regions will to rotate relative to each other. This rotation can be measured as the angle of rotation of the tissue as growth proceeds.

Monitoring of spatio-temporal growth patterns was originally performed on a leaf of *Nicotiana tabacum* (tobacco). Avery (1933) monitored the growth of tobacco leaves by placing landmarks on it (ink dots) and tracking those landmarks (Figure 9a). Landmarks displacements in time were used to estimate growth patterns in different parts of the leaf. The tobacco leaf grew more in the margin, central and basal portions of the leaf compared to the tip of the leaf. The leaf tip matured earlier than the leaf base, showing a tip to base increase in growth rates. According to Avery, these differences in growth rates caused the changes in leaf shape (Avery, 1933). Richard and Kavanagh (1943) used the tobacco leaf data from the Avery paper to calculate relative growth rates (Figure 9b). The relative growth rate is calculated as the growth rate per unit of quantity over a specified period of time (Richards, 1943). The leaf had a tip to base gradient in growth rates where the tip was always growing at slower rates than the leaf base (at the fourth stage, the tip had a 70% relative growth rate of the highest relative growth rate compared to 100% at the base, Richards, 1943). One other observation is that the growth was non-isotropic at early stages but then it became more isotropic at the last time points (Richards, 1943). Although this method could give an idea of how the leaf is growing, the problem is that the sample had to be large enough when applying the dots. In this case, when dots were placed, cell divisions (and likely vein patterning) had already almost stopped and the leaf was already close to its mature shape.

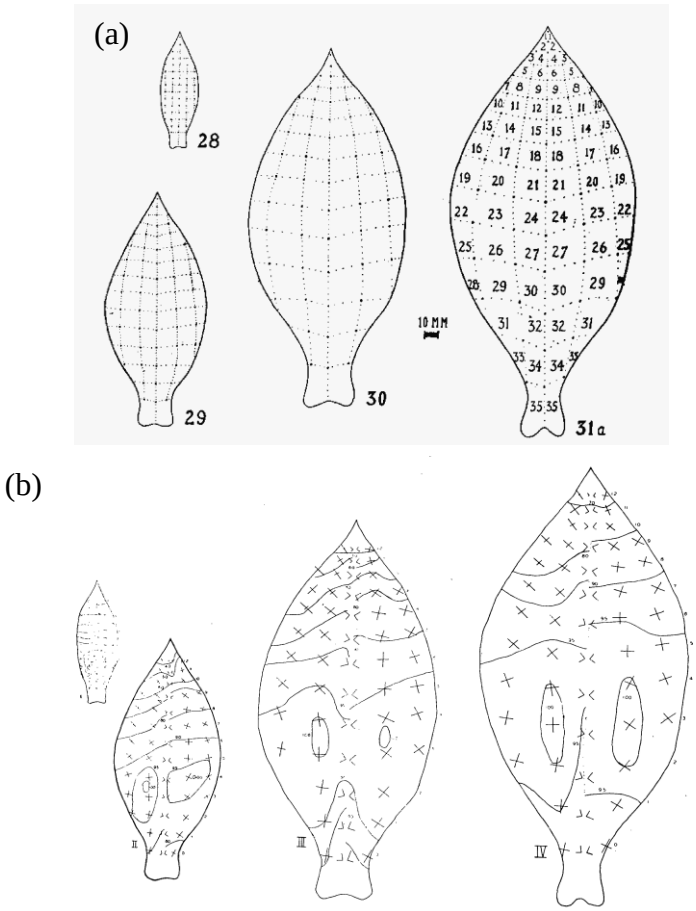

Figure 9: Growth of Tobacco leaf measured over time. (a) Placing ink dots on the tobacco leaf and following its growth. Reproduced from Avery (1933) with permission from The Copyright Clearance Center. (b) Growth rates measured by Richards and Kavanagh (1943) using the leaves in the Avery paper (Avery, 1933). The relative growth rate was calculated in percent of the maximum growth rate. The nature of the specific growth rate in length is shown at each point by a pair of crossed lines. The length of each line is proportional to the specific growth rate in length in that direction. Reproduced from Richards & Kavanagh (1943) with permission from The Copyright Clearance Center.

More recently, other methods have been developed to assess growth patterns of plant surfaces. Dumais & Kwiatkowska (2002) developed a method to measure growth of the surface of the shoot apical meristem in *Anagallis arvensis L* as the cells divide. First, they reconstructed the shoot apical meristem in 3D from stereoscopic images (Figure 10). The shoot apical meristem was monitored at different time points. For each time point, meristem curvature was calculated by determining how much a

part from the shoot apical meristem differs from a plane surface. To estimate growth between time points, the strain rates or in other words, how much a cell had grown or stretched was measured between two time points by using a method by Goodall & Green, (1986) and modified by the authors. Using such a method to track the growth of whole leaves would be very difficult due to the large number of cells involved and the difficulty to track cell lineages for multiple rounds of cell division.

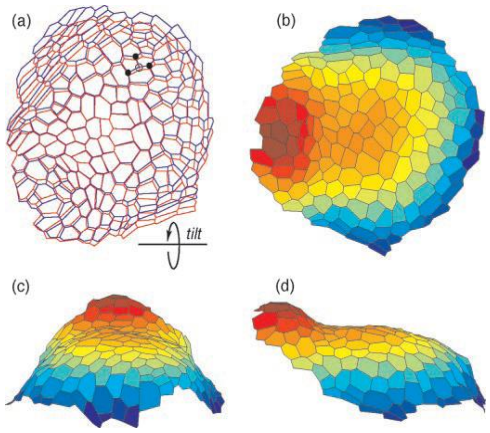

Figure 10: Stereoscopic reconstruction of the shoot apical meristem. (a) Cell pattern before and after tilting by 10°. (b-d). Top and side views of the reconstructed meristem. Colors indicate position along the meristem axis (red = high elevation, blue = low elevation). Reproduced from Dumais & Kwiatkowska (2002) with permission from The Copyright Clearance Center.

Wiese *et al.* (2007) measured the relative growth rate of two ecotypes of Arabidopsis Colombia (Col0) and Ler (Wiese *et al.*, 2007). The leaves were chosen depending on their size and position in the plants. The authors chose the 2nd to 4th youngest leaves when they were half the size of already grown leaves (5–10 mm in length). They used digital image sequence processing to calculate leaf growth over 24 hours. The leaves were fixed with clips and images were taken every 120s (Figure 11a). The authors found a basipetal gradient of growth for both ecotypes: the leaf base was growing faster than the leaf tip. Although this

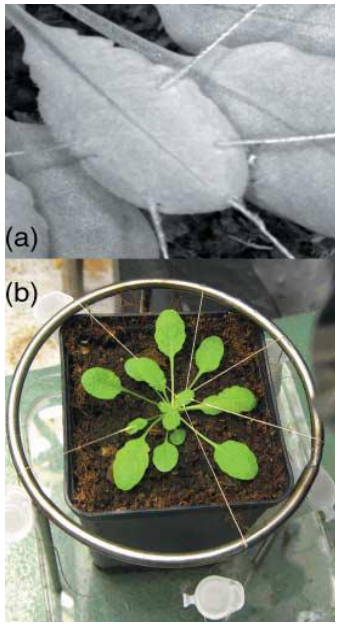

Figure 11: Leaf growth analysis of *Arabidopsis thaliana*. (a) Fixation of strings on a Col-0 leaf. (b) Fixation of a leaf with weights in a metal ring. Reproduced from with permission from Wiese *et al.* (2007) from The Copyright Clearance Center.

method showed a clear spatial gradient in the growth of leaves, imaging started at later stages of growth when the leaf is older. This does not suit our project objectives, we want to follow growth and patterning at very early stages until both growth and vein patterning have stopped. In addition, there is the inconvenience of having to hold the leaf flat for the whole experiment (Figure 11b).

As a plant tissue grows, cells initially enlarge and divide. Cell divisions stop before growth of the tissue stops (i.e., at later stages, cells expand but do not divide). The phase of growth during which cells enlarge and divide is sometimes referred to as the proliferation stage (Beemster *et al.*, 2005; Wiese *et al.*, 2007). During that phase, cell are actively subdividing and expanding. Donnelly *et al.*, (1999) used cyclin proteins to follow spatial and temporal patterns of cell division in leaves i.e. study leaf growth at the cellular level. They looked at rosette leaf number 8 of *Arabidopsis thaliana* ecotype Col0. Leaf 8 is initiated 18 days after germination of the seed. The cyclin proteins were labelled using the GUS (beta-glucoronidase) assay at different time points. At day 0, the cyclin proteins were distributed evenly in the developing leaf. In a cross section of the blade, GUS signal was seen in the mesophyll precursor cells, the protoderm and the procambium. At day 4, even though the signal was still abundant in the whole leaf, the signal was less diffused. In a cross section of the blade, GUS activity was only seen in the margins of the leaf and the midvein. A cleared leaf showed GUS in mesophyll cells and in the procambium of all the vein classes. At day 8, GUS activity was more localized at the leaf base. There was at this point a tip to base gradient. A cleared preparation of a leaf showed GUS more localized to the cells of the basal half of the blade and very reduced in the tip of the leaf, GUS was still expressed in

all vein classes throughout the leaf blade. At day 12, GUS activity was more localized to the leaf base and in the petiole. At Day 16, GUS activity was reduced to the petiole, and the secondary veins mostly in the basal half of the mid vein. This study showed apex to base pattern of the cyclin proteins expression i.e. cells have stopped dividing first in the tip then at the base (Donnelly *et al.*, 1999). This study does not truly encompass growth as it reflects cell division rates only, not cell expansion. Moreover, the study did not allow *in vivo* analysis, as GUS assays are destructive, (samples cannot be followed over time).

Therefore, to date there is no suitable technique for monitoring growth patterns during the vein patterning stage of leaf development. In the following, we propose a new methodology to quantitatively monitor leaf surface growth and vein patterning, where individual leaves are followed in many samples through time-lapse imaging. In the longer term, this methodology will provide a basis to investigate the interaction between vein patterning and growth.

Chapter 2

2. Materials and Methods:

2.1. Objectives:

In this thesis, we propose a new methodology to quantitatively monitor leaf surface growth and vein patterning *in vivo* throughout leaf development. The objectives of this study are to develop: 1) a way to image leaves *in vivo* over their development and follow vein formation at the same time without killing the plants, 2) a computational method to extract vein patterning and growth information from the acquired images, and 3) a methodology to combine data from many samples to obtain statistical data. The methodology will then be applied to a set of *Arabidopsis thaliana* plants of which individual leaves will be followed through time-lapse imaging. This will provide a basis to investigate the interaction between vein patterning and growth.

2.2. Experimental procedures

2.2.1. Plant material and growth conditions

The widely studied model plant *Arabidopsis thaliana* (commonly called Arabidopsis) has been used for this study, because most of the molecular work on vein pattern formation has been carried out on this species. In addition, transgenic plants are available that have fluorescent markers associated with the vasculature (Appendix B). Arabidopsis plants also have the advantage of being small, allowing easy imaging under a fluorescence microscope. In young plants, leaves of Arabidopsis form successively, with very short internode between two successive leaves, forming what is commonly called a rosette (Figure 12a). Leaves in the rosette are called rosette leaves. When the plant is ready to flower, the stem of the plant elongates, and leaves,

known as cauline leaves, are formed on the stem (Figure 12b-c). The focus of this work is the development of the first rosette leaf of Arabidopsis. The first two rosette leaves form almost simultaneously and it is not possible to distinguish between both; therefore, it is common practice to pick one of the first two leaves at random when analyzing development of the first leaf of Arabidopsis (Rolland-Lagan et al., 2009; Scarpella et al., 2004).

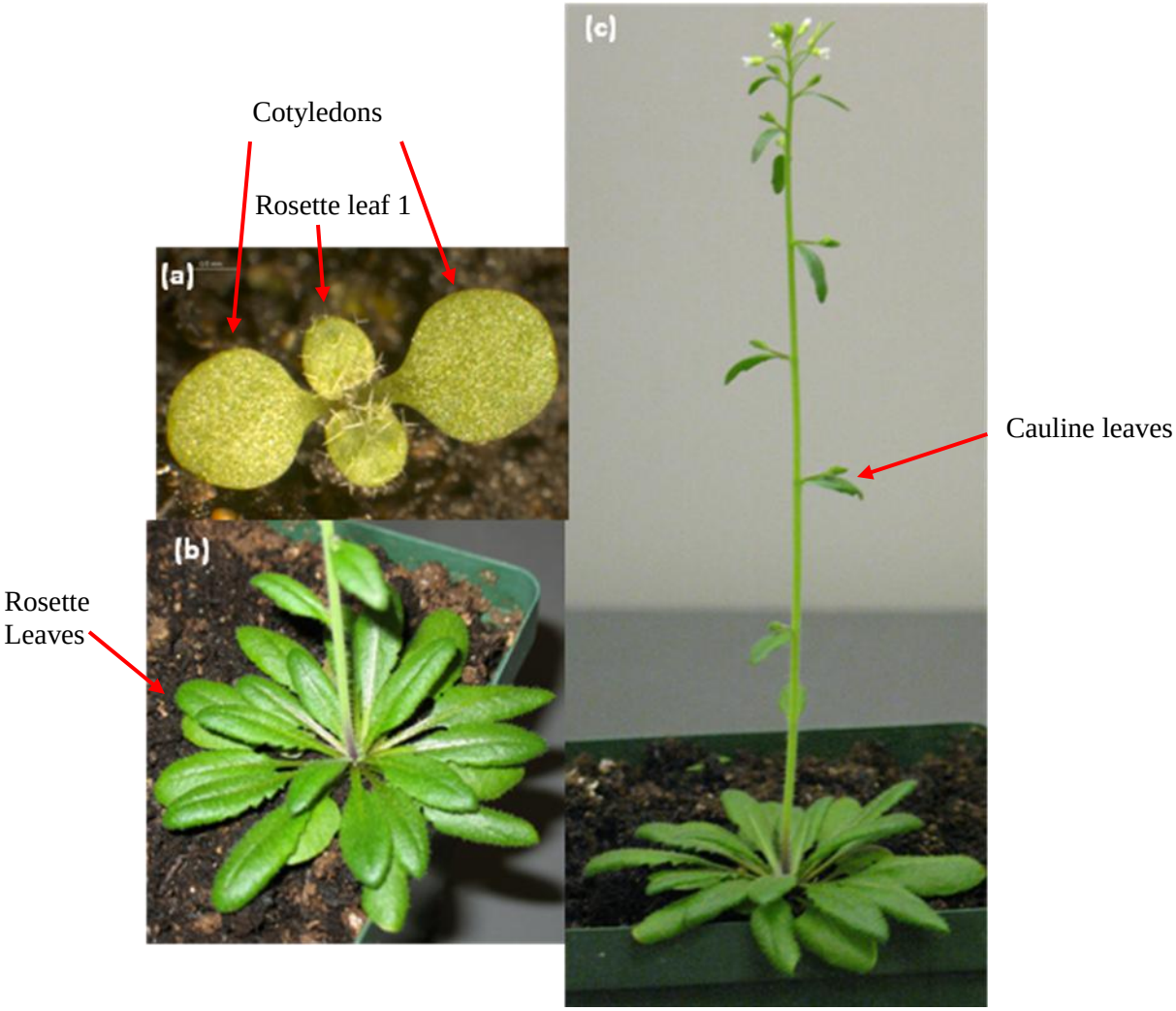

Figure 12: *Arabidopsis thaliana* (a) with 2 cotyledons and the first 2 leaves (b) rosette leaves. (c) The plant with a stem and the cauline leaves.

For this study, the focus is a line in which patterning and growth can be followed until both processes have stopped. The most suitable line is pEPS1 of ecotype C24 (AtSuc2prom: GFP). This line expresses free green fluorescent protein (GFP) in the phloem. The GFP marker appears at late stages of development, i.e. when the procambial cells differentiate into xylem and phloem. Other transgenic lines have been tested, but pEPS1 was ultimately selected to develop this methodology (for more details on the different lines tested check Appendix B).

The use of a fluorescent dye was tested as an alternative to using the transgenic lines with fluorescent markers expressed in the vasculature. This was mainly because getting suitable transgenic lines is not always easy, especially when we want to study vein patterning in different mutants. We attempted to use hydroponics medium to grow plants and then transfer them into a fluorescent dye solution for a short period of time (Roberts *et al.*, 1997) so the roots could take up the dye. Then, leaves could be imaged and vasculature could be visualised. Growing plants in liquid would be the best way to study the veins in different mutants without needing to get mutants with the fluorescence markers expressed in the vasculature. Two different approaches (Hetu *et al.*, 2005; Huttner & Bar-Zvi, 2003) were tested, but they both failed (for further details, check Appendix B). In the remainder of this study, pEPS1 will be used to follow the development of the first rosette leaf over time.

2.2.2. ***Growth conditions***

For each plant line, seeds were sterilized with one wash with 70% ethanol, one wash with bleach and then five washes with distilled water. Sterilized seeds were imbibed in the fridge at 4^0 C for four days, and then sown in soil in pots (~5 seeds per

pot, 5x5x10cm pots) and placed under light shelves (ArabiSun Lighting System, Lehle seeds, Texas, USA) in the microscopy room with 16 hr light: 8 hr dark cycles at 23^{o} C (Figure 13). All samples used in the analysis were imbibed and sown at the same time.

Figure 13: Light shelves used to grow plants in pots (green) in the lab also called ArabiSun.

2.2.3. Imaging and time lapse

When the first two rosette leaves were visible, which occurred approximately seven days after sowing (DAS07), one of these two leaves was randomly chosen to image over time. However, for pEPS1, imaging started at DAS10 because GFP fluorescence specific to the vasculature could not be visualized until then. Twenty pEPS1 plants were followed over 11 days (DAS10-DAS20). Pictures were taken at 24 hour intervals.

A motorized fluorescence macroscope (Leica Z16 APO A Macrofluo TM) was used to image the leaves according to the following procedure.

For each leaf sample, images were taken at different focal planes, which constitute a *z-stack*. Two z-stacks were taken for each leaf; the first z-stack was imaged under bright field (BF) illumination and the second z-stack under fluorescent light (FL). The bright field stack was used to obtain data on the leaf surface, whereas the fluorescent stack was used to obtain venation pattern data.

For each z-stack, the Leica Application Software (LAS) generated three different maps; a confidence map, a depth map and a multi-focus image (Figure 14a-d). These maps allowed the extraction of data for each leaf such as the leaf surface and the vein pattern. The *depth map* displays which focal plane is used to create the multi-focus image at each pixel, it is expressed as a grey scale where white is the highest point in the stack and black the lowest point (Figure 14d). *The confidence map* is an estimate of how accurate the depth map image is at each pixel, as well expressed as a grey level. White shows points of high confidence and black shows points of low confidence where several planes will appear to be in focus. By checking the confidence map, the user decides (qualitatively) if the stack taken is of good quality and could be used for further analysis (Figure 14c). Finally, *the multi-focus image* is an overlay of all the pictures taken in one stack and only keeping the areas in focus (Leica software, Figure 14a-b).

The BF depth map and the FL multi-focus image were used in combination to extract leaf data; the BF depth map was used to get the leaf surface data, and the

multifocus FL image was used to visualize the vasculature, which allowed the extraction of the venation data.

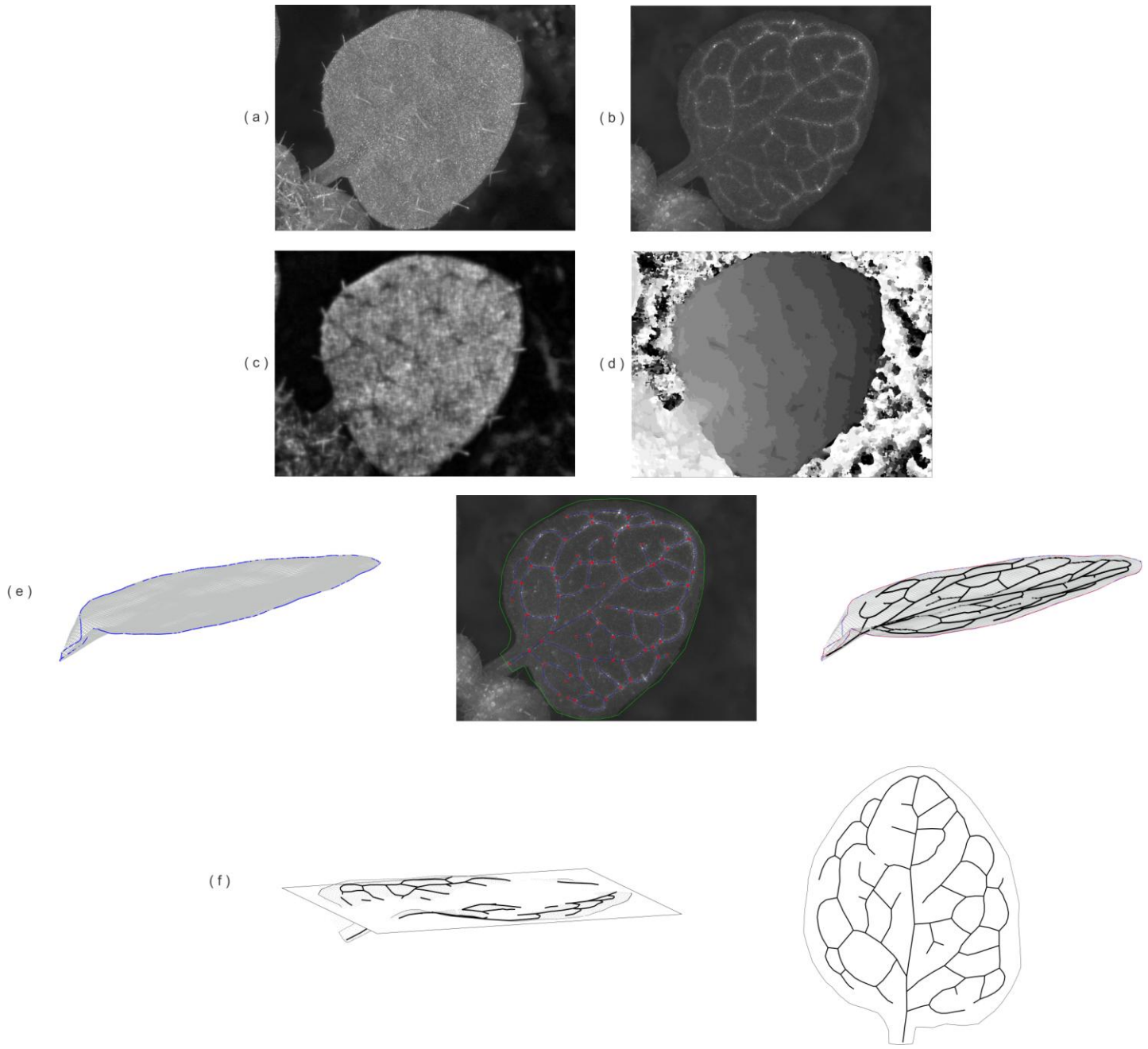

Figure 14: Extraction of leaf parameters. (a) Multi-focus image of a z-stack in bright field. (b) Multi-focus image of a z-stack under fluorescent light. (c) Confidence map of a z-stack in bright field. (d) Depth map of a z-stack in bright field. Depth map and confidence map for FL are generated but are not used (maps not shown). (e) (Left) Extracted 3D leaf surface, the selected outline by the user is shown in blue. (Center) Multi-focus image under FL is used to trace the vasculature displayed in blue, branching points and free vein endings are shown in red and the selected outline in green. (Right) Reconstructed leaf in 3D. (f) (Left) a 2D plane is fitted through the reconstructed 3D leaf. All points will be projected onto the 2D plane. (Right) Reconstructed leaf in 2D (2D projection onto a fitted plane).

2.3. Computational methods

2.3.1. Extraction of 3D leaf surface and vein pattern data:

Custom-made programs were written in Matlab (The Mathworks Inc., http://www.mathworks.com/). I was involved in deciding what was needed from the algorithms to extract the data, but my supervisor A.-G. Rolland-Lagan wrote the software. I was involved in writing one program to estimate growth (see section 2.3.3). The bright field depth map and fluorescent multi-focus image that are generated by LAS were used to extract the 3D leaf surface and the vascular patterns, respectively.

2.3.1.1. Extracting leaf parameters

Using software developed in the lab, the user traced the leaf outline from the BF depth map (Figure 14d). The pixel values in the depth map within the leaf outline gave the height of each point on the leaf surface. The 3D leaf surface could then be extracted (Figure 14e left). For the purpose of this study, only the leaf blade was taken into consideration, the petiole was not used because it was not clearly visible in most cases; it could be either hidden by other leaves, or it was too small to image.

The leaves used had trichomes, which in some cases affected the leaf surface. Trichomes were removed from the leaf surface by digital shaving to get a smoother leaf surface. After tracing the leaf outline, the area of the leaf blade, the coordinates of each point in space and the resolution of the image were recorded and saved as matrices in a Matlab-file.

The venation pattern was digitized in two dimensions (from the FL multifocus image) using a custom-user interface in Matlab (Figure 14b), based on previous work

in the lab (Rolland-Lagan *et al.*, 2009). The FL depth map was not used in the analysis because of the low FL confidence map. Moreover, once the 3D leaf surface information from the BF data was extracted, each point on the FL multifocus image was assigned a height (z-value). Each segment of the venation pattern was traced using a digital pen on a Cintiq21UX screen (Wacom Co, Ltd., Saitama, Japan) and points along those segments were saved as matrices in a Matlab-file (Figure 14e middle, Rolland-Lagan *et al.*, 2009).

2.3.1.2. Combining the leaf surface and the vein pattern

Once the leaf surface and vein pattern were extracted from the maps and saved, the leaf was reconstructed in 3D by projecting the extracted vein pattern onto the reconstructed 3D leaf surface (Figure 14e right).

2.3.1.3. From 3D to 2D

The plants used were wild type, with relatively small leaf blade curvature (Figure 14e left). Therefore, the leaf surface was approximated as a flat surface. A 2D plane was fitted through the 3D points of the leaf (Figure 14f left) and all the points of the leaf were projected onto the flat plane. The resulting 2D leaf was then re-oriented vertically along its proximo-distal axis (Figure 14f right). The flat outline, the topology of the vein pattern (segments, branching points and the free vein endings), the resolution of the pictures and the initial 3D information were saved as matrices. Data saved in Matlab-file would be later used to analyze vein patterning and growth.

2.3.2. Extracting the topology of the venation network

The topology of the vein pattern network was extracted from the segments saved previously, using a published method (Rolland-Lagan *et al.*, 2009). Each segment was identified by two sets of coordinates, a starting point and an ending point. The segments that had the same x, y coordinates were linked together. Branching points or nodes (which are defined by the intersection of more than two segments) and free vein endings were defined and numbered. Loops or reticulations were then identified by taking a starting node (branching point) at random and 'walking' along the network until getting back to a visited node. Different matrices were used to save the branching points, the free veins endings and the loops data (Rolland-Lagan *et al.*, 2009).

Knowing all the parameters of all the leaves and the orientation of the loops and their sizes, successive leaves could be displayed for each sample (Figure 18a).

2.3.3. Analysis of growth

2.3.3.1. Extracting growth information

In this thesis, the vasculature was used to track leaf growth; specifically branching points were used as fixed landmarks or vertices on the leaf to follow growth over time. I developed the programs for tracking growth under the guidance of my supervisor. Growth parameters between two successive time points t and *t+1* were calculated using the methodology outlined below.

Corresponding branching points of successive leaves were identified visually and then matched up (Figure 16a). The two successive branching points were given the same indices. The coordinates of the two matched branching points were saved in two

different matrices; one matrix for the coordinates of the identified branching points at time point t (i.e. before growth), it was called "*mat1*", and the other matrix was for the coordinates of the identified branching points at time point *t+1* (i.e. after growth), and it was called "*mat2*" (Figure 15).

For instance, in the case of three matched branching points:

$$mat1 = \begin{bmatrix} x1 & y1 \\ x2 & y2 \\ x3 & y3 \end{bmatrix} \qquad mat2 = \begin{bmatrix} x'1 & y'1 \\ x'2 & y'2 \\ x'3 & y'3 \end{bmatrix} \qquad \text{(eq. 1)}$$

Using a technique called *Delaunay triangulation* (function *Delaunay* in Matlab), the leaf surface was divided into non-intersecting triangles using the branching points of the leaf at time point *t*; the indices of each of these triangles were saved in a matrix called "*tri1*". Then the same indices were used to create another set of triangles for the leaf at time point *t+1* (Figure 15, Figure 16b). For example, if branching points 1, 2, 3 formed a triangle in the leaf at time point *t* then branching points 1, 2, 3 would form a triangle in the leaf at time point *t+1* (Figure 15).

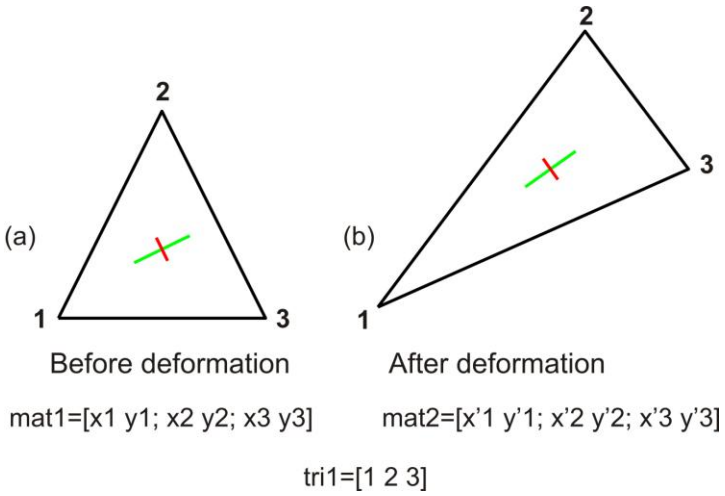

Figure 15: Measurements of deformation of a triangle by Goodall and Green (1986) for three landmarks. (a) "*mat1*" is the matrix for the points before deformation or growth, (b) "*mat2*" has the coordinates of points after deformation or growth, "*tri1*" contains the triangle indices generated by the *Delaunay triangulation*.

Following the above example of three matched branching points,

tri1 = [1 2 3] (eq. 2)

These triangles (Figure 16b) were used to measure growth over time, i.e. how much the first triangle has grown to become the triangle in the second leaf using a method described by Goodall & Green (1986, Figure 16c).

The deformation or growth of triangles was characterized by a *strain cross* (Goodall & Green, 1986) which represented the relative growth of the triangle in two principal directions. It was defined by the length of its two orthogonal arms "p" and "q" and two angles of rotation "θ" and "ψ" (Goodall & Green, 1986) . For all the generated triangles, the strain cross parameters (p, q, θ *and* ψ) were calculated and saved in a matrix (Figure 15, Figure 16c). The strain cross parameters were used to measure the growth of the triangles from one time point to the next.

To calculate the strain crosses parameters, a 2 x 2 matrix called "A" was required such that

$$mat1 \times A = mat2 \qquad \text{(eq. 3)}$$

The coordinates of two points out of the three landmarks of triangle suffice to calculate A. If equation (3) is multiplied by the inverse of the matrix "*mat1*",

$$mat1^{-1} \times mat1 \times A = mat1^{-1} \times mat2 \qquad \text{(eq. 4)}$$

Equation (4) becomes

$A = mat1^{-1} \times mat2$ Such that $A = \begin{pmatrix} a & b \\ c & d \end{pmatrix}$

Goodall and Green defined four intermediate quantities that they called “canonical parameters”. Using the elements of matrix A, theses parameters could be calculated so that,

$t = [(a+b)^2 + (b-c)^2]^{1/2}$ (eq. 5)

$w = [(a-d)^2 + (b+c)^2]^{1/2}$ (eq. 6)

$\tau = \arctan[(b+c)/(a-d)]$ (eq. 7)

$\omega = \arctan[(b-c)/(a+d)]$ (eq. 8)

These canonical parameters have physical meanings where t is the areal expansion, w is the anisotropy , $\tau/2$ is the average angle of inclination of the major axis to the horizontal and ω is the rate of rotation of the triangle.

Finally using the canonical parameters, the strain cross parameters were calculated,

$p = (t+w)/2$ (eq. 9)

$q = (t-w)/2$ (eq.10)

$\theta = (\tau-\omega)/2$ (eq. 11)

$\psi = (\tau+\omega)/2$ (eq. 12)

This method assumed that p and q were always positive and bigger than one and $p>q$. Using these parameters, different variables could be calculated;

$Relative\ growth\ rate = [(p \times q) - 1] \times 100$ (eq. 13)

$anisotropy = p \div q$ (eq. 14)

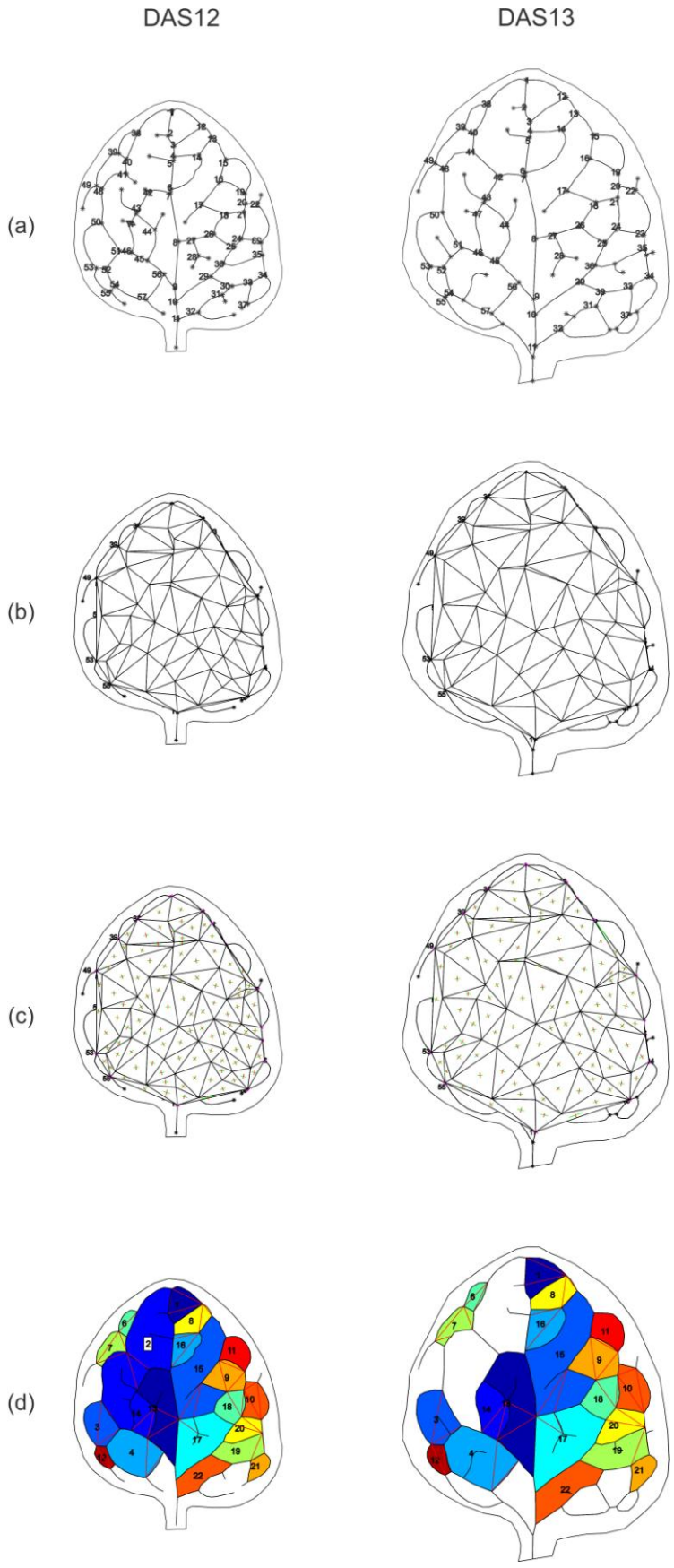

Figure 16: Successive leaves used to track loops and measure growth over time. (a) Leaves at DAS12 –DAS13 with matched up branching points labeled in black and numbered. (b) Leaves with the triangles generated by *Delaunay triangulation*. (c) These triangles will be used to measure growth of leaves by calculating the strain crosses for each set of triangles; *p,* the scaling factor along the main direction of growth is shown in green and *q*, the scaling factor along the direction of growth perpendicular to the main direction of growth is displayed in red. (d) The triangles are also used to track loops over time. The same loop at different time points is given the same identification number; once it splits the new loops are given new identification numbers. The colors used in (d) are only visual aids to help the user make sure that the tracking is done properly.

2.3.4. Analysis of pattern formation

2.3.4.1. Tracking Loops

As individual leaves are followed over time, features of the venation pattern can be tracked, in particular the individual loops. Using the triangles previously generated by the *Delaunay triangulation*, loops were tracked over time (Figure 16b-d) using software developed by A.-G. Rolland-Lagan. The triangles used to track growth were used to identify corresponding loops over time. Each tracked loop was given a unique tracking identification number. Hence, growth of any given loop over time could be calculated. The timing and location of newly forming loops could then be extracted, as well as the timing and position of 'disappearing' loops. A tracked loop could disappear due to loss of fluorescence signal (rare event, see Appendix H), or because the loop subdivided.

2.3.5. Obtaining spatial maps

Leaves from individual plants vary in their venation and growth patterns. We therefore wanted to calculate average spatio-temporal growth and vein patterning data from many samples. To do so, data was combined from many samples, based on a methodology first described in Rolland-Lagan *et al.*, (2009).

For each time point, the average leaf outline was calculated by spreading 70 points at equal distances along each of the outlines of all the samples (Figure 17a), and then all points with the same index were averaged into one point of the average outline (Figure 17a). Then for each time point, all leaf data (triangles and vasculature) were overlaid onto the average leaf outline and then warped to that average outline (Figure 17b). To get the spatial maps, at each (x, y) of the average leaf shape, the

average growth and loops data were calculated from all the data at that position (Figure17b, Rolland-Lagan *et al.*, 2009). Spatial maps were generated for the loops data, tracked loops data and growth data (triangles, Figure17b).

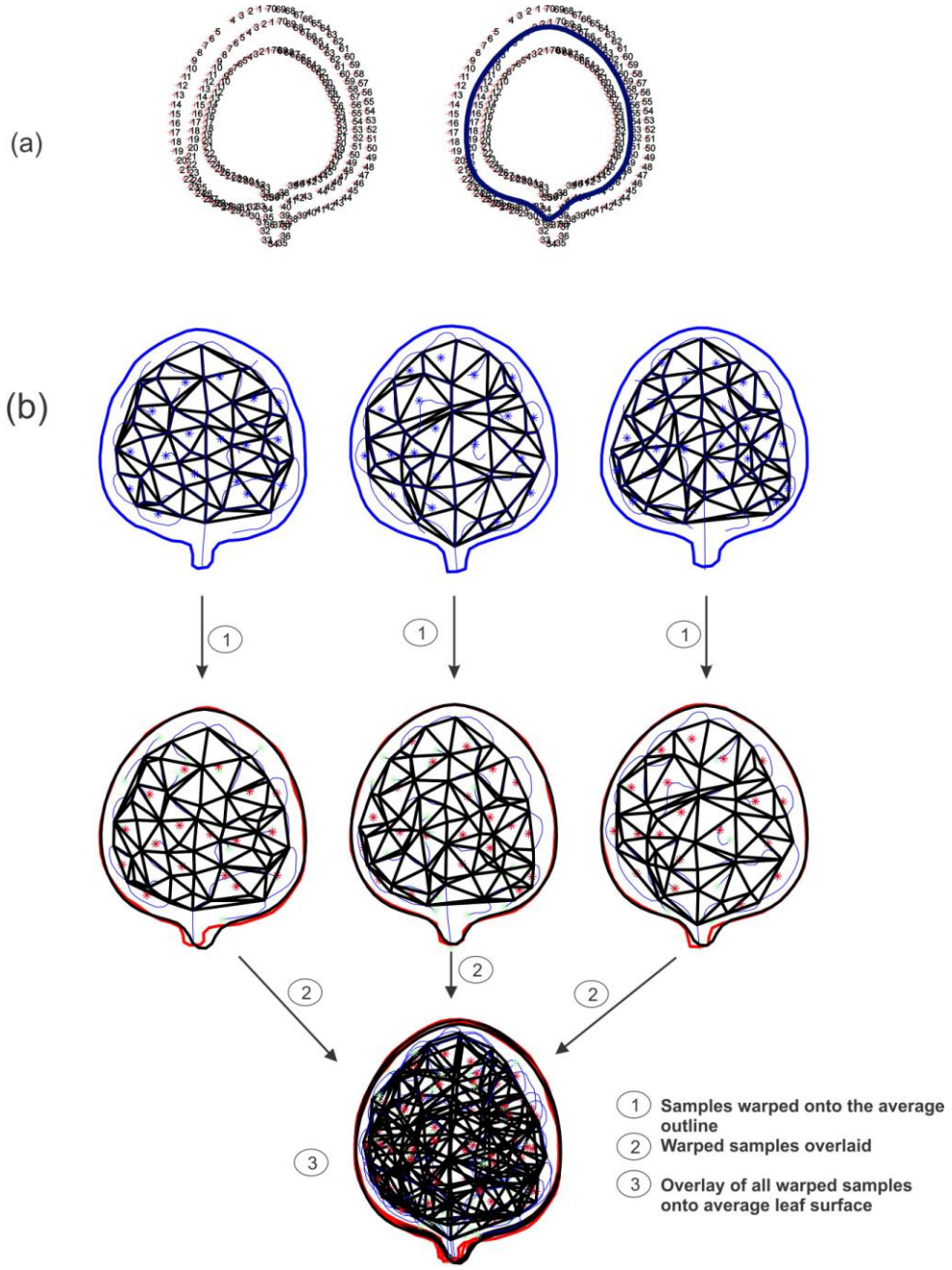

Figure 17: Obtaining average spatial maps. (a) Seventy points spread along the outlines of 3 samples at DAS12, and then the average outline for those three outlines is calculated and displayed in dark blue. (b) Three samples at DAS12 are warped onto the average outline and then all samples are overlaid and then finally average data is calculated at each (x, y). This is done for the triangles and the vein network.

2.3.6. Statistical analysis

Using the Matlab-file saved previously, excel files were generated to recapitulate much of the extracted data such as leaf blade area, branching point, segment and loop number, loop area, segment length, and free vein endings. These files could then be used to perform statistical analysis using statistical analysis software (SPSS Inc., http://www.spss.com/). A non-parametric test for repeated measures was used to test the significance of data such leaf blade area, vein density, loop number and segments number per leaf, branching point and free vein ending density with the day as a factor (for further details, check section 3.2.1, Figure 20).

Chapter 3

3. Results

We developed a new methodology to quantitatively monitor vein patterning and growth of leaf surfaces *in vivo*, where individual leaves were followed in many samples through time-lapse imaging. Vein patterns could then be quantified and tracked through successive time points. This new method will provide a way to investigate the formation of vein patterning as the leaf is growing.

3.1. Analysis for a single sample

3.1.1. Loops data

Once data was extracted from the z-stacks of each of the samples, different parameters were calculated and displayed such as sample number, tracked loops for individual samples over time, relative growth rate, anisotropy, and loop orientation (Figure 18). Using the topology of the venation network, samples over time were displayed, showing the vein pattern changing as the leaf develops (Figure 18a).

Then using the tracked loops data, tracked loops for individual samples over time can be displayed (Figure 18b). The same loop was given the same identification number until it splits into different loops, the resulting 'daughter loops' were then assigned a new identification number. New loops either can form via the splitting of pre-existing loops or by the addition of new segments on the periphery of the leaf (e.g. curved segments, Figure 27). Figure 18c displays how loops are formed. Five types of loops are seen, each type was assigned a color; loops that are newly formed are colored in red, loops that will subdivide in the next time point are in green, loops in yellow are newly formed but will have subdivided in the next time point, loops in light

blue are loops that have "disappeared" because of degradation of the fluorescent marker (rare event, Appendix H) and the segments are not visible anymore, and finally loops where patterning have stopped are in black. For the one sample displayed, most patterning happened between DAS10-13, and slowed down at DAS14. Loops formation stops at DAS15 where the last two loops are formed (red, Figure 18c); from that point on no patterning is seen. For DAS18-19 and DAS19-20, three loops have "disappeared", due to the degradation of the marker from certain veins.

The loop area over time was also calculated (Figure 18d) and displayed as a map. This sample showed smaller loops at early time points and larger loops at later stages. At the same time, loops at the center of the leaf blade were larger than loops at the edge. The gradient seen is a marginal to center increase in loop areas.

Relative growth rate can also be calculated and displayed. At early stages, the leaf grew at fast rates, with some of the loops growing by more than 20% from one time point to the next. Then growth slows down at DAS16 where the rates drop to 14-16%. Growth stops at DAS17 (rate becomes almost zero, Figure 18e).

Finally, loop orientations are estimated and displayed. Loops on different sides of the leaves are oriented in opposite directions. Loops near the center are more elongated and their directions are to the mid vein, while loops at the edge are parallel to the mid vein (Figure 18f).

3.1.2. Triangle data

Spatio-temporal growth patterns of the leaf blade can be calculated through the tracking over time of fixed landmarks on the leaf surface. In this study, the branching points of the venation pattern are used as fixed landmarks on the leaf (Figure 19a).

Those landmarks are triangulated to follow growth (Figure 19b-c, see Chapter 2). Maps can be displayed to show growth from one stage to the next for a set of triangles, i.e. how much each triangle at time point *t* will grow in different directions to become the corresponding triangle in the next time point *t+1*. The strain cross parameters can be used to compute the percentage relative growth rate and the growth anisotropy of each triangle.

Leaves grow until DAS16, then the growth slows down and then stops at DAS17 (Figure 19d). The temporal trend in growth parameters was similar to the data calculated using tracked loops. As for the orientation of growth, no obvious gradient was seen (Figure 19e).

Figure 18: Successive leaves displayed for one sample. (a) One sample displaying the network from DAS10 to DA20. (b) Tracked loops over time; the same loop is given the same color; once a loops splits the new loops are given new colors.(c) Loops can form either by one loop splitting into two loops (loops shown in green) , or formed from new segments (red loops), some loops will be new loops at one time point and will subdivide in the next time point outside of any loops (yellow loops), finally loops in light blue are loops that have "disappeared" because the GFP marker has degraded from the veins. (d) Loop areas are shown with smaller loops shown in blue and larger loops in red. The color code shows the loop areas in mm^2. (e) Relative growth rates are shown with blue showing slow growth rate and red higher growth rates. The relative growth rates are calculated from the loops data. The color code shows the relative growth rates in %. (f) Loops orientations are shown with a color gradient representing the angle of orientation of the loop in degrees. The data shown displays how a loop at the time point t will behave to become the loop at time point t+1.

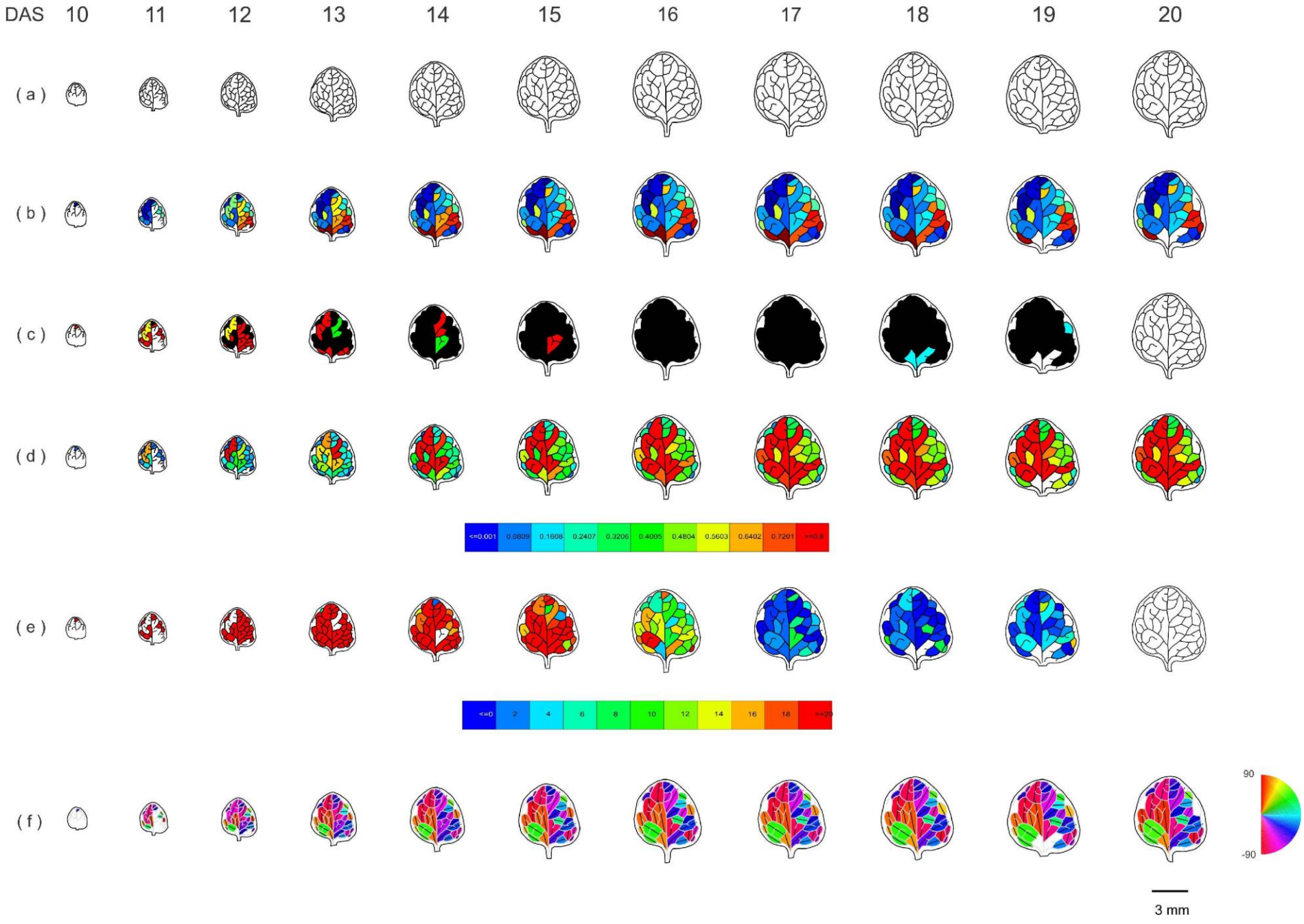
DAS
10
11
12
13
14
15
16
17
18
19
20
(a)
(b)
(c)
(d)
<=0.001
0.0809
0.1608
0.2407
0.3206
0.4005
0.4804
0.5603
0.6402
0.7201
>=0.8
(e)
<=0
2
4
6
8
10
12
14
16
18
(f)
90
-90
3 mm

Figure 19: Successive leaves displayed for one sample. The following maps show growth to the next time point for a set of triangles i.e. how will one triangle at time point t grow to become the same triangle at time point t+1. One sample is displayed over DAS10 to DAS20 showing: (a) the vasculature used to track growth. (b) The triangles generated for each set of leaves by the Delaunay triangulation. (c) The strain crosses calculated for each set of triangles by Goodall and Green (31); p, the scaling factor along the main direction of growth is shown in green and q, scaling factor along the direction of growth perpendicular to the main direction of growth is displayed in red. (d) The Relative growth rates in percent, with blue being the slowest growth rate and red the highest. The color code shows the relative growth rate in %. (e) The anisotropy over time, with blue showing triangles that grew isotropically and red, the triangles that grew anisotropically. The color code shows the degree of anisotropy.

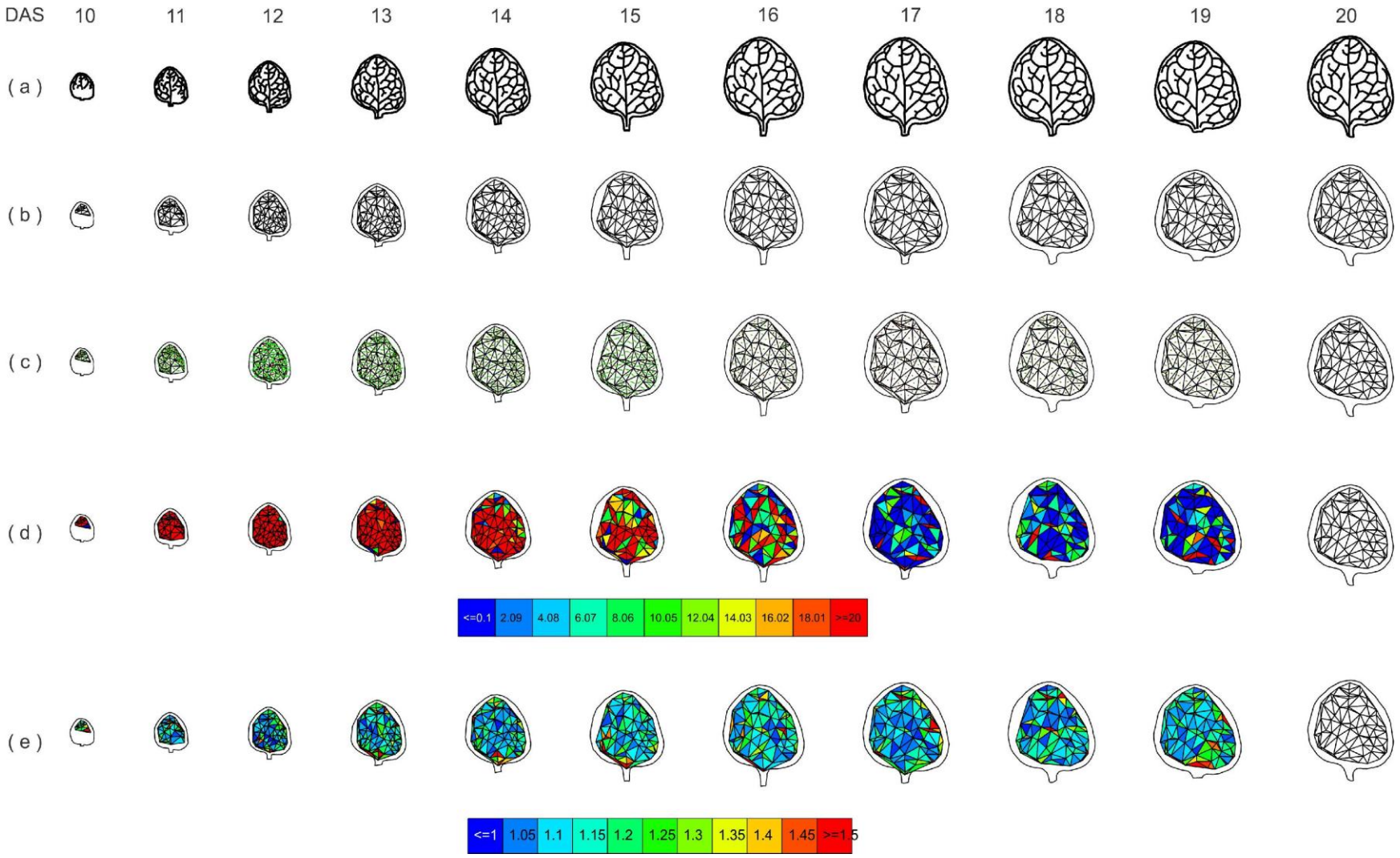
DAS
10
11
12
13
14
15
16
17
18
19
20
(a)
(b)
(c)
(d)
(e)
<=0.1
2.09
4.08
6.07
8.06
10.05
12.04
14.03
16.02
18.01
>=20
<=1
1.05
1.1
1.15
1.2
1.25
1.3
1.35
1.4
1.45
>=1.5

3.2. Analysis for multiple samples

3.2.1. Temporal analysis of vein patterning

The leaves were followed from DAS10 to DAS20; the leaf blades continue to grow until DAS20 (Figure 20a). A non-parametric test for repeated measures (Friedman test) on vein densities with day as a factor shows significant differences between the different days, for DAS10 to DAS20 (χ^2=198.791, df =10, P<0.001) and for DAS17 to DAS20 (χ^2=52.02, df=3, P<0.001). This shows that the leaves used kept on growing during the period analyzed. To determine how the vasculature and growth interact, different variables related to leaf size and to venation pattern, features were calculated and plotted over time.

To assess whether vein patterning and growth are coordinated, vein density can be measured across the leaf. The vein density is the total length of segments divided by the leaf area. The mean vein density increases from DAS10 to DAS12, decreases until DAS19, and became constant after DAS19 and DAS20. Accordingly, a non-parametric test for repeated measures on the mean vein density of pEPS1 with day as a factor shows significant differences in vein densities for DAS13 to DAS20 (χ^2=133.550, df=7, P<0.001) and from DAS17 to DAS20 (χ^2= 42.840, df =3, P<0.001). From DAS19 to DAS20, vein densities were not significantly different between days (χ^2=3.20, df =1, P=0.074, Figure 20b).

By measuring the number of segment number and loops in leaves through development, we can pin point at which stages patterning stops. The mean loop number per leaf is calculated by averaging the number of loops of all samples at each time point. The graph shows an increase in loop number from DAS10 to DAS16. Then

loop number stays constant from DAS16 to DAS20 (Figure 20c). A non-parametric test for repeated measures on the mean loop number of pEPS1 with day as a factor shows significant differences for DAS10 to DAS16 (χ^2=115.116, df=6, P<0.001). For DAS16 to DAS20, the mean loop number was not significantly different between the days (χ^2=2.829, df=4, P=0.587). The mean number of segments per leaf was calculated by averaging the number of segments of all samples at each time point. A Friedman test shows that the segment number was significantly different for DAS10 to DAS15 (χ^2=97.656, df =5, P<0.001). It was not significantly different for DAS15 to DAS20 (χ^2=3.066, df =5, P=0.690). The mean segment number per leaf increases until DAS15 before it becomes constant from DAS15 to DAS20 (Figure 20d).

Free vein ending density has been traditionally used as a measure of vein pattern complexity (Candela *et al.*, 1999). The mean free vein ending density per unit leaf area decreases from DAS10 to DAS19, before it becomes constant from DAS19 to DAS20. A Friedman test shows that the mean free vein ending density per unit leaf area is significantly different between days for DAS10 to DAS19 (χ^2=171.360, df=9, P<0.001). It shows that the mean free vein ending density is not significantly different for DAS19 to DAS20 (χ^2= 1.8, df = 1, P=0.180, Figure 20e). The mean number of branching points per unit leaf area increases from DAS10 to DAS12 and then decreases from DAS13 to DAS20 (χ^2=137.783, df =7, P <0.001, Figure 20f).

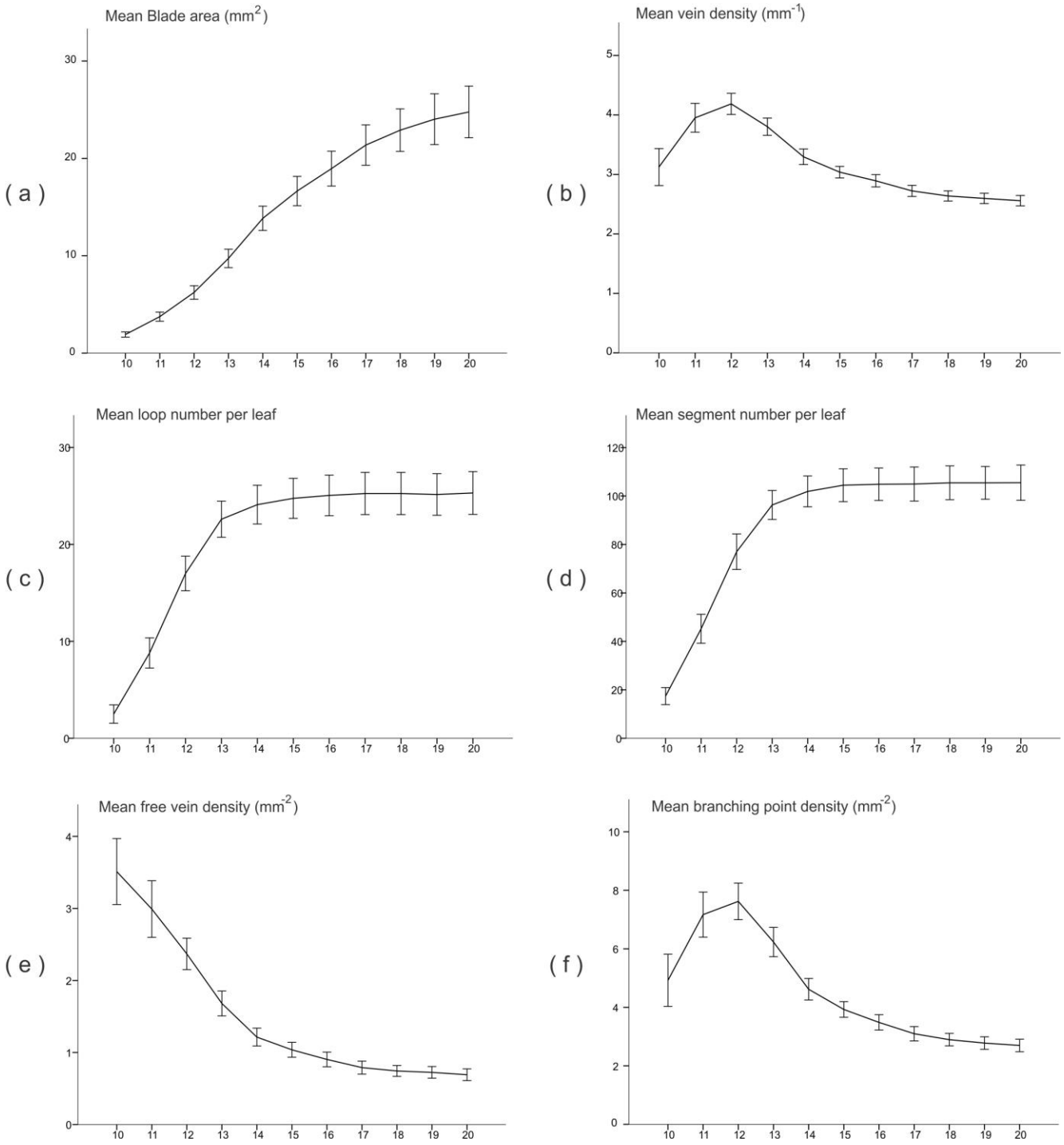

Figure 20: Temporal analysis of leaf vein pattern parameters as a function of time (from DAS10 to DAS20). (a) Mean blade area (mm^2). (b) Mean vein density (mm^{-1}). (c) Mean loop number per leaf. (d) Mean segment number per leaf. (e) Mean free vein density (mm^{-2}). (f) Mean branching point density (mm^{-2}). Error bars indicate the standard error of the mean.

3.2.2. Obtaining spatial maps

In order to assess whether vein patterning parameters vary both in space and in time, we obtain average spatio-temporal data on growth and vein patterning from multiple samples. This involves mapping data from samples at the same developmental stage onto a common average leaf shape (Rolland-Lagan *et al.*, 2009), and calculating average vein pattern parameters. Maps can be generated for loops data (Figure 21), tracked loops data (Figure 22, Figure 23), and growth data obtained from triangulations (Figure 24).

3.2.2.1. Loops maps

Twenty samples were used to generate spatial maps at each time point. Data extracted from loops were used to generate the following spatial maps.

The sample numbers map shows the number of samples used to get the average data at each point on the map i.e. at each (x, y) of the average leaf shape (Figure 21a).

The map of loop areas shows a clear gradient where the loops at the center of the leaf are of bigger size than the loops at the edge; loop areas increase in size from the margins to the center of the leaf (Figure 21b-c). From DAS17 onward, no changes are seen in the loop areas map. The marginal to center increase in loop areas is similar to the gradient observed in. Rolland-Lagan *et al*. (2009). Standard error maps for the loop area are presented in Appendix G (Figure S 15a).

Loop shape is defined as the ratio of the length along the major axis of the loop to the length along the minor axis (width) of the loop. Loop shape maps show more elongated loops along the bottom edge of the leaf and more rounded (isodiametric) loops at the center and tip of the leaf (Figure 21d). Loop shape has a tip to base

gradient. Standard error maps are calculated for loop shape (Appendix G, Figure S15b).

Loop orientation maps show loops oriented in a mirror-image direction to each other relative to the leaf midvein (Figure 21e). Loops closest to the center show an orientation that is parallel to the mid vein. The angles of orientation decrease from the tip to the base of the leaf; with smaller angles at the base of the leaf.

Loop subdivision is given as the total length of the segments cutting through a loop divided by the loop area, if the loop is not subdivided by any segments; it is identified by a zero. Loop subdivision maps show a gradient from margin to center gradient where loops at the edge of the leaf are not subdivided by any segments and loops at the center of the leaf are subdivided the most. This gradient is seen throughout the leaf development (Figure 21f).

Loop mean area and loop shape data on their own do not give information on the size at which loops split. This is because any spatial differences in loop, shape and area may result from spatial variation in growth patterns after loop formation. In order to analyze in more details, loops are tracked individually over the development of the leaves.

Figure 21: Average spatial maps of loops data for multiple samples. (a) Sample number for the different time points. (b) Loop areas over time with a common color code for the whole data set with smaller loops in blue and larger loops in red. The color code shows the loop areas in mm^2. (c) Loop areas with smaller color code for DAS10 to DAS13. The color code shows the loop areas in mm^2. (d) Loop shape with a common color code with areas in blue are loops more rounded and red with more elongated loops. The color code shows the loop shapes. (e) Loops orientations are showed with color wheel showing the different colors corresponding to the angles going from -90^o to 90^o. (f) Loop subdivisions map showing in red areas with the highest loop subdivision and blue loops with no subdivision. The color code shows the loop subdivisions. All leaves are too scale.

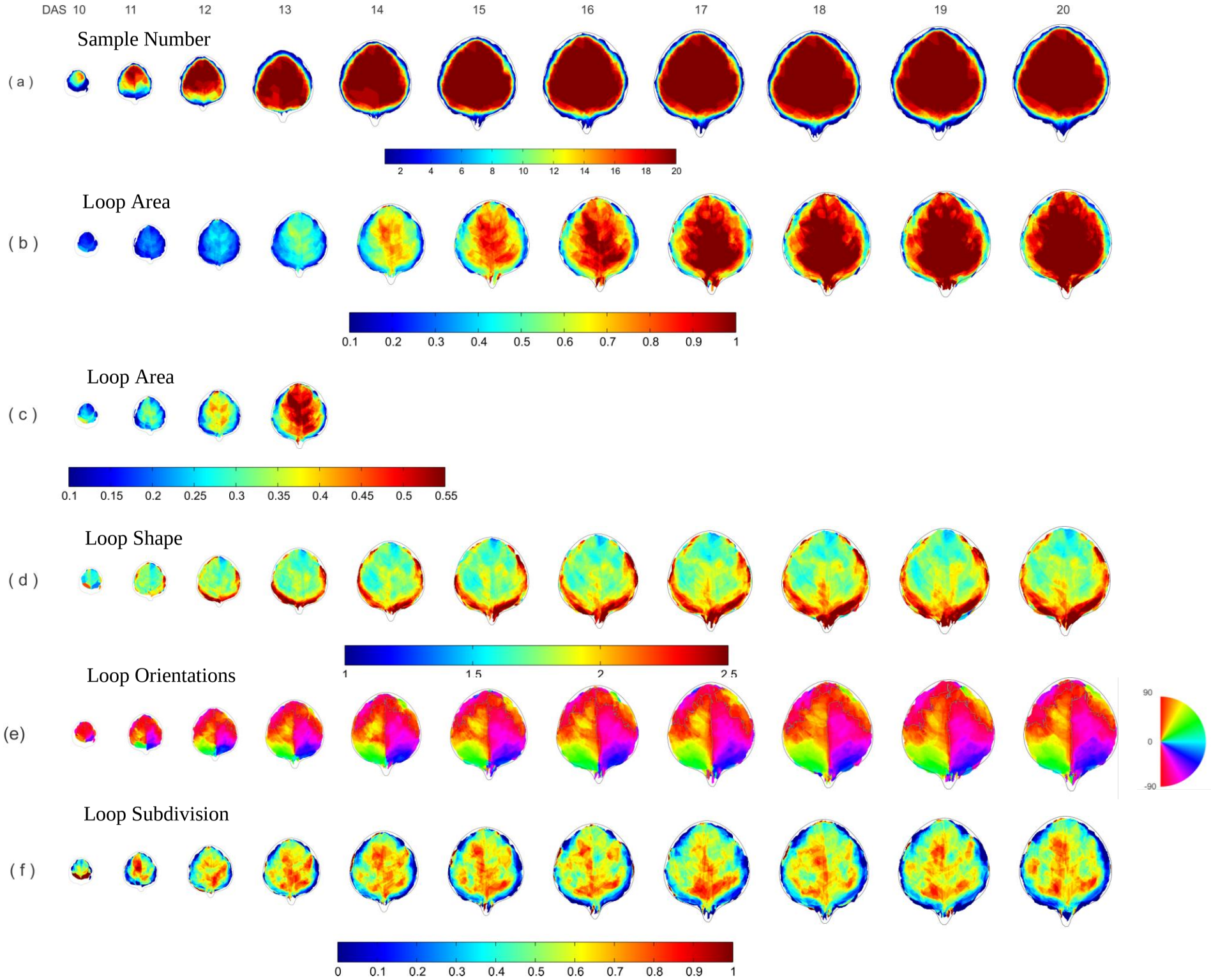
DAS 10
11
12
13
14
15
16
17
18
19
20
Sample Number
(a)
2 4 6 8 10 12 14 16 18 20
Loop Area
(b)
0.1 0.2 0.3 0.4 0.5 0.6 0.7 0.8 0.9 1
Loop Area
(c)
0.1 0.15 0.2 0.25 0.3 0.35 0.4 0.45 0.5 0.55
Loop Shape
(d)
1 1.5 2 2.5
Loop Orientations
(e)
90
0
-90
Loop Subdivision
(f)
0 0.1 0.2 0.3 0.4 0.5 0.6 0.7 0.8 0.9 1

3.2.2.2. Tracking maps

Using the tracked loops data, different maps can be generated to study how patterning is occurring; where the loops are added, which loops are subdividing and how these loops are growing knowing that the growth of the leaf is not uniform throughout the leaf surface, and knowing that patterning is different between the different parts of the leaf (Figure 22). Maps show tracking to the next time point; in other words, each spatial map at time point t shows how the leaf changes between time point t and time point t+1. Here, only maps for time points DAS10 to DAS16 are displayed. Little patterning occurs beyond DAS17; therefore, maps for DAS17 to DAS19 are only shown in Appendix E.

The map of sample numbers in Figure 21a shows the number of samples used to calculate map averages at each point on the average leaf surface. Figure 22a shows the ratio of newly formed loops across the leaf; at each point on the leaf surface, the ratio of newly formed loops is calculated as the number of loops that are present at the current time point but were not present at the previous time point, divided by the total number of loop samples. Most of the loops are added from DAS10 to DAS13. The addition of loops occurs mostly at the base of the leaf. At DAS14, some loops are still being added at the base of the leaf but patterning has stopped in the rest the leaf. From DAS15 onward vein patterning has stopped.

In order to visualize areas of the leaf where enlarging loops subdivide into new loops, we calculated for each time point, at each point on the average leaf surface, the number of loops that will split in the next time point divided by the total number of loops. This gives us a ratio of 'loops about to split'. The map of loops about to split

(Figure 22b) shows a marginal to center gradient, where loops in the center of the leaf subdivide more than the loops at the edge. The loops splitting slow down at DAS12 and stop at DAS14. A few loops split at DAS15 and DAS16; which are likely due to variations in developmental stages between the different samples.

In order to identify potential areas of the leaf where patterning occurs faster than in other areas, we identify, at any given time point, a 'fast forming loop' as a loop which was not present at the previous time point (so it is a newly formed loop), and will not be present at the next time point (so it is a 'loop about to split'). In other words, a fast forming loop is a loop that is both newly formed and about to split. For each time point, we calculate the ratio of fast forming loops to the total number of loops present at each point of the leaf surface. The corresponding map of fast forming loops is shown in Figure 22c. This map shows that the loops at the center and base of the leaf subdivide and disappear at a faster rate than the loops at the edge of the leaf. The formation of such loops slows down at DAS13, and ends at DAS14 with a few exceptions.

Growth rates were estimated using the tracked loops, in the same way as we used triangles. The last map displays the relative growth rates of loops in %. The relative growth rate is the growth rate per unit of quantity over a specified period of time (Richards, 1943) . Relative growth rate is calculated for each leaf from the tracked loops data. Average relative growth rate across samples can then be displayed (Figure 22d-e). The results show a proximo-distal gradient in growth rates across the leaf, where the tip is growing at slower rates than the base of the leaf. Growth rates decrease over time, and growth in the tip of the leaf stops at DAS16 while the base

continues to grow. Growth of leaves slows down at DAS17. The average growth rates and the maximum growth rates for each time point are in Table 1. The average relative growth rate decreases from 65% at DAS10 to 3.11% at DAS19. The average relative growth rate slows down and drops at DAS14 to almost the third of the relative growth rate at DAS10. Standard errors maps for relative growth rate are calculated (Appendix G, Figure S15d).

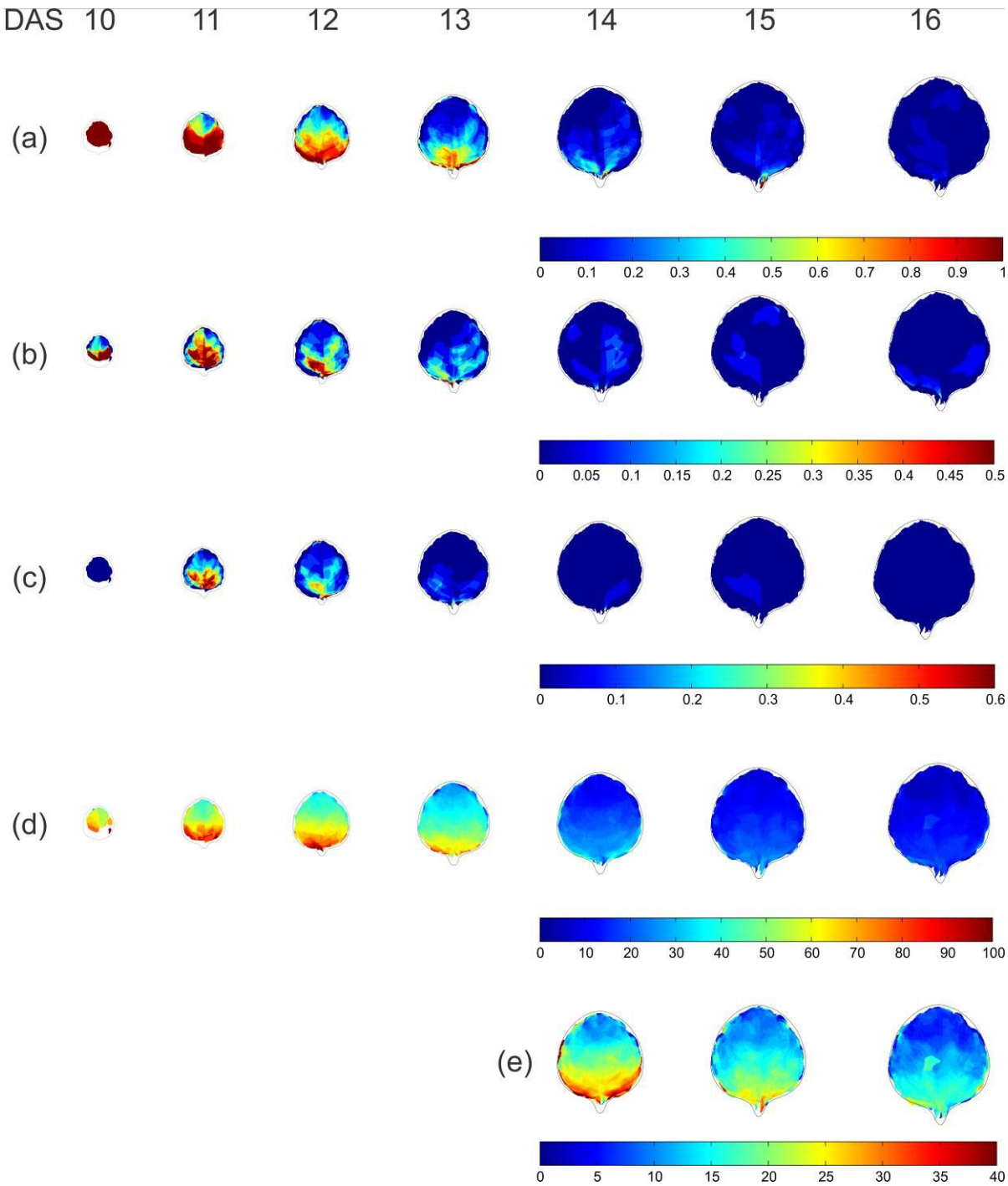

Figure 22: Spatial maps for multiples samples for the tracked loops data. (a) Maps of newly formed loops (the color code shows the percentage of newly formed loops), (b) Maps displaying the percentage of loops that will split into two or more smaller loops (the color code shows the loops that will split). (c) Some loops will be newly formed at time point t but will subdivide at time point t+1. These loops are called fast forming loops. (a-c) The color code shows the percentage of newly formed loops (a), the percentage of loops about to split (b) or the percentage of fast forming loops (c) to the total number of loops at each point on the surface. (d) Spatial maps of average relative growth rates using the loops data. The color code shows the relative growth rates in percent. (e) DAS14-DAS16 displayed with a different color scale for relative growth rates. The color code shows the relative growth rates in %.

3.2.2.3. Tracking loops areas

As mentioned in the introduction, we postulated that loops will split at an optimal size to maintain proper irrigation of the tissue enclosed by the vein segments. For each time point, a map of average areas of loops about to split was generated, as well as an associated map showing the number of samples (i.e. number of loops about to split) available at each point on the leaf surface (Figure 23). Only DAS10 to DAS16 is shown because from DAS17 to DAS 20 patterning has stopped completely. The maps of areas of loops about to split show a tip to base gradient at early stages of development, loops at the tip split at larger size than the loops at the base. Therefore, loops split when reaching a smaller size in areas of fast growth. From DAS14 to DAS 15, only a few loops subdivide. After this stage, patterning stops except for three loops that are still subdividing at DAS15 and DAS16 (Figure 23a). This might be due to variations in developmental stages between the samples used (Figure 23b-c). Alternatively, patterning might still occur in rare cases (see Chapter 4). Standard error map for areas of loops about to split is shown in Appendix G (Figure S15c).

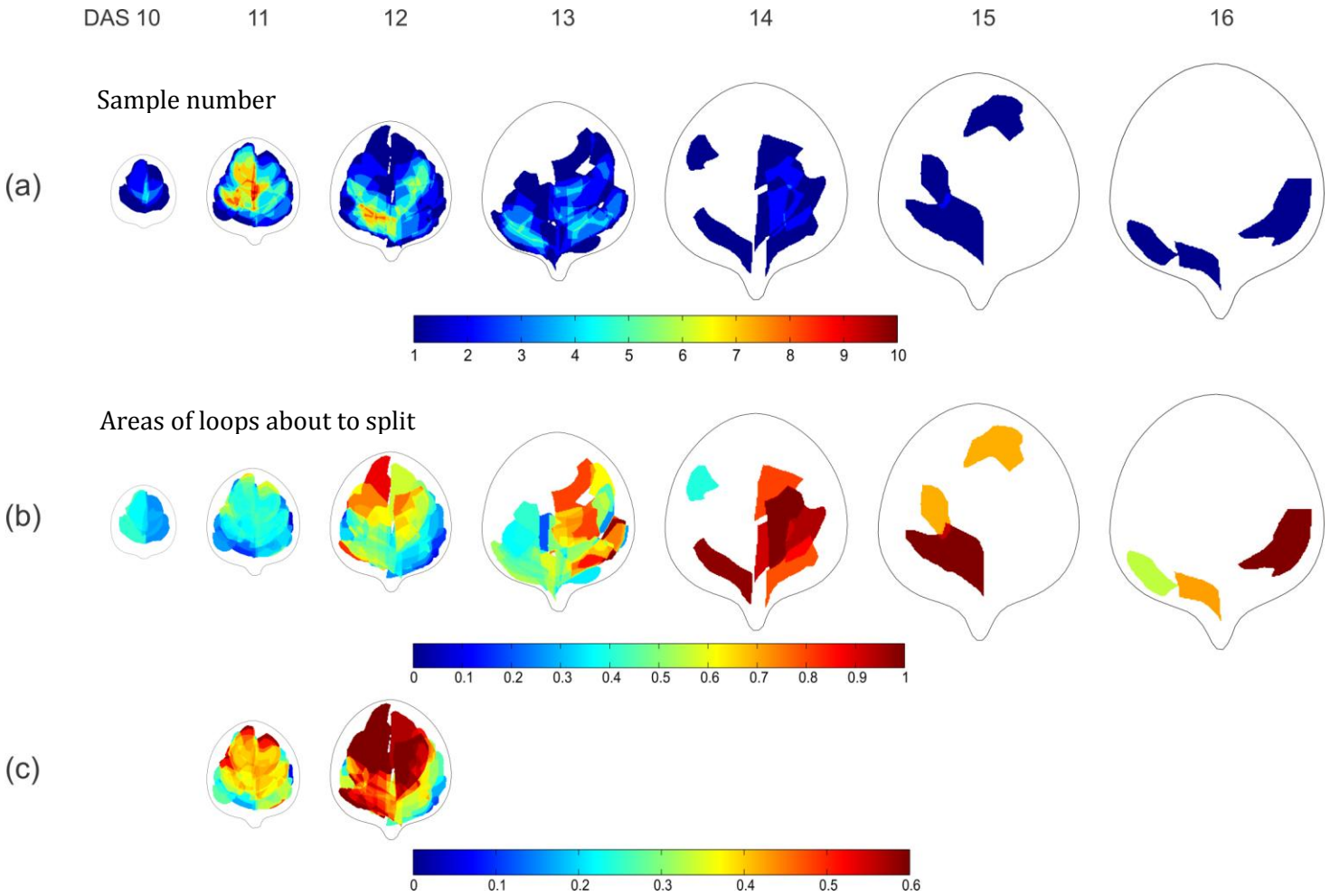

Figure 23: Loops subdivide at different sizes in different parts of the leaf. (a) Sample number for the maps of areas of loops that will split. (b) Spatial maps of areas of loops that will split. The color code shows the areas of loops about to split (mm^2). (c) Spatial maps of areas of loops that will split for DAS11-DAS12 showed with a different color scale. The color code shows the areas of loops about to split in mm2. Most splitting is happening at DAS11 and DAS12

3.2.2.4. Growth maps

Branching points of the venation patterns are triangulated to obtain detailed growth parameters across the leaf, not only in terms of growth rates, but also in terms of strain rates along the principal directions of growth (see section 2.3.3). Having calculated strain cross parameters for individual triangles from individual leaves tracked over time, we can calculate, for each time point, the average strain cross parameters from multiple samples at each point on the average leaf surface. The number of samples used for the growth maps is shown in Figure 24a.

The strain cross parameter *p* indicates the scaling factor along the main direction of growth between two time points. The average spatial map of *p* shows a tip to base increase in the growth along the proximo-distal axis of the leaf, where triangles at the base of the leaf grow more than triangles at the tip of the leaf (Appendix F- Figure S 13 b-c). From DAS14 onward, *p* is very close to one; which means the growth along the main direction has slowed down and in some areas, it has stopped.

The strain cross parameter *q* indicates the scaling factor along the direction perpendicular to the main direction of growth between two time points. The average spatial map of *q*, like the map of *p*, shows a tip to base increase in growth rates; *q* is smaller at the tip of the leaf (Appendix F- Figure S 13d-e). The growth in the direction of *q* slows down at DAS15 where *q* is close to one (Appendix F- Figure S 13d-e).

The anisotropy is the ratio of *p* divided by *q*. The anisotropy indicates to what extent growth occurs preferentially along a main direction, while the individual sample analyzed in a previous section (see section 3.1.2) does not show a clear spatial gradient in anisotropy, the spatial maps of anisotropy for all samples show a spatial

patterns which seems to indicate that growth is more anisotropic along the edges of the leaf blade (Figure 24b).

The average spatial map of the relative growth rate in percentage shows a tip to base gradient, with faster growth at the base of the leaf, which matches the observed gradients in *p* and *q* (Appendix F- Figure S 13b-e). This gradient is similar to the % relative growth rate maps generated for the tracked loops; where the tip is growing at slower rates than the base of the leaf (Figure 22c-d and Figure 24d-e). The growth rates slow down at DAS14 and drop below 40% (Figure 24c-d). Finally, the average map of the growth orientation (θ) of triangles is shown in Figure 24i. We expected that the triangle orientation maps would have a spatial gradient probably similar to the one seen in the orientation maps generated for the loops data (Figure 23e), but this map has no clear gradient or recognizable pattern; different parts of the leaves are growing in different directions. Standard error maps for *p*, *q*, relative growth rate and the growth anisotropy are calculated and displayed (Appendix G, Figure S 14).

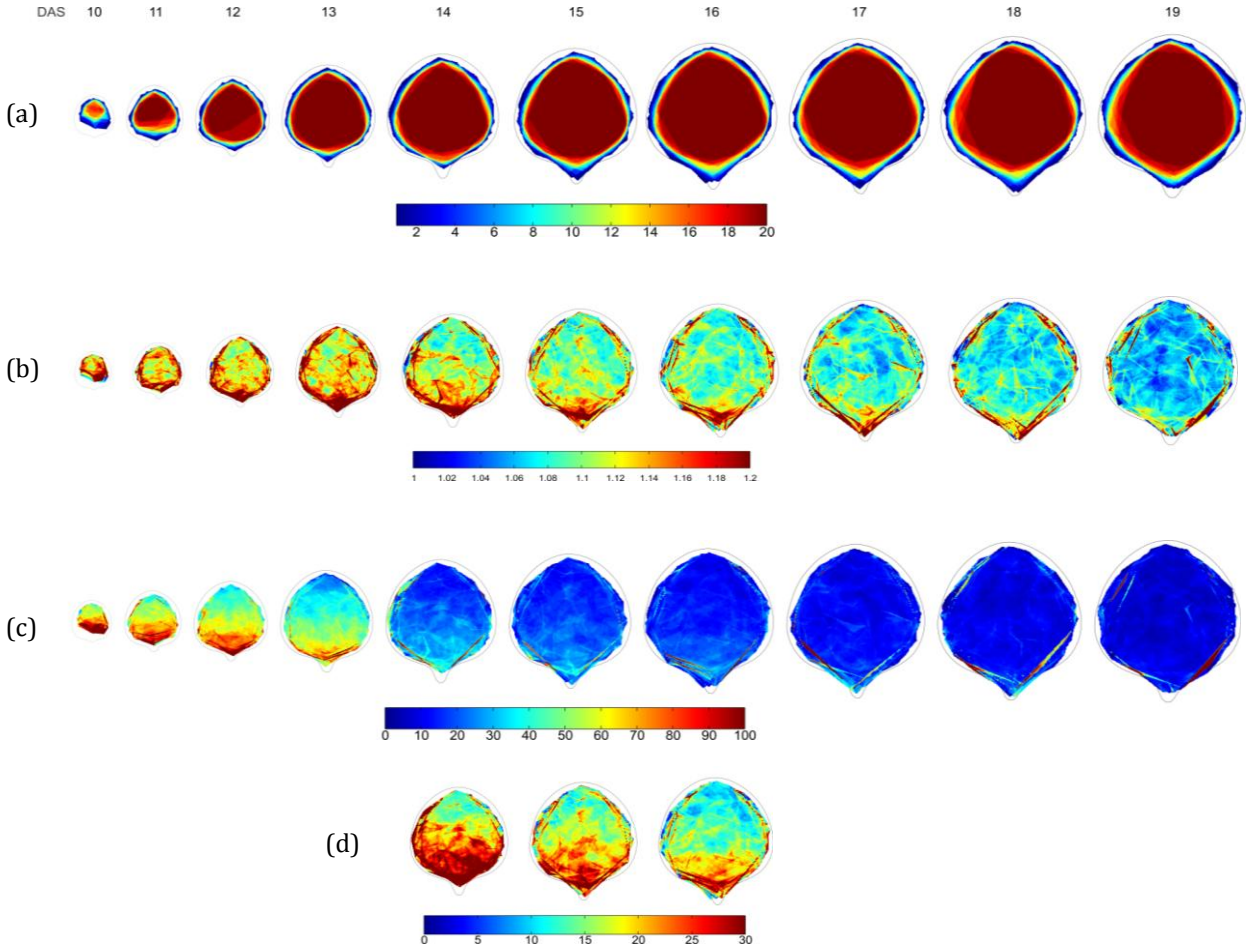

Figure 24: Growth spatial maps for pEPS1. (a) Triangle number maps. (b) Spatial maps of anisotropy. (c-d) Growth maps of relative growth rates calculated from the triangles from one time point to the next.

Chapter 4

4. Discussion

We developed a microscopic and computational methodology to track leaf vein formation over time in intact plants (*in vivo* imaging). This methodological development involved developing 1) a microscopic protocol to repetitively image veins in young leaves over successive time points as the leaves grew and 2) a computational method to extract quantitative information about leaf vein patterns, which allowed us to track features of vein patterns and growth over time. This methodology was used as a basis to investigate mechanisms of vascular patterning in growing leaves. Although we did not have time to apply the methodology to vascular pattern mutants, the quantitative data obtained from wild type analyses provided some new insights into vein patterning.

4.1. Need for in vivo quantitative analyses of vein pattern formation

Vein pattern formation in plant leaves has long intrigued biologists, mathematicians and physicists alike. Vein patterns form an intricate network within the leaf, and vein network architectures have been used to classify plant species (Hickey, 1973). However, upon close inspection no two leaves have the exact same vascular pattern. A reason for this variability may be due to the close relationship between vein pattern formation and growth (Fujita & Mochizuki, 2006a), and the sensitivity of growth to local environmental conditions and varies between samples (Granier & Tardieu, 2009; Poire *et al.*, 2010).

Some physicists have proposed that mechanic forces as the tissue grows generate stresses that drive vein formation (Couder *et al.*, 2002), while molecular biologists focus on the role of genes and proteins involved in auxin transport (Berleth, 2000; Mattsson *et al.*, 2003; Sachs, 1981; Vieten *et al.*, 2007). Indeed, numerous genes have been shown to affect vascular pattern phenotypes (Dengler & Kang, 2001; Krogan & Berleth, 2007; Scarpella & Meijer, 2004), and the expression pattern of PIN proteins, which are involved in polar auxin transport, has been shown to prefigure vein formation (Scarpella *et al.*, 2006). However, the mechanism by which veins arise in a growing tissue remains unknown.

Several models have been proposed to account for vascular formation (Corson *et al.*, 2009; Rolland-Lagan & Prusinkiewicz, 2005; Sachs, 1981). Those models can in principle account for the formation of vascular strands, but up until now, models could not be tested against experimental data, due to the lack of quantitative data on vein patterning.

In this project, we therefore set out to develop a methodology that would allow quantitative evaluation of vein pattern formation as leaves grow, which could be used to provide new insights into the vein pattern formation mechanisms, and a link between molecular experimental work and theoretical models of leaf vein patterning.

4.2. Advantage of quantifying vein patterns in vivo using a fluorescence macroscope

Vein patterns in developing leaves have traditionally been visualized using destructive methods; leaves can be cleared so that xylem patterns can be visualized in

dark field microscopy. In this context, our lab recently developed a method to quantify vein patterns in cleared leaves (Rolland-Lagan *et al.*, 2009), which can be used to classify vein pattern mutants (*in prep*). However, destructive imaging means that quantitative data on venation patterns from cleared leaves cannot be related to growth.

Recently, transgenic lines with fluorescent vasculature at various stages of vascular differentiation have been constructed (Haseloff, 1999; Imlau *et al.*, 1999; Sawchuk *et al.*, 2007; Scarpella *et al.*, 2004). After choosing the most suitable fluorescent line (see Appendix B), we could therefore set up a microscopy methodology to image leaf surfaces in 3D along with associated fluorescent vasculature. An advantage of the method is that we can expose the plant to microscopy light for relatively short times, which does not affect normal leaf growth (Lauren Remmler, unpublished data). The plants can be grown in soil and just placed under a motorized microscope for imaging. This contrasts with previous methods developed to track plant organ growth, where plants had to be placed upside down in liquid medium for imaging under a confocal microscope (Reddy *et al.*, 2004), or had to be covered with casting material to make replica of the organ to be imaged under a scanning electron microscope (Dumais & Kwiatkowska, 2002). The microscopy setup is relatively inexpensive (a motorized fluorescence macroscope), and image acquisition is fast.

By imaging each leaf twice (once in bright field, once in fluorescence) at different focal planes, we could extract not only the venation pattern but also the leaf surface in 3D.

4.3. Quantitative vein pattern data – a comparison between destructive and live imaging method

Our lab recently developed a method to quantify vein patterns in 2D (Rolland-Lagan *et al.*, 2009), based on images of cleared leaves. We will refer to the 2D method in the following as destructive method and our new method as live imaging method.

The data reported in Rolland-Lagan *et al*. (2009) are based on the analysis of Arabidopsis wild type ecotype Columbia (Col0), whereas in this study the transgenic line pEPS1 (of ecotype C24) is used. Both methods gave the same results concerning vein patterning, and any difference may be ascribed to differences between ecotypes. However, the general trends in vascular pattern parameters appeared much more consistent in the live imaging method compared with the destructive method, with much smoother curves and less overall variation between samples.

Col0 grew until DAS14 and then growth slowed down; while C24 (pEPS1) grew until DAS19. The mean loop number and mean segment number for both lines showed similar trends but with a slight temporal shift. Patterning stopped at DAS12 for Col0 (Rolland-Lagan *et al.*, 2009), while patterning stopped at DAS16 for C24. For both methods, the development of the first rosette leaf is divided into 3 different phases. The live imaging method has the same 3 phases as the destructive method (Rolland-Lagan *et al.*, 2009) but with a temporal shift. For C24, phase 1 goes from DAS10 to DAS12 where vein patterning and growth are occurring at the same time, vein density is increasing and the leaf blade is growing, at the same time loop, number and segment number are increasing. Phase 2 goes from DAS13 to DAS15 where the vein density is decreasing because patterning has stopped in most parts of the leaf but some

segments are still being added; a very small increase in segment number and loops number is noticed. Phase 3 is from DAS15 to DAS20, the loop and segment numbers are constant and the leaf is still growing, which explains why the vein density is decreasing.

In terms of spatial analyses, both lines showed a marginal to center increase in loop areas (i.e. loops are larger at the center of the leaf and smaller at the edge). In addition, in both cases, loops that have started subdividing have a larger loop area than loops that have not. This is consistent with the idea that loops enlarge, and then subdivide after reaching a given size. In the destructive method, it was postulated that the observed spatial gradient in loop areas could reflect a spatial gradient in the level of factors that affect patterning. This statement will be discussed below in light of the live imaging data (see section 4.6). Loops shapes showed a distal to proximal gradient in both methods; more isodiametric loop shapes at the distal end of the leaf and more elongated loops of the proximal end. It was previously postulated that this gradient in loop shapes is due to the growth patterns of the leaf (Rolland-Lagan *et al.*, 2009). However, in Rolland-Lagan *et al.* (2009), no growth data was available to test this idea. An advantage of the live imaging method is that quantitative data for both vein patterning and growth is available, so we can compare vein patterning and growth maps. The relation between vein patterning and growth will be discussed in a later section (see section 4.5).

Even though, both methods showed similar trends in most parts, the advantage of the new method is that we can study patterning as the veins are arising in time, and simultaneously growth of the leaf blade can be quantified. This new method provides a

way to track loops over time, and determine at what size a loop subdivide, how the leaf is growing in different parts, and how growth and vein patterning interact.

4.4. Using vein patterns to monitor growth – comparison with results from other growth estimation methods

As we tracked venation patterns over time in individual leaves, leaf growth patterns were estimated in two ways: 1) Using the branching points of the venation pattern as fixed landmarks, we triangulated the branching points and quantified the growth of leaves by calculating the growth of the resulting triangles, using a method proposed by Goodall & Green (1986). This method allowed us to characterize growth patterns in terms of the growth along the principal directions of growth, overall growth rates, and growth orientation. 2) Using loops tracked over time, we measured relative growth rates of leaves in percentage over time. Spatial maps of growth rates based on both methods showed similar results, with slight differences. In both cases, spatial maps revealed that growth slowed down over time, and that growth decreased from the tip to the base of the leaf. More precisely, the leaf grew more at the lower edge of the leaf than the central and basal part of the leaf. Growth in the tip of the leaf stopped at around DAS14, and the average relative growth rate dropped below 7.55% per day at DAS17 to reach a 3.11% per day at DAS19 (Table 1). The first method (based on triangles) allowed us to calculate growth rates along the principal directions of growth, and the ratio of growth along the principal directions of growth (anisotropy). Anisotropy is higher along the bottom edge of the leaf (Figure 24b), which matches with the elongated shape of the loops in that area (Figure 21d).

Growth along *p* and *q* might in principle be controlled by different factors, i.e. we could in principle see different spatial gradients for growth along each principal direction. However, this is not the case; both *p* and *q* maps have similar spatial trends in increasing from tip to base (Appendix F).

As mentioned in the introduction, leaf growth has been analyzed and quantified by other studies (Avery, 1933; Wiese *et al.*, 2007). In all the stated studies on leaf growth, growth has a tip to base gradient, where the leaf tip is growing at slower rates than the leaf base, which conforms to our data. Wiese *et al. (*2007) estimated growth patterns in Arabidopsis leaves (but not the first rosette leaf). The authors measured the relative growth rate of two ecotypes of Arabidopsis Col0 and Ler (Wiese *et al*., 2007). A basipetal gradient of growth for both ecotypes was seen for both ecotypes; the leaf base was growing faster than the leaf tip. The peak growth relative growth rate was >5% h^{-1}or 120% d^{-1}. The average relative growth rate was 1% h^{-1} or 24% d^{-1}. This value compares to the average relative growth rate of DAS14 in our data (Table 1).

Donnelly *et al*. (1999) studied cell divisions patterns instead of growth per se. Their results qualitatively resemble ours. Specifically, at DAS10, more growth is observed at the lower half of the leaf that is similar to the pattern of GUS expression at day 8. At DAS12, growth has slowed down except for the area closest to the petiole. Finally, at DAS17, growth had slowed down, which corresponds to the reduction of GUS expression at day 16 where there was only cell division in the petiole. Cell division and cell expansion have stopped in the distal part of the leaf first which cause the formation of a gradient in growth from tip to base (Donnelly *et al*., 1999).

Wolf *et al.* (1986) used vein branching points to calculate the relative growth rate of *Vitis vinefera* leaves during expansion (i.e. after the vein pattern was formed). The leaves were originally 2 cm long. Each leaf was subdivided into 120 triangles with different shapes and orientations. The authors calculated the relative growth rates for 100 plants, and each area was subdivided into 5 different growth categories <20 % d^{-1}, 20-39% d^{-1}, 40-59% d^{-1} and >60% d^{-1}. These leaves showed a tip to base increase in growth rates, as well. This paper (Wolf *et al.*, 1986) displays the growth of two leaves where slower growth rates at the tip is seen (20-39% d^{-1}), intermediate growth in the center (40-59% d^{-1}) and the highest growth rates in the base of the leaves (>60% d^{-1}, Wolf *et al.*, 1986), which corresponds to the growth gradient seen in our leaves.

4.5. Relation between growth and shape

It has been recognized that shape changes during growth results from spatio-temporal variations in growth patterns (Coen *et al.*, 2004; Thompson, 1942). Interestingly, in our case the shape of the leaf blade remains similar over time; even though growth patterns are heterogeneous. Therefore, spatial heterogeneities in growth patterns do not necessarily trigger changes in shape. Instead, there must be a very high control of growth patterns to maintain the leaf shape as it grows.

4.6. *Mechanism underlying loop formation and subdivision*

Most loops are added at the base of the leaf as it grows. Loops arise in two ways (Figure 22, Figure 27), they are either formed by new segments (*de novo*) at the edge of the leaf (Figure27c), or they arise as a result of older loops subdivision (Figure 27a-b).

4.6.1. *Control of loop subdivision: Proposed link between vein patterning and growth*

Any growing tissue, once reaching a certain size, needs a transport system to move nutrients over large distances (Bonner, 2006). Therefore, we expect that as a loop enlarges, the growing area of tissue enclosed by veins will reach a size at which point the irrigation system will become insufficient. New segments (veins) will then form to maintain proper growth of the area and proper transport from and to the cells in the leaf (Figure 6). In the introduction, we proposed the hypothesis that there may be an optimal size at which a loop subdivides, which could be dependent on the number of cells within that area, the area itself, or the level of a vein forming factor.

If loop subdivision only depends on loop area, we would expect all loops to subdivide at a similar size. With previous studies, this could not be proven because leaves keep growing after the arrest of vein patterning so tracking loops over time will allow us to check when loops do split. In other words, loops could have split at the same size but because growth carries on, the size of loops at the time of imaging would not reflect sizes at time of splitting. Moreover heterogeneities in growth would lead to heterogeneities in loop sizes, even if loops have split at the same size. Using the live imaging method, loops were tracked over time and loop areas and subdivision levels were calculated. We therefore tracked individual leaves over time to follow when and where vein patterning occurs, which loops subdivide and at what size they subdivide in different parts of the leaf for different time points. Contrarily to what was expected, different loops split at different sizes depending on the part of the leaf they are in (Figure 23). Loops split at smaller sizes in the basal parts of the leaf than in the distal

parts. Therefore, loop area does not directly control the size at which a loop will subdivide. Instead, we propose that there is a link between leaf growth patterns and the control of loop splitting. Figure 25 shows that as the leaf is growing, the initial parts of the base of the leaf are moved further upwards, so that loops that were initially at the base of the leaf become in more distal positions (areas 1 and 2 in Figure 25a) while other areas start to growing more (areas 3 and 4 in Figure 25a). This is due to the spatial gradient in growth rates, with more growth at the leaf base (Figure 25b). At the same time loops about to split display a tip to base gradient where loops at the base are smaller than loops at the tip of the leaf (Figure 25c). Therefore, we propose that as loops find themselves in areas of lower growth, the loops will split later, hence at larger sizes, while loops that are in areas with higher growth rates will split sooner, hence at smaller sizes. In that scenario, loop splitting depends on the growth rate of the tissue where the loop is (Figure 25d). This would be consistent with the idea that fast growing tissues would synthesize more of the substance that causes vein formation (maybe auxin), or could relate to the role of physical forces, which may be stronger in fast growing areas.

Auxin is a candidate for the signal allowing loops to split. Some studies proposed a hypothesis to explain how auxin controls the differentiation of veins within leaves (Sachs, 1981) based on the shifting of auxin maxima. According to this hypothesis, a first auxin maximum initially appears at the tip of the fast forming primordium; this maximum blocks the production of auxin in any other part of leaf. The next maxima are seen in lower half of the leaf and the blade. As the auxin maxima shift between the different parts of the leaf, they will cause the differentiation of vasculature (Aloni,

2001). Other studies showed the formation of auxin maxima in the margin of the leaves but exclude the gradual shift of auxin maxima to the blade area (Scarpella *et al.*, 2006; Wenzel *et al.*, 2007).

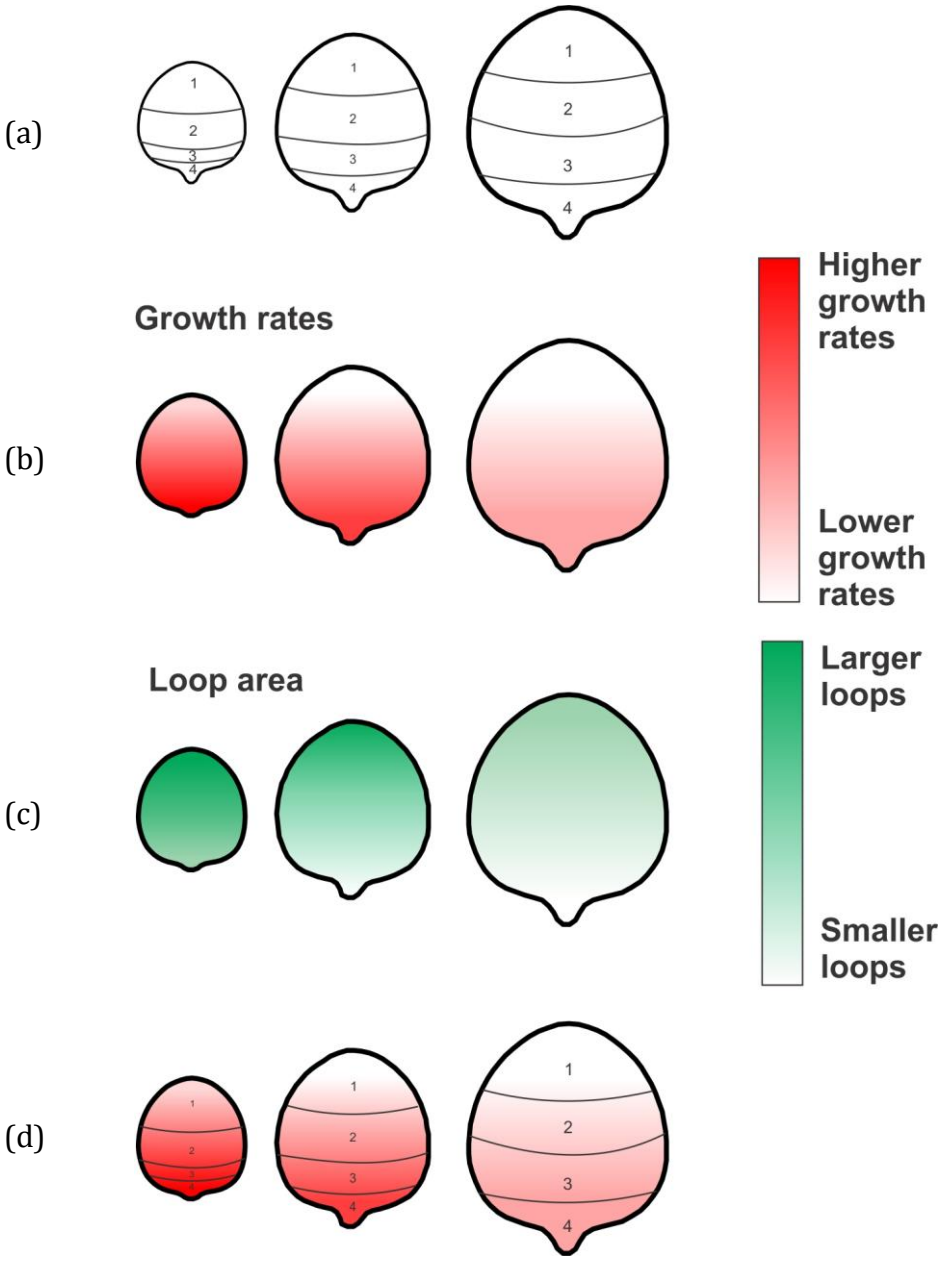

Figure 25: Proposed link between vein patterning and growth. As a leaf grows, initial parts of the base (areas 1 and 2) of the leaf are pushed upwards, so that loops that were initially at the base of the leaf become in more distal positions as other areas (3 and 4) start growing at higher rates (a). This is due to the spatial gradient in growth rates, with more growth at the leaf base (b), while loops about to split display a tip to base gradient (c). Proposed link: Loop splitting depends on the growth rate of the tissue where the loop is located (d).

4.6.2. Formation of loops at the edge

Loops do not always form by subdivision of older loops. Some loops form *de novo* at the edge of the leaf, and they are usually smaller than loops arising from loop splitting. Loops forming at the leaf edge might arise due to the formation of new auxin maxima along the edge of the leaf at later developmental stages (Figure 26b). However, no current data support this hypothesis. Scarpella's data (Scarpella *et al.*, 2006) on the expression of PIN1 protein in the leaf is very early and do not show any formation of auxin convergence points at the edge of the leaf beyond early stages of development when the first loops form.

Another possible mechanism for *de novo* loop formation may relate to the re-specification of the *MONOPTEROS* (*MP*) gene expression domain. The *MP* gene has been shown to have a major role in vein patterning (Berleth & Jurgens, 1993; Przemeck *et al.*, 1996; Wenzel *et al.*, 2007). First, *MP* is expressed all over the leaf blade and is excluded from the leaf margin. Then its expression becomes very high in pre-procambial strands as it decreases elsewhere (Wenzel *et al.*, 2007). It is therefore likely for MP to play a major role in the control of vein patterning. MP domains of expression during vein patterning are highly dynamic, so it is possible that as the leaf grows and *MP* expression domains are respecified, new MP domain boundaries form at the leaf edge, triggering the formation of new loops (Figure 26a). However, this has not been formally tested.

It is interesting to note that theoretical models of vein patterning have more difficulty generating loops *de novo*, than connecting vasculature to existing loops during loop splitting. Indeed, some models only try to model vasculature within

existing loops once the first two loops of veins have formed (Dimitrov & Zucker, 2006). Our observations make it clear that any theoretical model of vein patterning should be able to account for *de novo* loop formation continuously as the leaf grows, and that it is not only the first two loops of the leaf that form *de novo*.

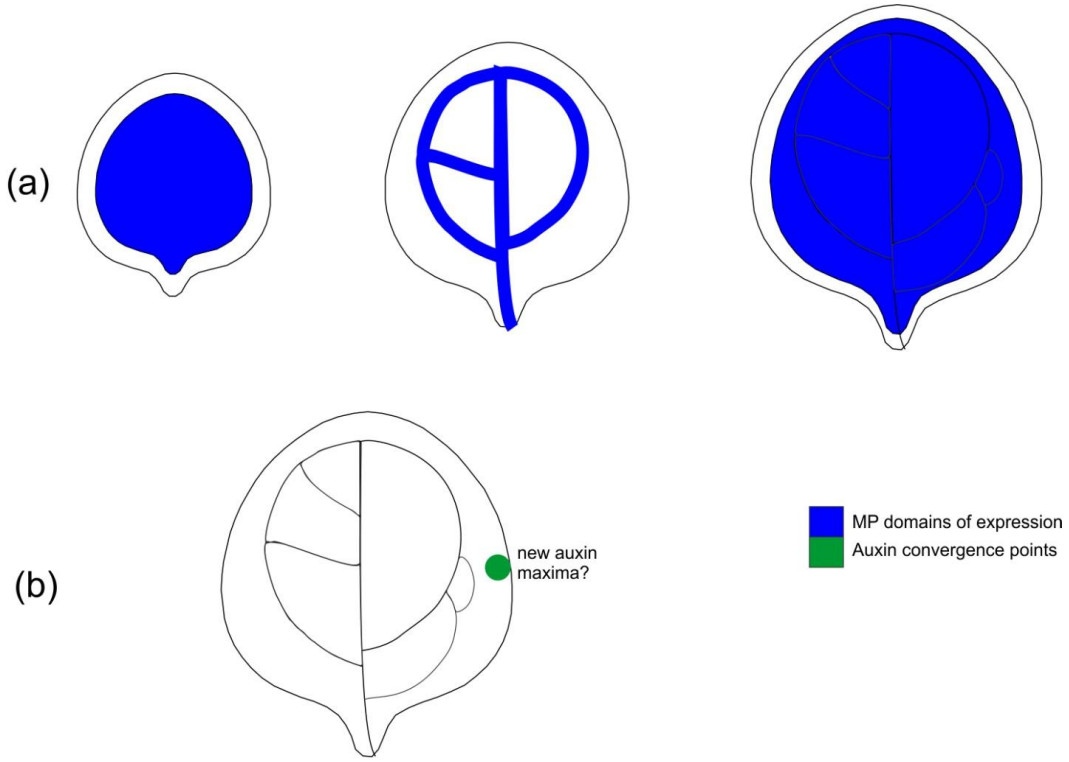

Figure 26: Loops formation at the edge of the leaf. These loops might form either because (a) MP domain is re-specified. (b) New auxin maxima form in the margin of the leaf.

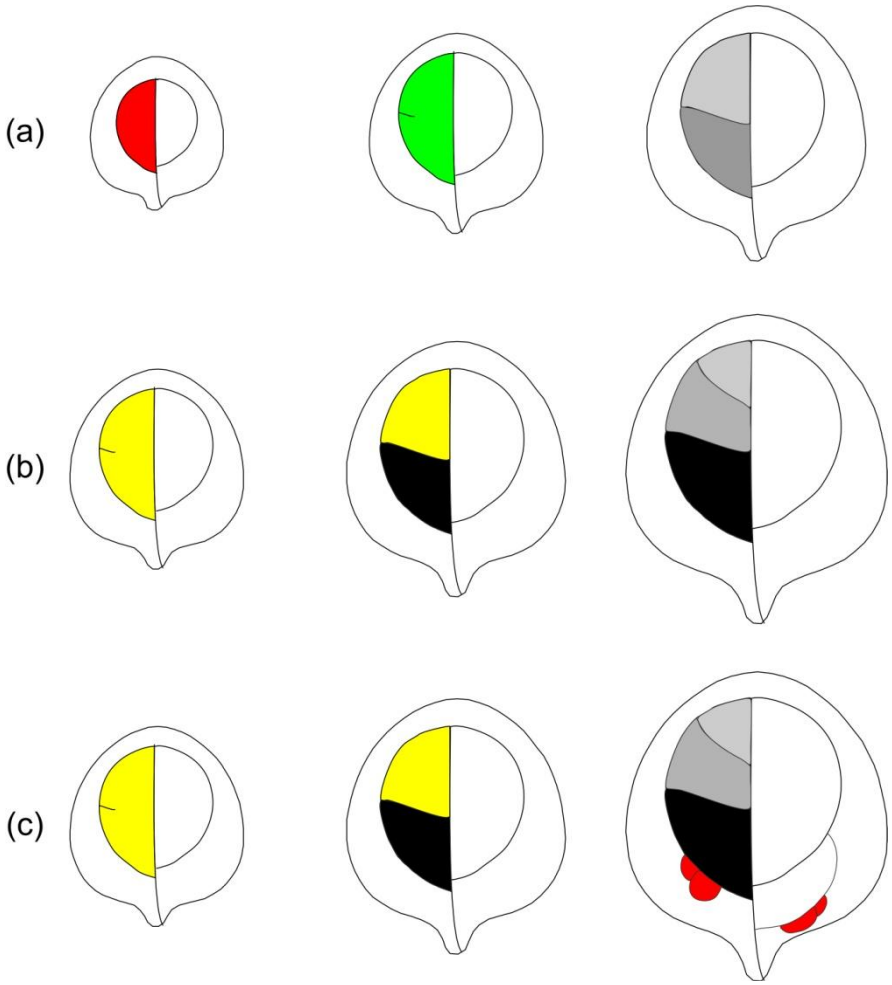

Figure 27: Formation of different types of loops. Loops are classified in different categories: loop splitting from existing loops (a), Loops that are newly formed by spilt right away (b), and finally smaller loops formation at the edge.

Chapter 5

5. Future directions

In this thesis, we developed a new method to study the interaction of vein patterning and growth. We present results for twenty samples over a period of 11 days and including spatial maps of vein patterning and growth. These maps were used to determine how different parts of the leaf grow, how loops arise and at what time loops split (i.e. subdivide) if they split.

After analysis of the wild type and to further study the interaction between growth and patterning, we need to alter either process to study the relationship between them. The first step is to analyse vein patterning and growth in mutants affected in either processes. The Micol group (Spain) has many mutants affected in leaf shape and/or vein patterns. Currently, our lab is working in collaboration with this group and analysing vein patterns in many mutants only at two time points using the destructive method (Rolland-Lagan *et al.*, 2009). Comparing phenotypes of wild type and mutant plants at maturity may reveal differences in vein patterns that are not due to differences in vein patterning but on differences in growth patterns.

Leaf growth is affected by the environmental cues. For instance, environmental stress can affect the final leaf size (Poire *et al.*, 2010). To study the effect of the environmental conditions on growth and patterning, we can alter these conditions such as temperature, light quantity and quality, water availability, nutrients and CO_2 concentrations (reviewed in Granier & Tardieu, 2009).

In order to investigate mechanisms of vein patterning and growth, leaves can also be treated with different chemicals that affect either process. For instance,

phytohormones such as auxin, cytokinins and brassinosteroids are involved in the maintenance and differentiation of procambial cells (Reviewed in Fukuda, 2004). Application or inhibition of these phytohormones is expected to disturb patterning and possibly growth of the leaf.

In the case of auxin, hormone transport can be inhibited by auxin transport inhibitors such as 1-N-naphthylphtalamic acid (NPA), 2, 3, 5-triiodobenzoic acid (TIBA) and 2-chloro-9-hydroxyfluorene-9-carboxylic acid (HFCA, Bennett *et al.*, 1998). These chemicals interfere with the auxin efflux carriers (Bennett *et al*., 1998; Mattsson *et al*., 1999). When auxin is inhibited, leaves have increased number of vascular strands (Mattsson *et al*., 1999). We could therefore compare growth and vein patterning in control plants versus plants treated locally or systemically with auxin transport inhibitors.

The role of phytohormones on leaf vein patterning and growth may also be studied by comparing wild type plants with mutants defective in phytohormone synthesis or signalling. For instance, lines with mutations in any Brassinosteroid gene are dwarf plants and have altered vein patterning with less xylem tissue and increased phloem tissue (reviewed in Fukuda, 2004; Jung & Park, 2007; Ohashi-Ito & Fukuda, 2010). As another example, a mutation in the WOL (wooden leg) gene, a gene involved in a cytokinin receptor, causes ectopic differentiation of xylem cells (reviewed in Fukuda, 2004; Ohashi-Ito & Fukuda, 2010). In light of these findings, our new live imaging method will enable us to study the effect of particular hormones on growth and patterning by comparing growth and patterning data in wild type and mutants.

As for the analysis of the data and the software used, some parts can be improved to make the analysis more user-friendly and more time-efficient, such as automated of the matching of the branching points to generate the triangles for measuring growth and tracking loops over time.

In our lab, another Master's student, Lauren Remmler, has developed a method to measure growth of leaves in 3D using fluorescent beads. Using live vein patterning tracking in combination with fluorescent beads tracking, we can follow patterning and growth separately. It is shown that cell division along the veins is parallel to the direction of growth (Scarpella & Meijer, 2004; Scarpella *et al.*, 2004); it is therefore unclear how growth directions are specified in the inter-veinal tissue between two perpendicular veins, for instance. In order to study growth of the inter-veinal tissue, purple fluorescent beads can be applied on pEPS1 (C24) leaves. This will allow us to monitor how individual loops are growing.

Finally, we would like to explore the formation of auxin convergence points and MP expression in leaves to further study the formation of smaller loops at the edge of the leaf which will allow us to test our hypothesis that the formation of smaller loops at the edge is caused by the re-specification of MP gene expression domains.

Table 1: Mean relative growth rates over time for C24 (pEPS1)

DAS	Relative Growth Rate (% per d)*
10	65.00
11	63.22
12	56.90
13	43.50
14	21.75
15	15.23
16	11.84
17	7.55
18	5.14
19	3.11

*The averages are calculated from the tracked loops data.

Appendix A: Mean area blade for 20 samples of C24 (pEPS1)

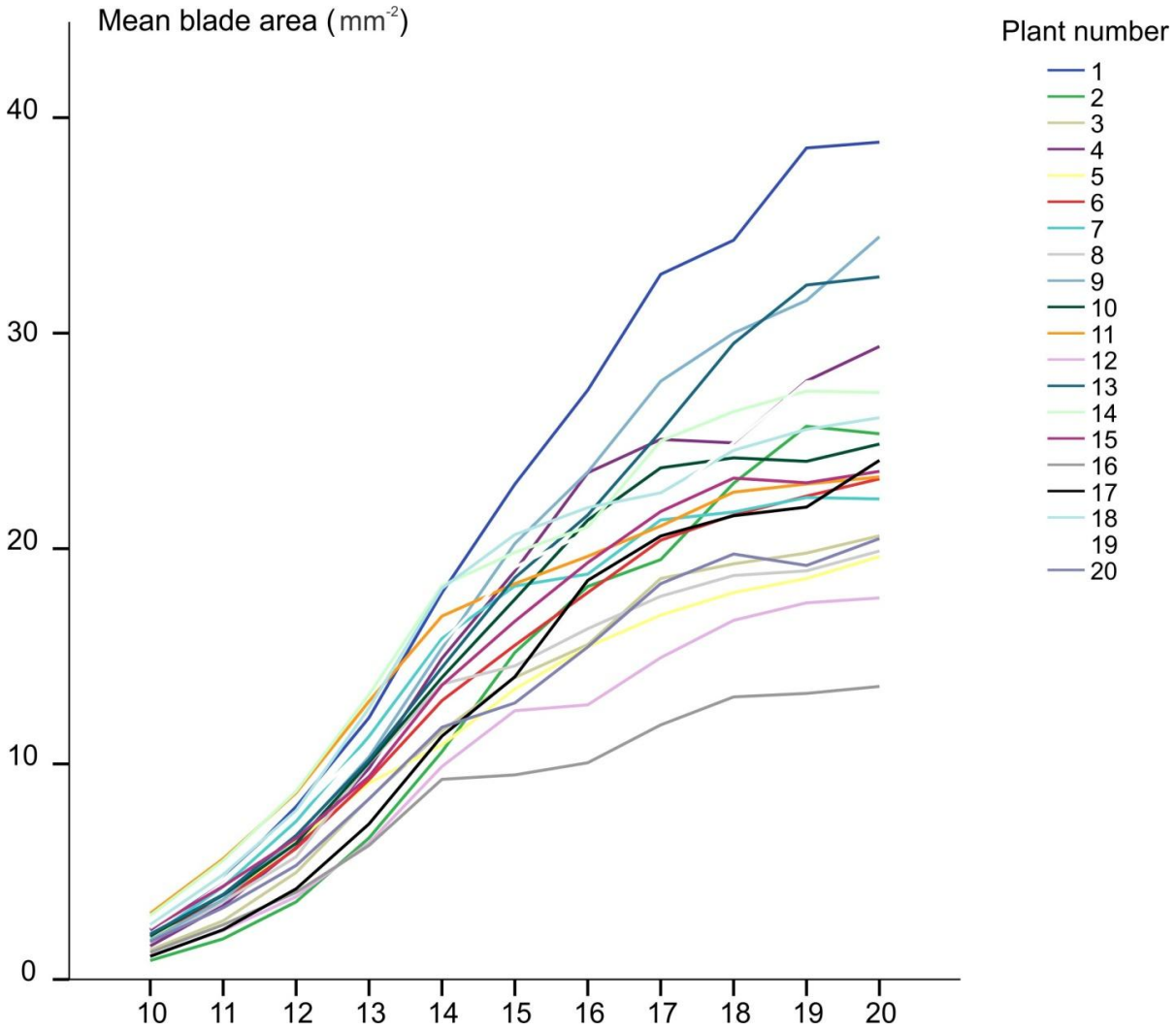

Figure S 1: Blade area for individual samples over time.

Appendix B: Choice of plant

1. Use of transgenic plants with fluorescent vasculature

In order to visualize venation patterns over time, we wanted a plant line with fluorescence in the vasculature, which would appear at early stages of patterning and still be present in the veins until development stops.

Five different lines are tested, which could be divided into early markers and late markers plants. *Early markers* display fluorescence early in the vein differentiation process, when future vascular cells have not yet acquired vascular cells morphology. Fluorescing cells are at the procambial or pre-procambial stage (Kang & Dengler, 2004; Scarpella *et al.*, 2004, Figure S2). *Late markers* display fluorescence in phloem cells, i.e. when the vasculature has already differentiated.

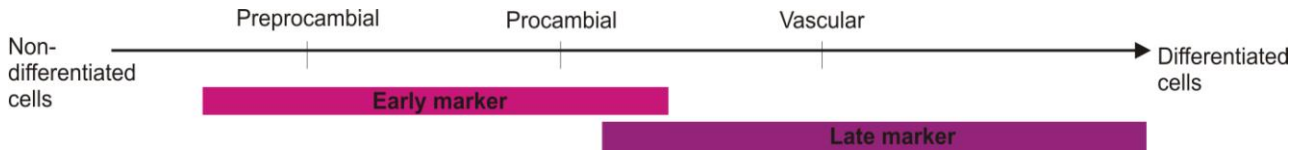

Figure S 2: Early vs. Later markers in leaves. Early markers are expressed before the preprocambial cells differentiate into vascular tissue. Late markers are expressed once the cells differentiate into xylem and phloem.

The five different lines tested are described below.

- SHR::mcherry:3xNLS have the mcherry (red) marker expressed in the vasculature, this marker shows up at early stages of patterning. The promoter of the vascular marker SHORT-ROOT (SHR) is fused to the mcherry marker and is targeted to the nucleus. The problem with this line is the descendants of the initial seeds gave patchy vasculature. The fluorescence started to fade away around 14 days after sowing (stage referred to as DAS14, Rolland-Lagan *et al.*,

2009). This line was provided by E. Scarpella, University of Alberta, Edmonton, Alberta, Canada.

- J1721 and Q0990 are of ecotype C24. These lines are two of the 250 lines of a GFP-enhancer trap (Haseloff, 1999). In J1721, the GFP marker appears in vasculature at early stages of patterning; it labels preprocambial cells (their length was not significantly different from their width, Sawchuk *et al.*, 2007). The GFP marker in Q0990 follows the appearance of GFP in J1721. GFP is expressed in Q0990 when cells are more procambial like. The Scarpella lab screened the 250 lines collection for lines that express GFP specifically in the vasculature and they chose J1721 and Q0990 (Sawchuk *et al.*, 2007). Both lines were provided to us by E. Scarpella, University of Alberta, Edmonton, Alberta, Canada. For J1721, the fluorescence fades around DAS11-DAS13, for Q0990, the fluorescence disappears at DAS08.
- SHR::NLS:YFP has the yellow fluorescent protein (YFP) fused to the SHR and is also targeted to the nucleus. In this case, the fluorescence is not properly visible in the leaf *in vivo*. This line was provided by E. Scarpella, University of Alberta, Edmonton, Alberta, Canada.
- The pEPS1 line is a transgenic line of ecotype C24. The transgenic construct is AtSuc2prom: GFP (pEPS1). This line has been previously described by *Imlau et al.* (1999). The GFP marker appears at late stages of development, i.e. when the procambial cells have differentiated into xylem and phloem. It expresses free green fluorescent protein (GFP) in the phloem. The line was provided to us by R.

Stadler and N. Sauer, Molecular Plant Physiology, University of Erlangen, Germany.

Originally, J1721 was the line of choice. It has a GFP marker expressed in its vasculature; it is bright enough at early stages. But the GFP protein degrades very early from the veins. In addition, there was a variation when the fluorescence in the veins degraded between different samples. In some cases, we could image the leaves up until DAS15 but that was only for very few samples, in each trial. For these reasons, we decided to use pEPS1 instead. We chose pEPS1 to follow venation patterns *in vivo*. Even though it is a late marker, it is very bright and the fluorescence keeps being generated until DAS20. Vascular patterns obtained from *in vivo* imaging and destructive imaging (Rolland-Lagan *et al.*, 2009) are the same (Figure S 3). Therefore to monitor venation patterns *in vivo*, the pEPS1 line is used.

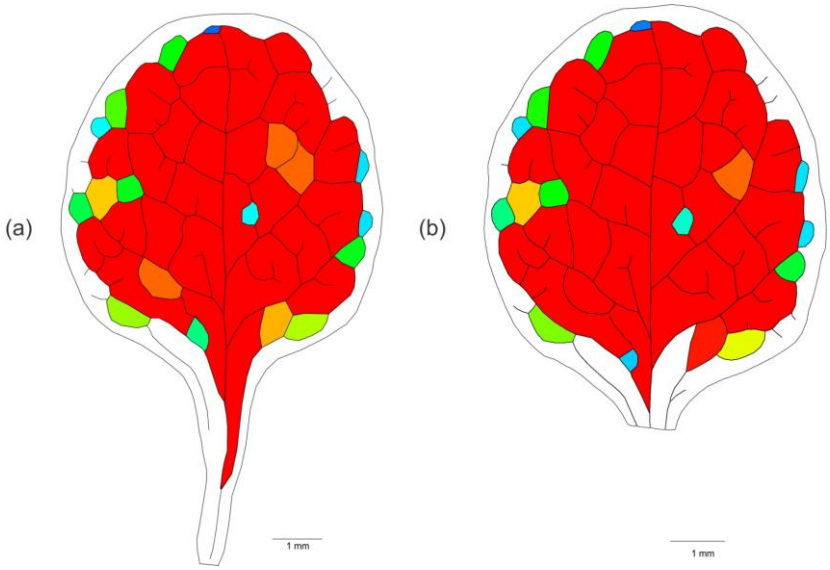

Figure S 3: Comparison of pEPS1 leaf imaged using two different methods. Leaf imaged (a) with the destructive method and (b) Live imaging method. Colors represent the loop areas with red being the biggest area and blue the smallest.

2. ***Use of fluorescent dyes in non-transgenic plants***

We tried to use hydroponics and grow plants in liquid media. Plants would be regularly transferred into a solution with a fluorescent dye, for the necessary amount of time to allow the dye to move in the vasculature. We could therefore visualize veins without the need for transgenic plants. This technique required two optimization steps; 1) find a suitable dye which would stain the vasculature and 2) find a good hydroponic setup for easy transfer of plans to and from the fluorescent dye (the plants would only be left in the dye for a short amount of time before and during imaging, and would then be returned to the hydroponic system). Different protocols were tried out with some modifications (Hetu *et al*., 2005; Huttner & Bar-Zvi, 2003).

We chose the Texas Red lysine-fixable dextran 3-kD (Invitrogen, CA, USA) for our hydroponics experiment because even after several minutes of dextran uptake by leaves it remains confined in the vasculature because of its high molecular weight and then none of the cells around it would be stained, it is water soluble (1 $mg.mL^{-1}$ in water) so plants can take it up easily, and it is not toxic for plants (Roberts *et al.*, 1997).

Two different approaches were tested for the best setup for growing plants. First, we tried a method developed by Huttner & Bar-Zvi (2003). Using a 5L plastic container with holes drilled in the plastic cover, plastic plugs were stuffed with rock wool pieces; these plugs were used to hold the plants in the holes. The plants grew and were healthy enough to use for studying vein formation. Our plan was that as soon as the roots came out, the plants would be placed in the Texas red solution, so the roots could take up the dye. But this attempt failed because of the length of the rock wool pieces used and the time it took roots to grow out of the rock wool.

Our second approach was to use a method developed by Hetu *et al.* (2005). This method consists of growing plants on stainless steel screens, first in petri dishes, then moving the screens to liquid media in Erlenmeyer flasks under sterile conditions. In our case, plants were grown on the metal screens in petri dishes, and then moved to the plastic containers used in the previous method (Huttner & Bar-Zvi, 2003). This passage from sterile conditions to non-sterile killed the plants.

Both approaches failed for the purpose of our experiment. For future trials, some features of both approaches need to be combined: first plants have to be grown on the screens in soil then once the plants are big enough they should be moved to the plastic containers with punched holes in the cover. The screens are very stable and easy to move. These screens are very thin so we see roots early on. The plastic covers (with punched holes) are easy to use; plants are easily moved from the medium solution into the Texas red dye solution.

Appendix C: Comparing pEPS1 vs. J1721

Knowing that pEPS1 and J1721 have the same background ecotype (C24), we decided to combine and compare both lines. We assumed that both lines would have similar behavior when it comes to vein patterning and growth, but this is not the case.

The expression of GFP in pEPS1 in the veins follows the expression of GFP in J1721. It was noticeable that the two lines behaved differently (Figure S 4). The mean leaf blade area for both lines was almost the same at DAS10 and the two mean graph lines correspond (Figure S 4a). While the mean vein density of J1721 is decreasing from DAS08 to DAS10, for pEPS1 it increased from DAS10 to DAS12 and then decreased (Figure S 4b). J1721 had almost constant mean loop number and mean segment number per leaf, while for pEPS1 the mean loop number and mean segment number per leaf were increasing at a high frequency from DAS10 to DAS15 (Figure S 4c-d).

This difference in behaviour of both lines could be due to differences in vein patterns between the lines, or could be due to the fact that early markers may not be reliable. It is possible that some cells do show the GFP marker but then do not differentiate into veins, and that some cells that differentiate into veins never show the GFP marker.

In order to discriminate between those two possibilities, we grew 15 plants of each line and imaged them using the live imaging technique (this method) at DAS10. Then at DAS18, we cleared the leaves and used the destructive technique to quantify the vasculature of the leaves (Rolland-Lagan *et al.*, 2009). At DAS18, patterning and growth have stopped and all veins have differentiated.

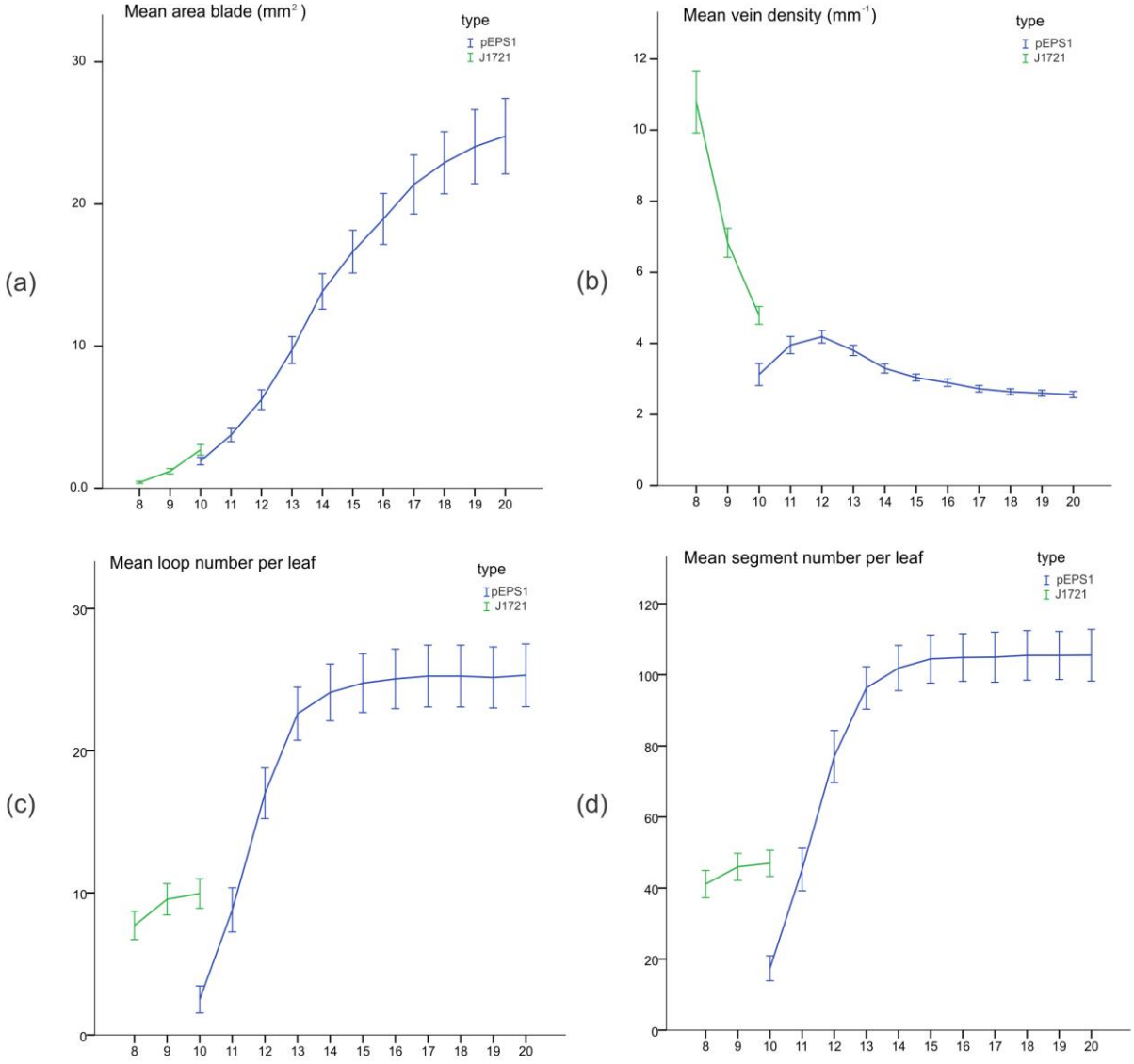

Figure S 4: Comparison between pEPS1 and J1721. (a) Mean blade area (mm^2). (b) Mean vein density (mm^{-1}). (c) Mean loop number per leaf. (d) Mean segment number per leaf. Error bars indicate the standard error of the mean.

First, we compared J1721 at DAS10 and DAS18 to see if the marker is showing the same loops and segments numbers. The leaves showed the same vasculature at both time points with a slight change (Figure S 5), which is expected because patterning does not stop until DAS14 and the leaf is still growing (Scarpella *et al*., 2004, also confirmed by our data). The leaf blade area increased in size from DAS10 and DAS18 while the vein density decreased. The number of loops and segments per leaf increased slightly between the two time points indicating that the patterning was almost done at DAS10.

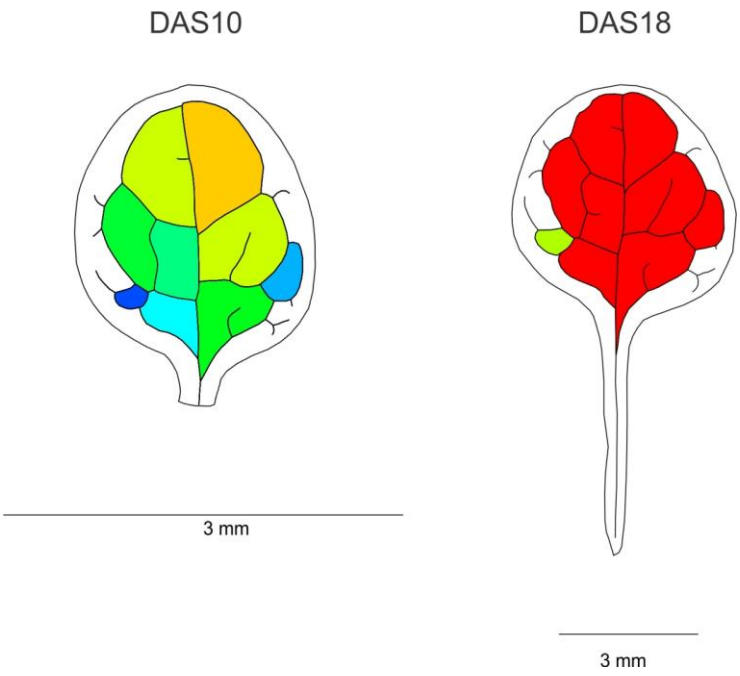

Figure S 5: Comparison of a J1721 leaf at two time points. (a) DAS10 and (b) DAS18. Colors represent the loop areas with red being the biggest area and blue the smallest.

We then compared the DAS18 data from the digitized cleared leaves for pEPS1 and J1721 (Figure S 6, Rolland-Lagan *et al.*, 2009). At DAS18, J1721 leaves were smaller than pEPS1 leaves but the difference is very minimal between the two lines (Figure S 6a). However, in terms of loops and segments numbers per leaf, pEPS1 had almost twice as many veins as the J1721 line. A non-parametric test for unpaired measures (Mann-Whitney test) with the type as factor showed that the mean leaf area of the blade of both lines is not significantly different (U=69.00, Z= -1.804, *P*=0.71), while the loop

number and the segment number were significantly different (for loop number: U=0, Z= -4.678, *P*<0.01, for the segment number: U=0, Z= -4.667, *P*<0.01)._

J1721 showed similar vasculature at DAS10 and DAS18 and a slight increase in segment per leaf between DAS10 and DAS18 (Figure S 7), while the loop number stayed constant (Figure S 7). A non-parametric statistical test for two related samples with day as a factor (Wilcoxon-signed rank test) showed that the blade area was significantly different between DAS10 and DAS18 (Z = -3.408, *P* =<0.01), while the loop number was not significantly different between the two days (Z = -0.734, *P* =0.463), while the segment number was significantly different between the two time points (Z = -2.591, *P* <0.01).

Finally, both lines are from the same background but they behave differently. We cannot combine their data to study patterning and growth over longer periods. J1721 was used by the Scarpella group (Sawchuk *et al*., 2007) to study patterning at early stages. But for the purpose of our study, this line used on its own was not useful. In the appendix D, we show the results for 20 samples of J1721 imaged from DAS08 to DAS10 and analysed vein patterning using the live imaging method.

(a)

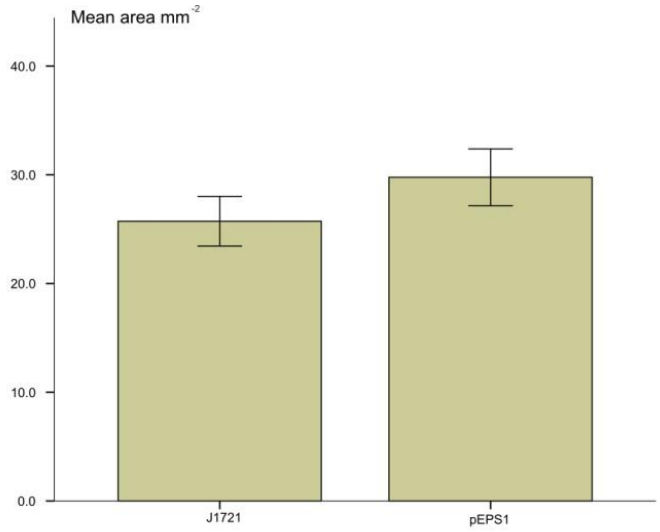

(b)

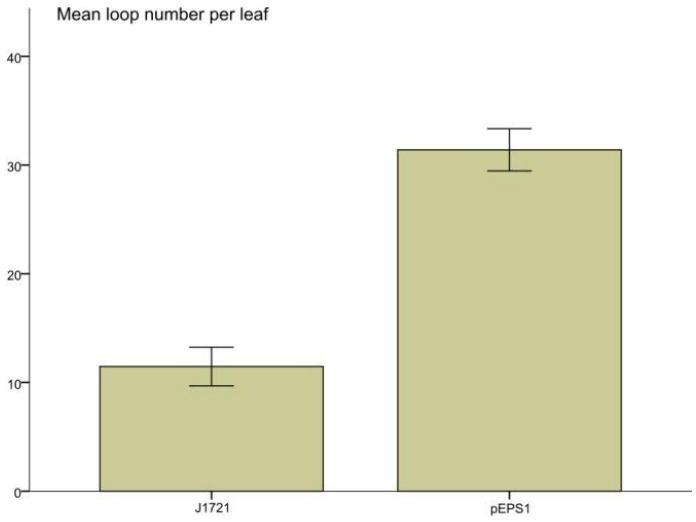

(c)

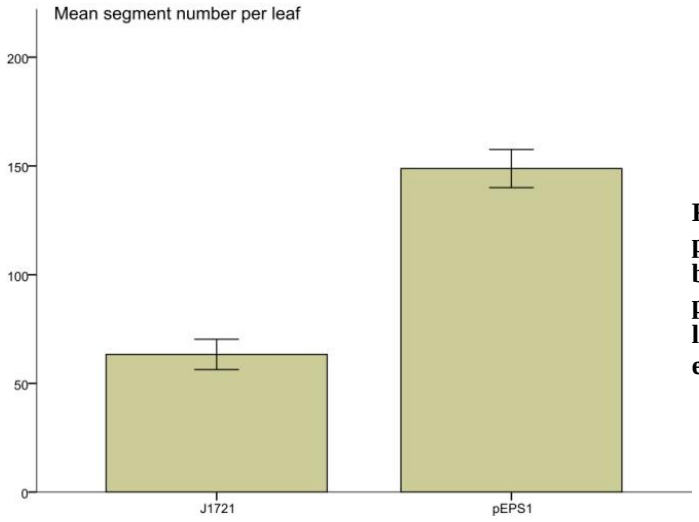

Figure S 6: Averages of cleared leaves of pEPS1 and J1721 at DAS18. (a) Mean blade area (mm^2). (b) Mean loop number per leaf. (c) Mean segment number per leaf. Error bars indicate the standard error of the mean.

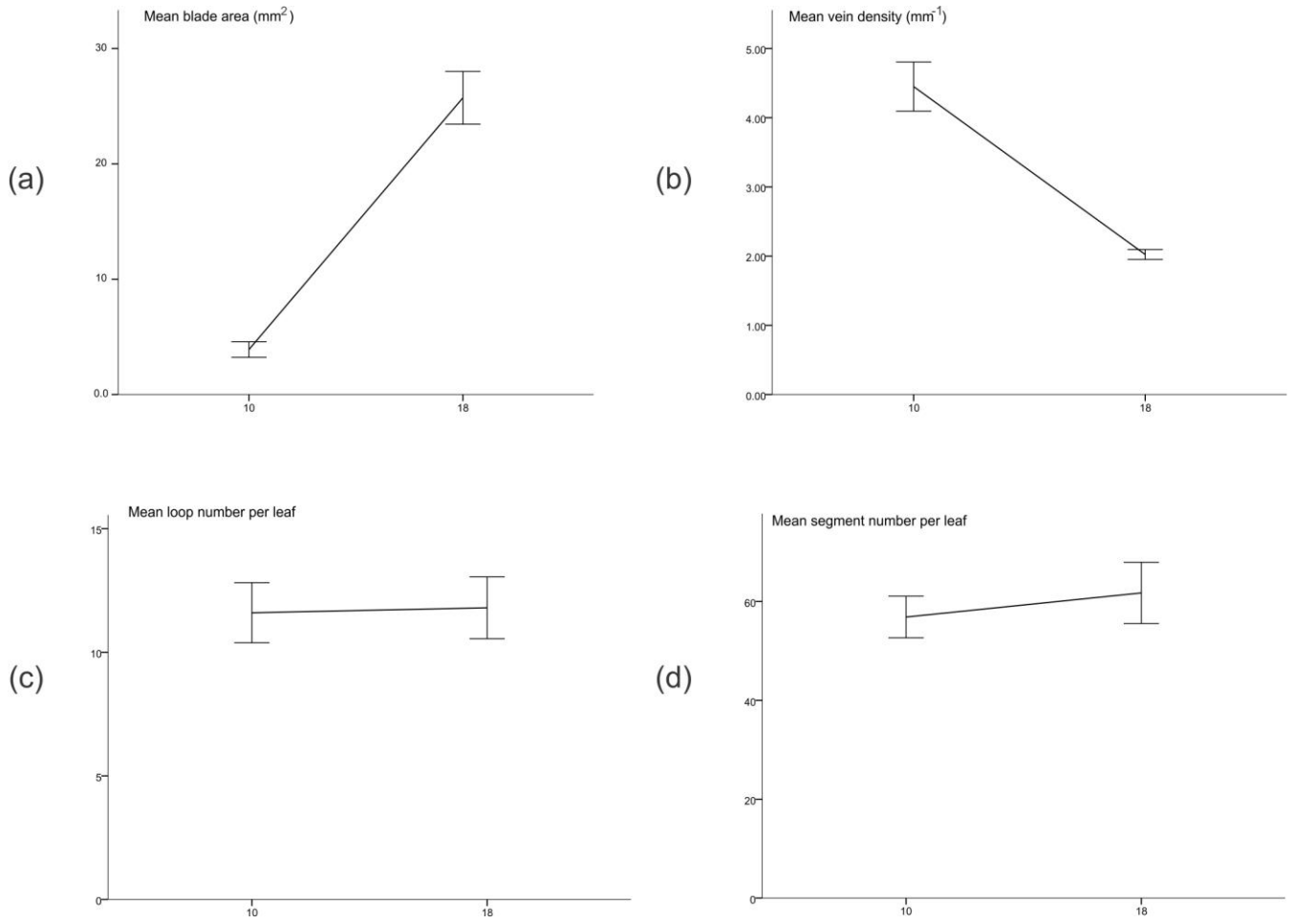

Figure S7: Average data of J1721 at DAS10 and DAS18. (a) Mean blade area mm^2. (b)Mean vein density (mm^{-1}). (c) Mean loop number per leaf. (d) Mean segment number per leaf. Error bars indicate the standard error of the mean.

Appendix D: Analysis of patterning and growth for multiples samples for J1721

The expression of GFP in J1721 shows up after the expression of PIN1 (Sawchuk *et al.*, 2007). J1721 marker expression starts from previously existing veins, these newly formed segments are initially free veins ending and progress to connect to the pre-existing vein (Sawchuk *et al.*, 2007). In the following, we are analyzing 20 samples of J1721 imaged and analyzed using the live imaging method (see Chapter 2).

Spatial analysis for multiple samples:

Temporal analysis:

From DAS08 to DAS10, J1721 leaves are imaged. The leaf blade increases six times in size within two days. Moreover, the mean vein density decreases drastically within those time points. As the leaf blade grows during these time points, the loop number and segment number per leaf are almost constant between the three time points (Figure S 8).

Loops data

Average data is calculated, and spatial maps are generated for DAS08 to DAS10 (Figure S 9). The number of samples maps shows the number of samples at each (x, y) of the map (Figure S 9a). Loop areas decrease from tip to base, where loops at the tip and center of the leaf are larger than loops at the base (Figure S 9b). Loops shape maps show a tip to base gradient, where loops are more rounded at the tip and center of the leaf and more elongated at the base (Figure S 9c). Loops orientation maps show a tip to base decrease in angles of orientation (Figure S 9d). As for the level of subdivision, loops are subdivided at the center of the leaf and base then the tip, this map shows a gradient from tip to base.

Tracking data

For the tracked loops maps, not much can be seen, because we have only three time points. These maps are showing growth from one stage to the next for a set triangles, i.e. how much each triangle at time point t will grow in the different directions to become the corresponding triangle in the next time point *t+1* (Figure S 10). When comparing the temporal analysis with the tracking maps, patterning is mostly happening between DAS08 and DAS09, while fewer loops are added from DAS09 to DAS10. At those time points, a gradient from tip to base is seen in terms of new loops addition but most of the loops are added to the right half of the leaf. The map of loops about to split confirms that patterning is mostly happening between DAS08 and DAS09 with an increase in splitting from tip to base. As for DAS09 to DAS10, low levels of splitting are occurring in the center of the leaf. The leaf has very high relative growth rate. In these maps, we only see the initial very high rate of growth while patterning has apparently slowed down.

Growth data

We generated growth spatial maps for J1721 (Figure S 11). First, the number of samples for each point of the spatial maps is displayed (Figure S 11a). The maps of the arms of the strain cross *p* and *q* showed a tip to base increase in *p* and *q* (Figure S 11b-c). This gradient is similar to the gradient seen for the growth maps of pEPS1. The anisotropy shows a center to edge increase, where the triangles at the edge are anisotropic (Figure S 11d). The map of relative growth rate percentage shows very high growth rates. Some areas are growing more than 3 times from one time point to the next. These maps show a tip to base increase, where the tip is growing slower than the

rest of the leaf. This gradient is similar to the maps of pEPS1. Relative growth rate maps using loops data and the triangles are very similar (Figure S 11e).

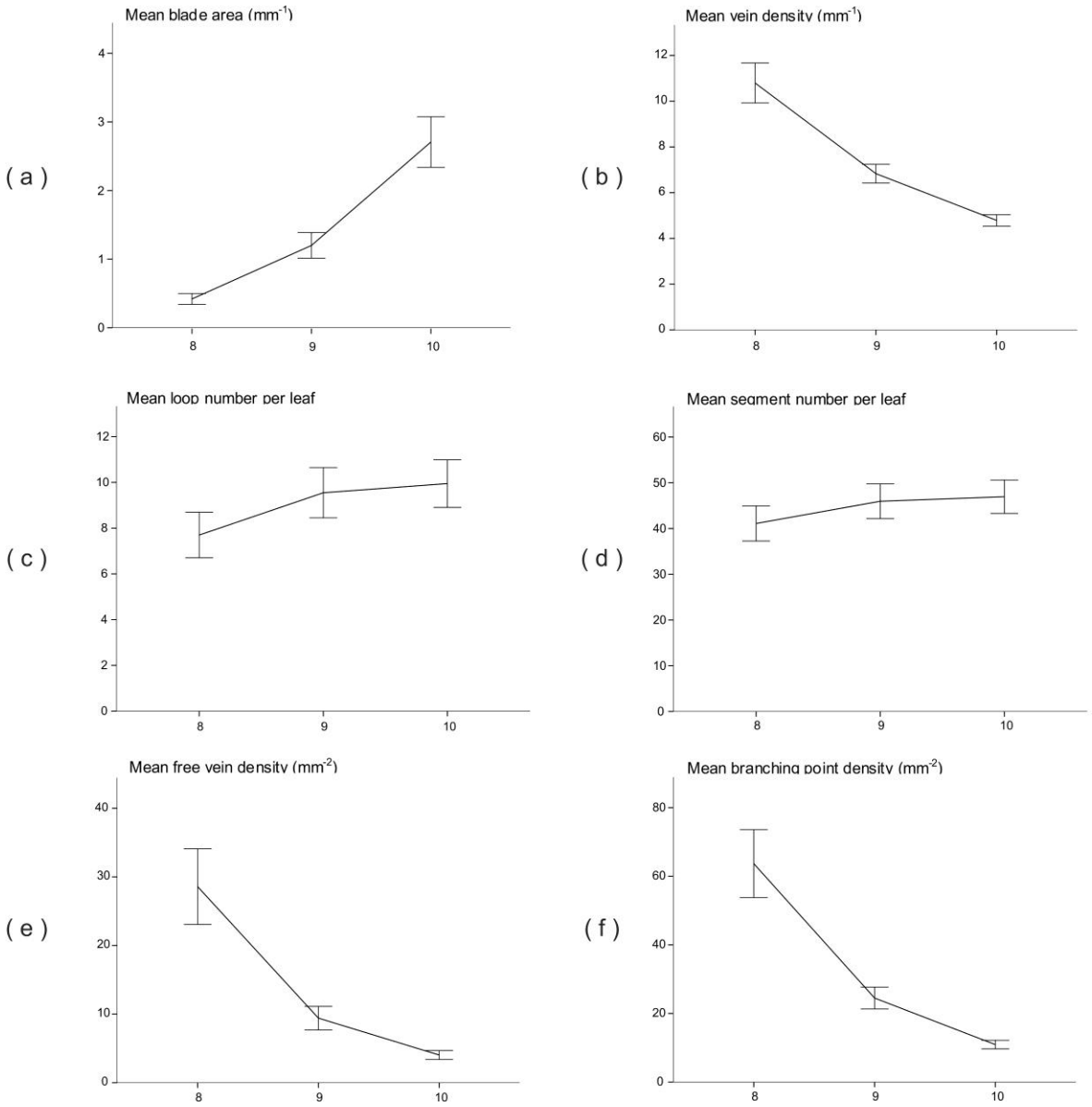

Figure S 8: Temporal analysis of J1721. (a) Mean blade area (mm^2). (b) Mean vein density (mm^{-1}). (c) Mean loop number per leaf. (d) Mean segment number per leaf. (e) Mean free vein density (mm^{-2}). (f) Mean branching point density (mm^{-2}). Error bars indicate the standard error of the mean.

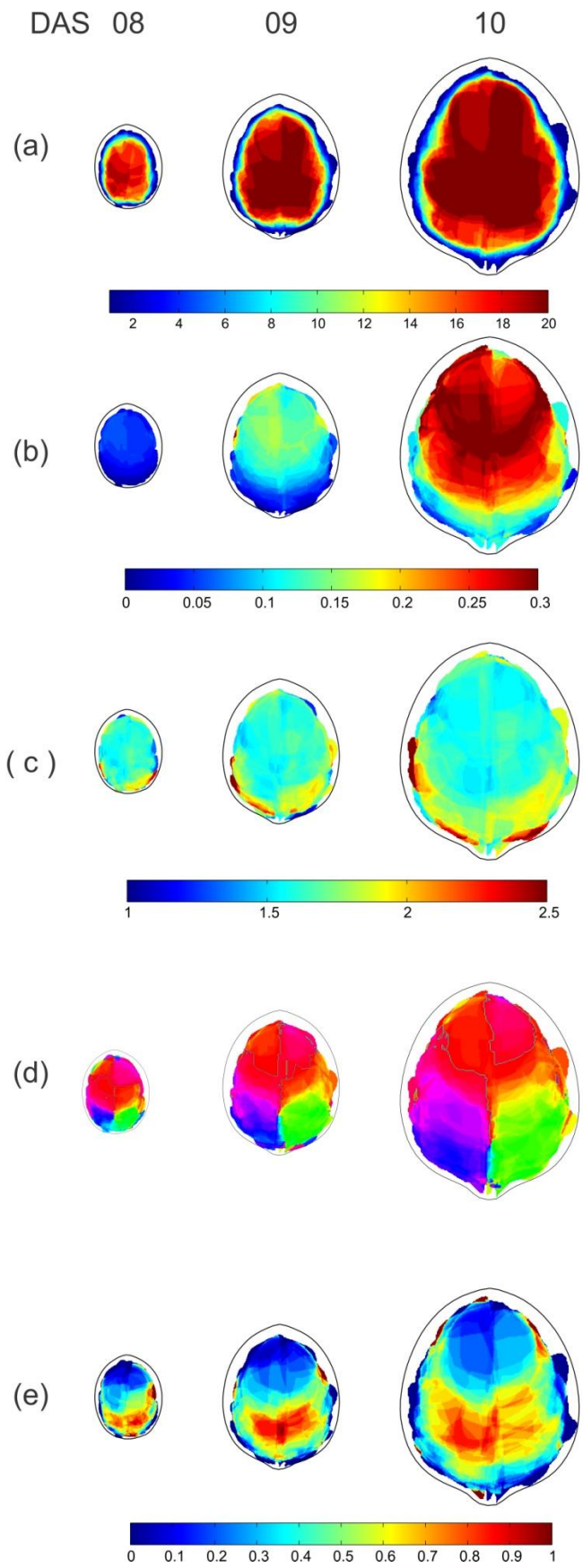

Figure S 9: Average loops data for 20 samples. (a) Sample number for each (x, y). (b) Loop areas over time. The color code shows the loop areas in mm^2. (c) Loop shapes over time. The color code shows the loop shapes. (d) Loops orientations with color wheel showing the different colors corresponding to the angles going from -90^o to 90^o. (e) Loop subdivision over time.

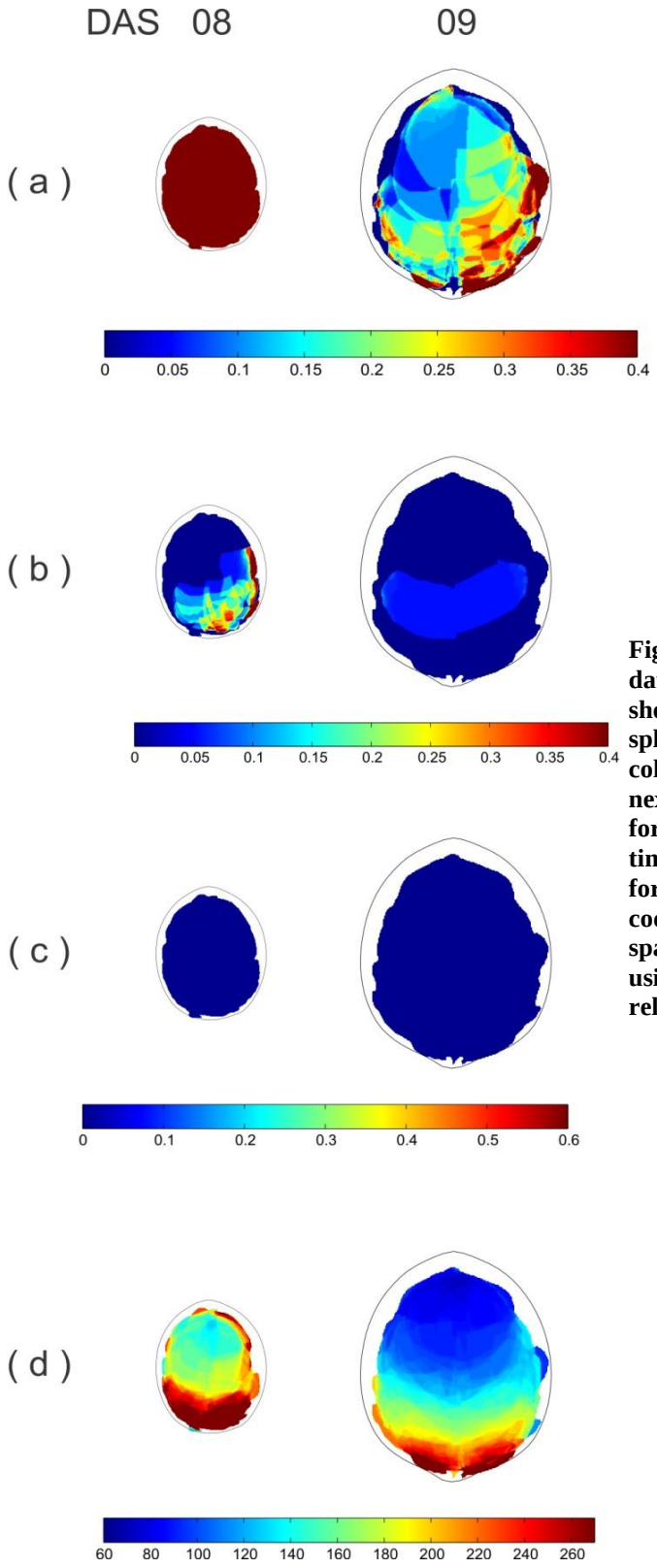

Figure S 10: Spatial maps for tracked loops data. a) Newly formed loops. The color code shows the newly formed loops. (b) Loops splitting into two or more smaller loops. The color code shows the loops that will split at the next time point. (c) Some loops will be newly formed at time point t but will subdivide at time point t+1. But in this case there is not formation of fast forming loops. The color code shows the fast forming loops. (d) The spatial maps for the relative growth rates using the loops data. The color code shows the relative growth rates in %.

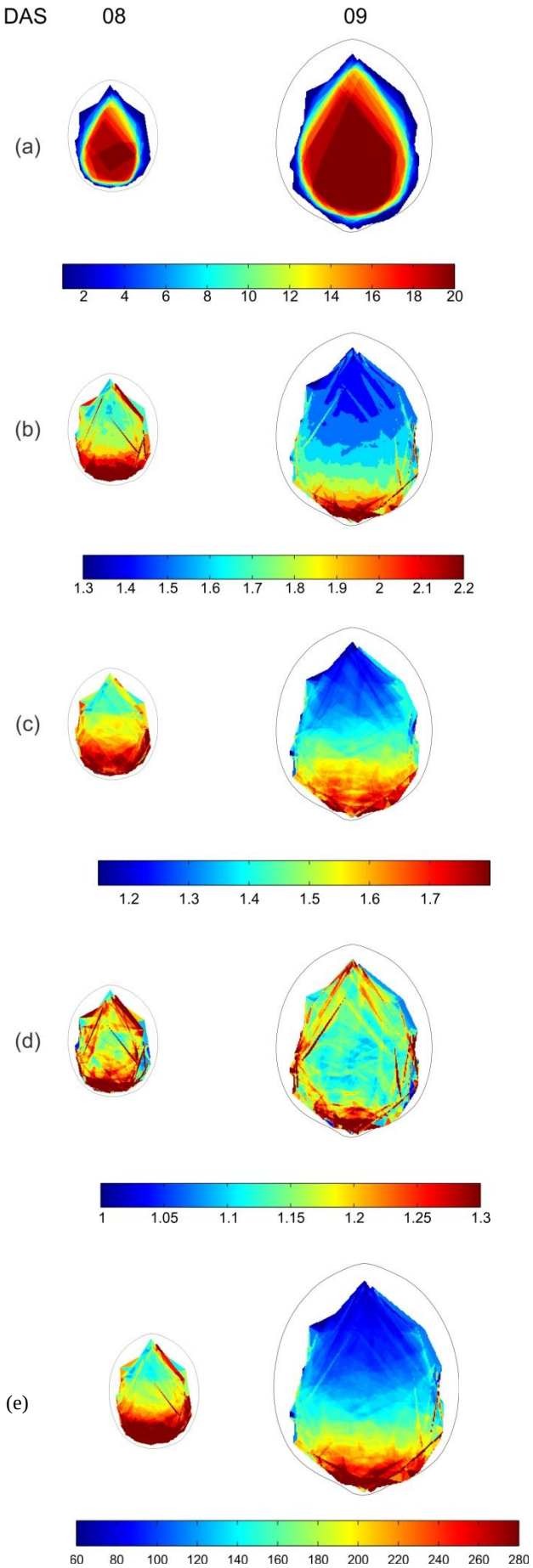

Figure S 11: Growth spatial maps. (a) Samples numbers. (b) Main direction of growth p. (c) q. (d) Anisotropy. (e) Relative growth rate (%).

Appendix E: Spatial maps for multiples samples for the tracked loops data for DAS17 to DAS19.

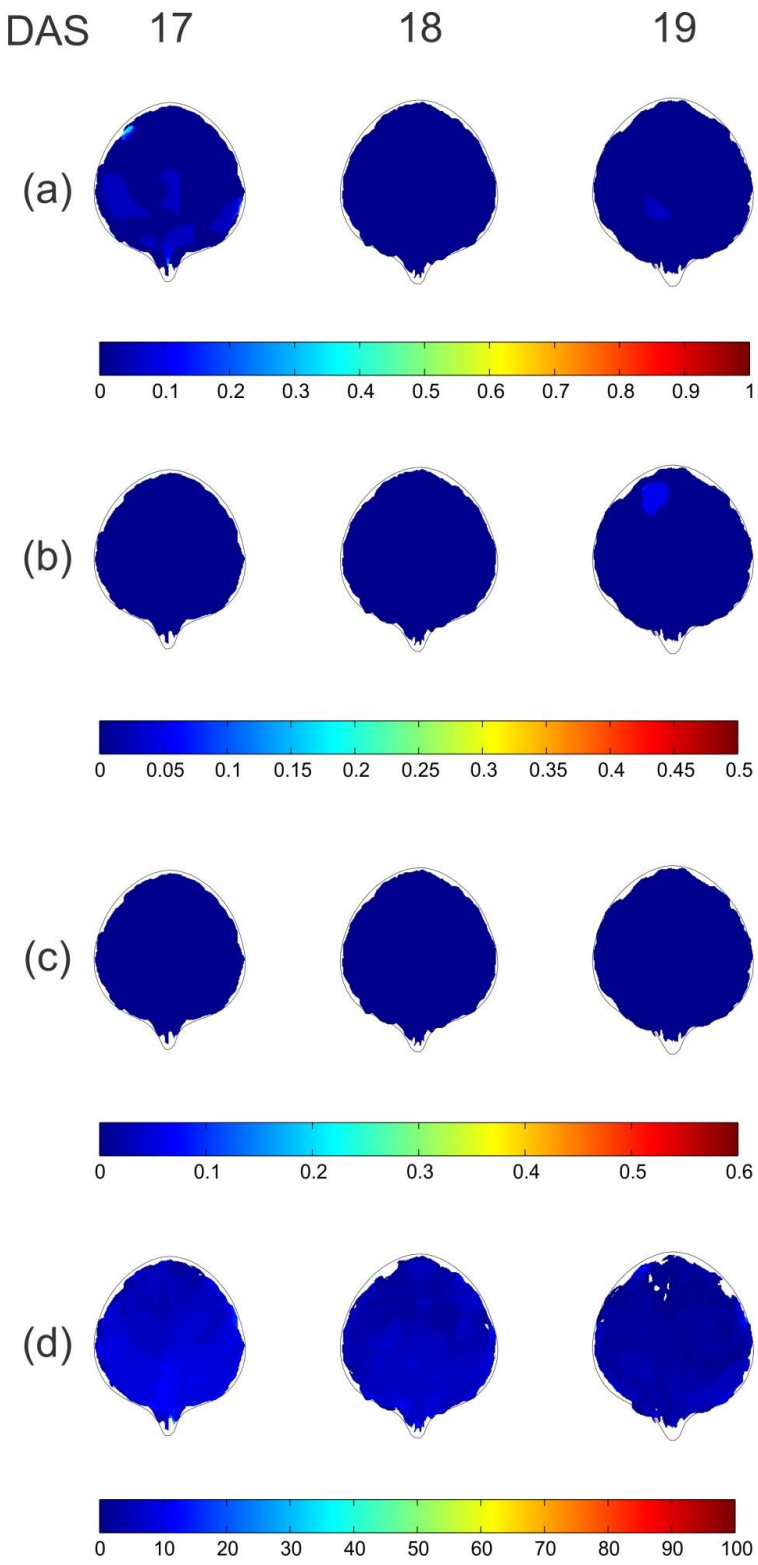

Figure S 12 : From DAS17-DAS19, patterning has almost stopped. (a) Newly formed loops maps (the color code shows the newly formed loops), (b) map of loops splitting in the next time point (the color code shows the loops that will split). (c) Map of fast forming loops. The color code shows the fast forming loops. (d) The spatial maps for the relative growth rates using the loops data. The color code shows the relative growth rates in %.

Appendix F: Growth spatial maps for pEPS1

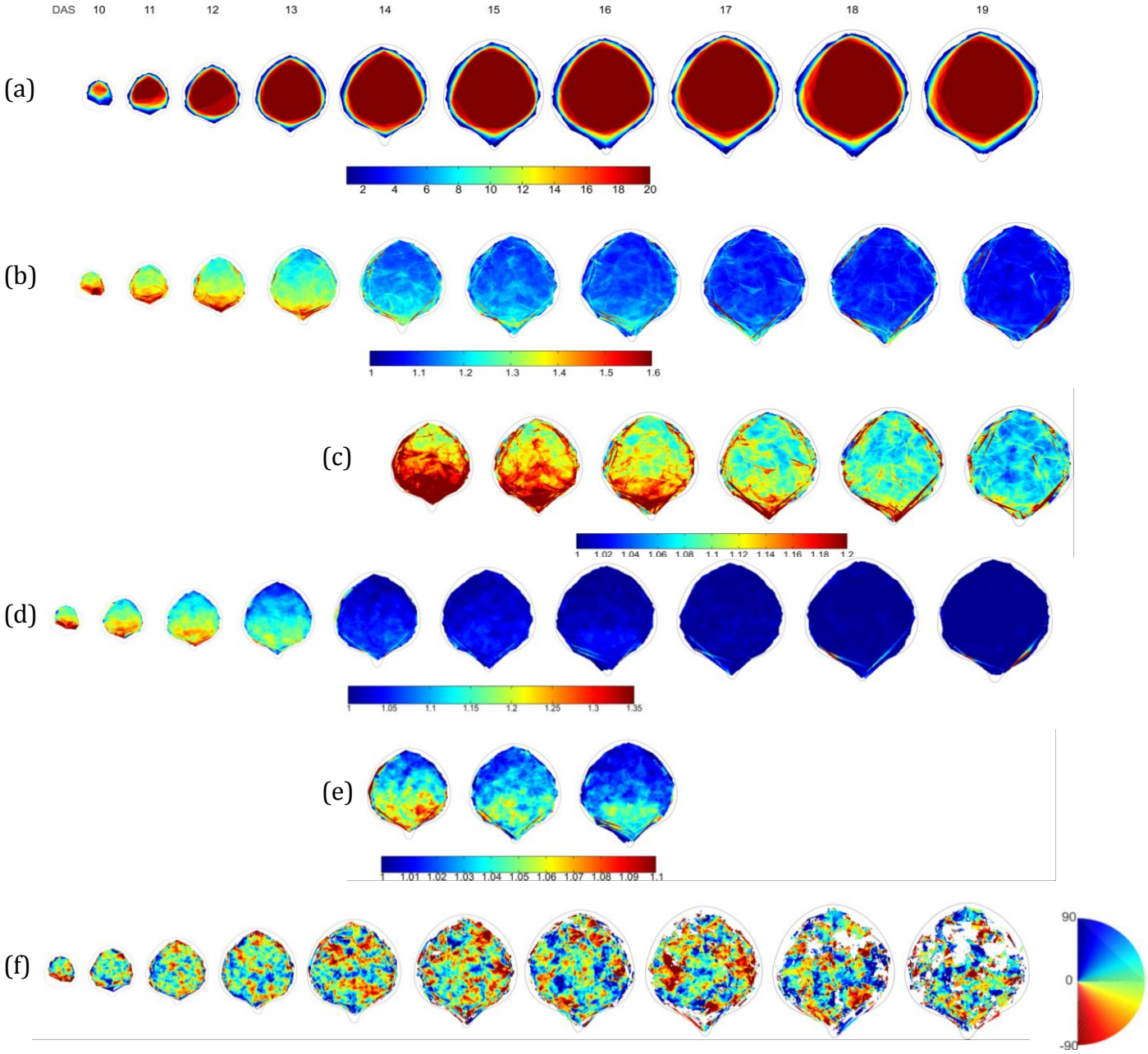

Figure S 13: Growth spatial maps for pEPS1 (a) Triangle number maps. (b-c) Spatial map of p, the scaling factor along the main direction of growth between two successive time points. (d- e) Spatial maps of q, the scaling factor along the direction perpendicular to the main direction of growth. (f) Spatial maps of angles of orientation.

Appendix G: Standard errors maps for the spatial maps

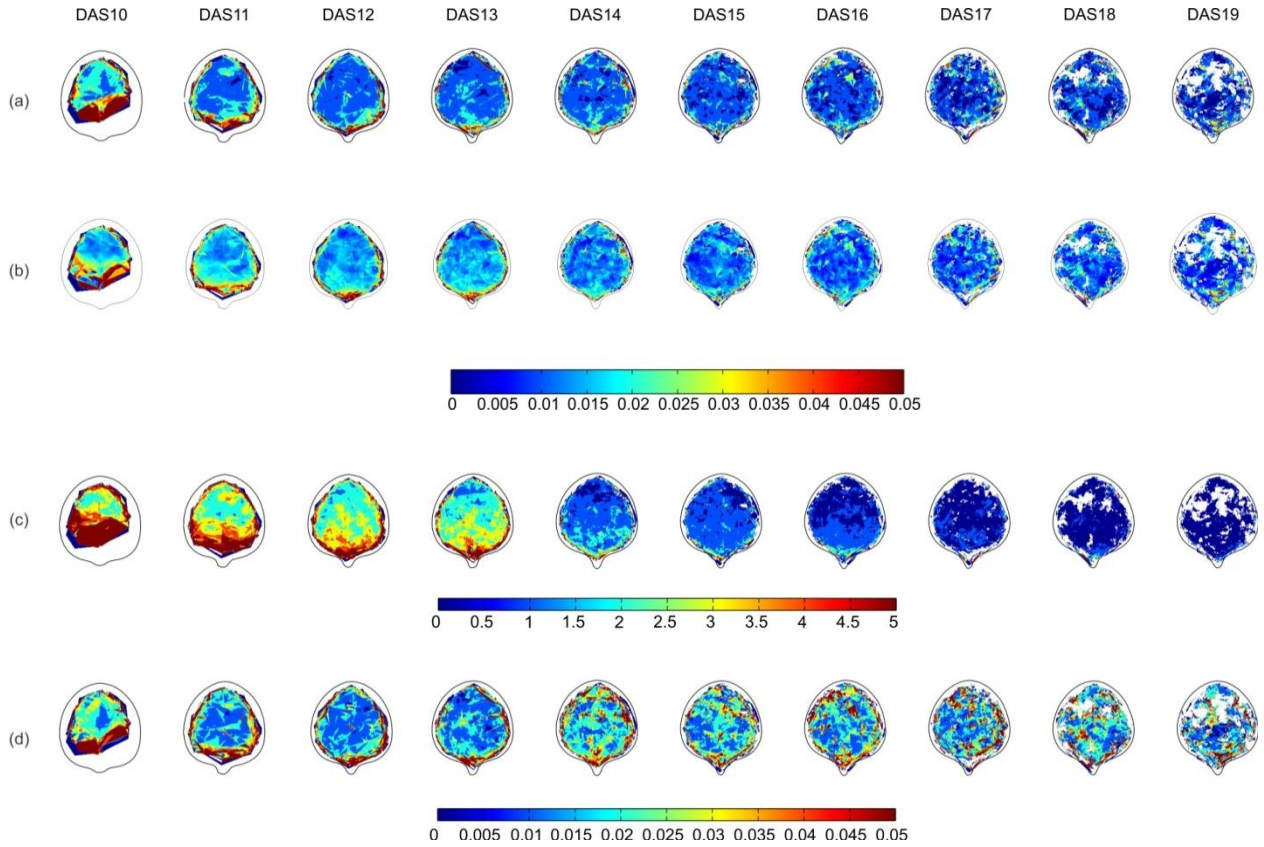

Figure S 14: Standard error for growth maps: (a) Scaling factor along the main direction of growth, p. (b) scaling factor along the main direction of growth, q. (c) Relative growth rate. (d) Anisotropy.

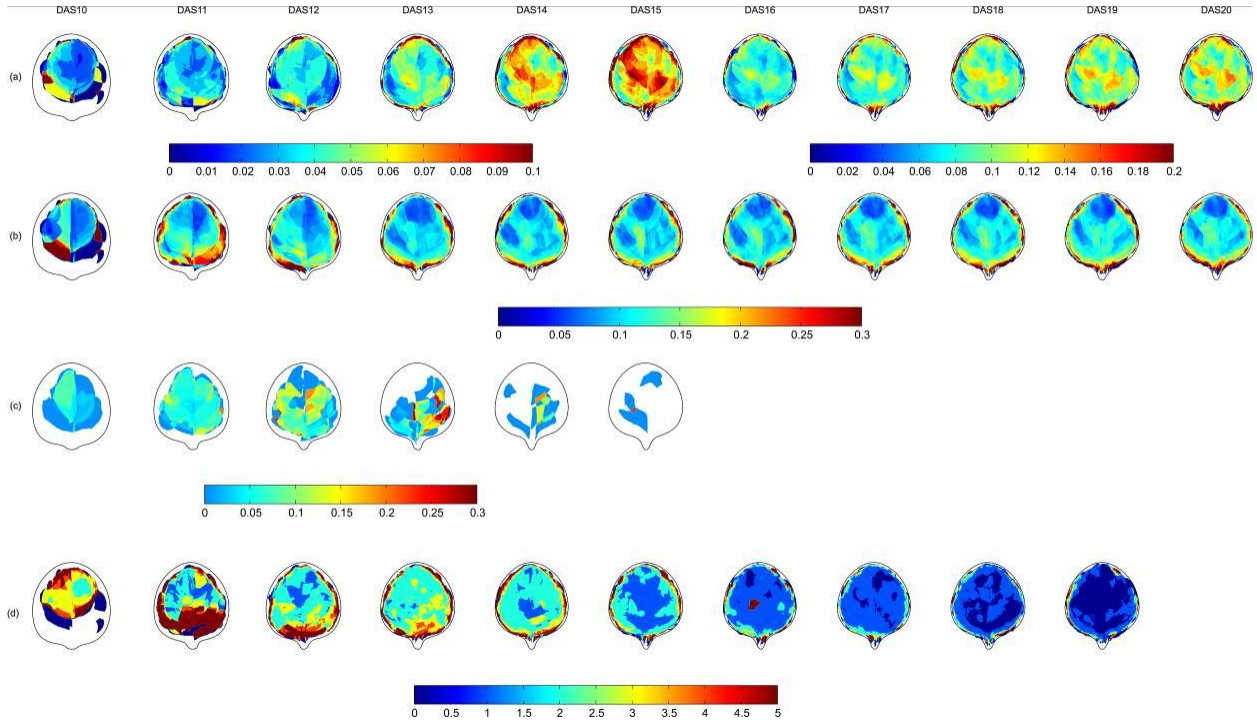

Figure S 15: Standard error maps for (a) loops area (b) loop shape (c) areas of loops about to split (d) Relative growth rates calculated from loop areas.

Appendix H: Disappearing Fluorescence

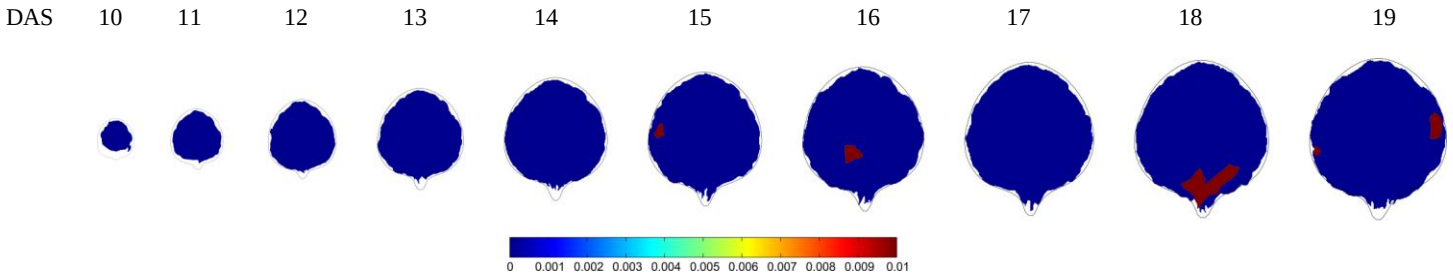

Figure S 16: Map showing the spatial map of loops that disappeared, i.e. which time points had degradation of the GFP marker, and in which part of the leaf.

References

Aloni, R. (2001). Foliar and axial aspects of vascular differentiation: Hypotheses and evidence. *Journal of Plant Growth Regulation, 20*(1), 22-34.

Aloni, R., Schwalm, K., Langhans, M., & Ullrich, C. (2003). Gradual shifts in sites of free-auxin production during leaf-primordium development and their role in vascular differentiation and leaf morphogenesis in Arabidopsis. *Planta, 216*(5), 841-853.

Avery, G. (1933). Structure and development of the tobacco leaf. *American Journal of Botany, 20*(9), 565-592.

Beemster, G. T. S., De Veylder, L., Vercruysse, S., West, G., Rombaut, D., Van Hummelen, P., Vuylsteke, M. (2005). Genome-wide analysis of gene expression profiles associated with cell cycle transitions in growing organs of Arabidopsis. *Plant Physiology, 138*(2), 734-743. doi:10.1104/pp.104.053884

Bennett, M. J., Marchant, A., May, S. T., & Swarup, R. (1998). Going the distance with auxin: Unravelling the molecular basis of auxin transport. *Philosophical Transactions of the Royal Society of London Series B-Biological Sciences, 353*(1374), 1511-1515.

Berleth, T. (2000). Plant development: Hidden networks. *Current Biology, 10*(18), R658-R661.

Berleth, T., & Jurgens, G. (1993). The role of the MONOPTEROS gene in organizing the basal body region of the Arabidopsis embryo. *Development, 118*(2), 575-587.

Berleth, T., & Sachs, T. (2001). Plant morphogenesis: Long-distance coordination and local patterning. *Current Opinion in Plant Biology, 4*(1), 57-62. doi:DOI: 10.1016/S1369-5266(00)00136-9

Bonner, J. T. (2006). *Why size matters : From bacteria to blue whales*. Princeton: Princeton University Press.

Bowman, J. L., Eshed, Y., & Baum, S. F. (2002). Establishment of polarity in angiosperm lateral organs. *Trends in Genetics, 18*(3), 134-141.

Candela, H., Martinez-Laborda, A., & Micol, J. L. (1999). Venation pattern formation in *Arabidopsis thaliana* vegetative leaves. *Developmental Biology, 205*(1), 205-216.

Cheng, Y. F., Dai, X. H., & Zhao, Y. D. (2006). Auxin biosynthesis by the YUCCA flavin monooxygenases controls the formation of floral organs and vascular tissues in Arabidopsis. *Genes & Development, 20*(13), 1790-1799.

Cheng, Y., Qin, G., Dai, X., & Zhao, Y. (2008). NPY genes and AGC kinases define two key steps in auxin-mediated organogenesis in Arabidopsis. *Proceedings of the National Academy of Sciences of the United States of America, 105*(52), 21017-21022. doi:10.1073/pnas.0809761106

Coen, E., Rolland-Lagan, A., Matthews, M., Bangham, J., & Prusinkiewicz, P. (2004). The genetics of geometry. *Proceedings of the National Academy of Sciences of the United States of America, 101*(14), 4728-4735.

Corson, F., Adda-Bedia, M., & Boudaoud, A. (2009). In silico leaf venation networks: Growth and reorganization driven by mechanical forces. *Journal of Theoretical Biology, 259*(3), 440-448. doi:10.1016/j.jtbi.2009.05.002

Couder, Y., Pauchard, L., Allain, C., Adda-Bedia, M., & Douady, S. (2002). The leaf venation as formed in a tensorial field. *European Physical Journal B, 28*(2), 135-138. doi:10.1140/epjb/e2002-00211-1

Dengler, N., & Kang, J. (2001). Vascular patterning and leaf shape. *Current Opinion in Plant Biology, 4*(1), 50-56. doi:DOI: 10.1016/S1369-5266(00)00135-7

Dimitrov, P., & Zucker, S. W. (2006). A constant production hypothesis guides leaf venation patterning. *Proceedings of the National Academy of Sciences of the United States of America, 103*(24), 9363-9368.

Donnelly, P., Bonetta, D., Tsukaya, H., Dengler, R., & Dengler, N. (1999). Cell cycling and cell enlargement in developing leaves of Arabidopsis. *Developmental Biology, 215*(2), 407-419.

Donner, T., Sherr, I., & Scarpella, E. (2009). Regulation of preprocambial cell state acquisition by auxin signalling in Arabidopsis leaves. *Development, 136*(19), 3235-3246.

Dumais, J., & Kwiatkowska, D. (2002). Analysis of surface growth in shoot apices. *Plant Journal, 31*(2), 229-241.

Fujita, H., & Mochizuki, A. (2006a). The origin of the diversity of leaf venation pattern. *Developmental Dynamics, 235*(10), 2710-2721. doi:10.1002/dvdy.20908 ER

Fujita, H., & Mochizuki, A. (2006b). The origin of the diversity of leaf venation pattern. *Developmental Dynamics, 235*(10), 2710-2721. doi:10.1002/dvdy.20908

Fukuda, H. (2004). Signals that control plant vascular cell differentiation. *Nature Reviews Molecular Cell Biology, 5*(5), 379-391. doi:10.1038/nrm1364 ER

Gierer, A., & Meinhard.H. (1972). Theory of biological pattern formation. *Kybernetik, 12*(1), 30-39.

Goldsmith, M. H. M. (1977). Polar transport of auxin. *Annual Review of Plant Physiology and Plant Molecular Biology, 28*, 439-478.

Goodall, C. R., & Green, P. B. (1986). Quantitative-analysis of surface growth. *Botanical Gazette, 147*(1), 1-15.

Granier, C., & Tardieu, F. (2009). Multi-scale phenotyping of leaf expansion in response to environmental changes: The whole is more than the sum of parts. *Plant Cell and Environment, 32*(9), 1175-1184. doi:10.1111/j.1365-3040.2009.01955.x

Haseloff, J. (1999). GFP variants for multispectral imaging of living cells. *Methods in Cell Biology, Vol 58, 58*, 139-+.

Hetu, M. F., Tremblay, L. J., & Lefebvre, D. D. (2005). High root biomass production in anchored Arabidopsis plants grown in axenic sucrose supplemented liquid culture. *BioTechniques, 39*(3), 345-+.

Hickey, L. J. (1973). Classification of architecture of dicotyledonous leaves. *American Journal of Botany, 60*(1), 17-33.

Huttner, D., & Bar-Zvi, D. (2003). An improved, simple, hydroponic method for growing *Arabidopsis thaliana*. *Plant Molecular Biology Reporter, 21*(1), 59-63.

Imlau, A., Truernit, E., & Sauer, N. (1999). Cell-to-cell and long-distance trafficking of the green fluorescent protein in the phloem and symplastic unloading of the protein into sink tissues. *Plant Cell, 11*(3), 309-322.

Jung, J. H., & Park, C. M. (2007). Vascular development in plants: Specification of xylem and phloem tissues. *Journal of Plant Biology, 50*(3), 301-305.

Kang, J., & Dengler, N. (2004). Vein pattern development in adult leaves of *Arabidopsis thaliana*. *International Journal of Plant Sciences, 165*(2), 231-242.

Krogan, N. T., & Berleth, T. (2007). From genes to patterns: Auxin distribution and auxin-dependent gene regulation in plant pattern formation. *Canadian Journal of Botany-Revue Canadienne De Botanique, 85*(4), 353-368. doi:10.1139/B07-029

Lehesranta, S. J., Lichtenberger, R., & Helariutta, Y. (2010). Cell-to-cell communication in vascular morphogenesis. *Current Opinion in Plant Biology, 13*(1), 59-65. doi:10.1016/j.pbi.2009.09.004 ER

Mattsson, J., Ckurshumova, W., & Berleth, T. (2003). Auxin signaling in Arabidopsis leaf vascular development. *Plant Physiology, 131*(3), 1327-1339. doi:10.1104/pp.013623

Mattsson, J., Sung, Z., & Berleth, T. (1999). Responses of plant vascular systems to auxin transport inhibition. *Development, 126*(13), 2979-2991.

Nelson, T., & Dengler, N. (1997). Leaf vascular pattern formation. *Plant Cell, 9*(7), 1121-1135.

Ohashi-Ito, K., & Fukuda, H. (2010). Transcriptional regulation of vascular cell fates. *Curr Opin Plant Biol, 13*(6), 670-676.

Paciorek, T., Zazimalova, E., Ruthardt, N., Petrasek, J., Stierhof, Y. D., Kleine-Vehn, J., . . . Friml, J. (2005). Auxin inhibits endocytosis and promotes its own efflux from cells. *Nature, 435*(7046), 1251-1256. doi:10.1038/nature03633

Poire, R., Wiese-Klinkenberg, A., Parent, B., Mielewczik, M., Schurr, U., Tardieu, F., & Walter, A. (2010). Diel time-courses of leaf growth in monocot and dicot species: Endogenous rhythms and temperature effects. *Journal of Experimental Botany, 61*(6), 1751-1759. doi:10.1093/jxb/erq049

Przemeck, G. K. H., Mattsson, J., Hardtke, C. S., Sung, Z. R., & Berleth, T. (1996). Studies on the role of the Arabidopsis gene MONOPTEROS in vascular development and plant cell axialization. *Planta, 200*(2), 229-237.

Reddy, G. V., Heisler, M. G., Ehrhardt, D. W., & Meyerowitz, E. M. (2004). Real-time lineage analysis reveals oriented cell divisions associated with morphogenesis at the shoot apex of *Arabidopsis thaliana*. *Development, 131*(17), 4225-4237. doi:10.1242/dev.01261 ER

Richards, O. W. (1943). The analysis of the relative growth gradients and changing form of growing organisms illustrated by the tobacco leaf. *American Naturalist, the, 77*, 385-399.

Roberts, A. G., Cruz, S. S., Roberts, I. M., Prior, D. A. M., Turgeon, R., & Oparka, K. J. (1997). Phloem unloading in sink leaves of nicotiana benthamiana: Comparison of a fluorescent solute with a fluorescent virus. *Plant Cell, 9*(8), 1381-1396.

Rolland-Lagan, A. G. (2008). Vein patterning in growing leaves: Axes and polarities. *Current Opinion in Genetics & Development, 18*(4), 348-353. doi:10.1016/j.gde.2008.05.002 ER

Rolland-Lagan, A. G., Bangham, J. A., & Coen, E. (2003). Growth dynamics underlying petal shape and asymmetry. *Nature, 422*(6928), 161-163. doi:10.1038/nature01443 ER

Rolland-Lagan, A. G., Coen, E., Impey, S. J., & Bangham, J. A. (2005). A computational method for inferring growth parameters and shape changes during development based on clonal analysis. *Journal of Theoretical Biology, 232*(2), 157-177. doi:10.1016/j.jtbi.2004.04.045 ER

Rolland-Lagan, A. G., & Prusinkiewicz, P. (2005). Reviewing models of auxin canalization in the context of leaf vein pattern formation in Arabidopsis. *Plant Journal, 44*(5), 854-865. doi:10.1111/j.1365-313X.2005.02581.x ER

Rolland-Lagan, A., Amin, M., & Pakulska, M. (2009). Quantifying leaf venation patterns: Two-dimensional maps. *The Plant Journal : For Cell and Molecular Biology, 57*(1), 195-205.

Runions, A., Fuhrer, M., Lane, B., Federl, P., Rolland-Lagan, A. G., & Prusinkiewicz, P. (2005). Modeling and visualization of leaf venation patterns. *Acm Transactions on Graphics, 24*(3), 702-711.

Sachs, t. (1981). the control of the patterned differentiation of vascular tissues. *Advances in Botanical Research, 9*, 151-262.

Sauer, M., Balla, J., Luschnig, C., Wisniewska, J., Reinohl, V., Friml, J., & Benkova, E. (2006). Canalization of auxin flow by Aux/IAA-ARF-dependent feedback regulation of PIN polarity. *Genes & Development, 20*(20), 2902-2911. doi:10.1101/gad.390806

Sawchuk, M. G., Head, P., Donner, T. J., & Scarpella, E. (2007). Time-lapse imaging of Arabidopsis leaf development shows dynamic patterns of procambium formation. *New Phytologist, 176*, 560-571. doi:10.1111/j.1469-8137.2007.02193.x ER

Scarpella, E., Barkoulas, M., & Tsiantis, M. (2010). Control of leaf and vein development by auxin. *Cold Spring Harbor Perspectives in Biology, 2*(1) doi:10.1101/cshperspect.a001511 ER

Scarpella, E., Francis, P., & Berleth, T. (2004). Stage-specific markers define early steps of procambium development in Arabidopsis leaves and correlate termination of vein formation with mesophyll differentiation. *Development, 131*(14), 3445-3455. doi:10.1242/dev.01182 ER

Scarpella, E., Marcos, D., Friml, J., & Berleth, T. (2006). Control of leaf vascular patterning by polar auxin transport. *Genes & Development, 20*(8), 1015-1027. doi:10.1101/gaf.1402406 ER

Scarpella, E., & Meijer, A. H. (2004). Pattern formation in the vascular system of monocot and dicot plant species. *New Phytologist, 164*(2), 209-242. doi:10.1111/j.1469-8137.2004.01191.x ER

Sieburth, L. E. (1999). Auxin is required for leaf vein pattern in Arabidopsis. *Plant Physiology, 121*(4), 1179-1190.

Sieburth, L. E., & Deyholos, M. K. (2006). Vascular development: The long and winding road. *Current Opinion in Plant Biology, 9*(1), 48-54. doi:10.1016/j.pbi.2005.11.008 ER

Thompson, D. W. (1992; 1942). *On growth and form* (2nd ed.). New York: Dover.

Turing, A. M. (1952). The chemical basis of morphogenesis. *Philosophical Transactions of the Royal Society of London Series B-Biological Sciences, 237*(641), 37-72.

Vanneste, S., & Friml, J. (2009). Auxin: A trigger for change in plant development. *Cell, 136*(6), 1005-1016. doi:10.1016/j.cell.2009.03.001

Vieten, A., Sauer, M., Brewer, P. B., & Friml, J. (2007). Molecular and cellular aspects of auxin-transport-mediated development. *Trends in Plant Science, 12*(4), 160-168. doi:10.1016/j.tplants.2007.03.006

Wenzel, C. L., Schuetz, M., Yu, Q., & Mattsson, J. (2007). Dynamics of MONOPTEROS and PIN-FORMED1 expression during leaf vein pattern formation in *Arabidopsis thaliana*. *Plant Journal, 49*(3), 387-398. doi:10.1111/j.1365-313X.2006.02977.x

Wiese, A., Christ, M., Virnich, O., Schurr, U., & Walter, A. (2007). Spatio-temporal leaf growth patterns of *Arabidopsis thaliana* and evidence for sugar control of the diel leaf growth cycle. *New Phytologist, 174*(4), 752-761.

Wisniewska, J., Xu, J., Seifertova, D., Brewer, P. B., Ruzicka, K., Blilou, I., . . . Friml, J. (2006). Polar PIN localization directs auxin flow in plants. *Science, 312*(5775), 883-883. doi:10.1126/science.1121356

Wolf, S. D., Silk, W. K., & Plant, R. E. (1986). Quantitative patterns of leaf expansion - comparison of normal and malformed leaf growth in vitis-vinifera cv ruby red. *American Journal of Botany, 73*(6), 832-846.